A Holistic Transformation Towards a Techno-Economic Model with Bilateral Contracts in Smart Building(s)

A Dissertation
Presented By

Syed Muhammad Ahsan Razvi
2017-06-0064

In Partial Fulfillment
of the requirements of the degree of
Doctor of Philosophy in
Electrical Engineering

Supervisor: Dr. Hassan Abbas Khan

Department of Electrical Engineering
Syed Babar Ali School of Science and Engineering
Lahore University of Management Sciences
May 2022

To my beloved Parents and loving Family

Acknowledgments

I thank **Almighty ALLAH** for giving me the strength to finish this thesis. All respect and admiration to the Holy Prophet **Hazrat MUHAMMAD** (peace be upon him) and his Holy Progeny, who all came as a source of knowledge for the seekers.

I feel profoundly obliged in my most deep and sincerest appreciation to my regarded instructor and honorable supervisor **Dr. Hassan Abbas Khan**, for his persistent help, generous consideration, imperative and scholarly ideas throughout this research work. I'm profoundly obliged to him for his generously offered assistance to finish this PhD postulation. May God favor him with well being, joy and long life. I consider it as my honor to offer my heartiest appreciations to recognize the assistance provided by my co-supervisor, **Dr. Naveed-ul-Hassan** for his recommendations, all the moral help, motivating direction and challenging criticism all through the exploration at LUMS.

I would like to thank the research group at **Auckland University of Technology (AUT)** for the research collaboration and linkage. In addition, my visit to **Aalborg University (AAU)** as a guest-PhD student provided me with the opportunity to learn about and experience the university's world-class research facilities and atmosphere.

Finally, I'd want to express my gratitude to **Dr. Abubakr Muhammad**, Chair of Department of Electrical Engineering, for providing me with the resources and assistance I needed to finish this thesis. I'd also want to thank **Lahore University of Management Sciences (LUMS)** for giving me the opportunity to work on my thesis and finish it on time.

Syed Muhammad Ahsan Razvi

Table of Contents

List of Figures

List of Tables

List of Acronyms

PV	Photovoltaics
c-Si	Crystalline Silicon
TF	Thin Film
MILP	Mixed Integer Linear Programming
CO_2	Carbon Dioxide
FiTs	Feed-in Tariffs
Li-ion	Lithium ion
PPAs	Power Purchase Agreements
DA	Day ahead
RT	Real-Time
TOU	Time of Use
ESS	Energy Storage System
LCOE	Levelized Cost of Electricity
RE	Renewable Energy
SOP	State of Power
P2P	Peer to Peer
B_1	Primary Building (Smart Building)
B_2	Secondary Building
B_3	Secondary Building
DRE	Distributed Renewable Energy
SOP	State of Power
LV	Low Voltage
THD	Total Harmonic Distortion
DG	Distributed Generation
PCC	Point of Common Coupling
EV	Electric Vehicle
PEV	Plug-in electric vehicle
PHEV	Plug-in hybrid electric vehicle
V2X	Vehicle-to-everything
V2G	Vehicle-to-grid
V2B	Vehicle-to-Building
V2H	Vehicle-to-Home
V2L	Vehicle-to-Load
CS	Charging Station
HEMS	Home energy management system
HDPV	Home distributed photovoltaic

List of Relevant Publications

[Paper A] **Ahsan, S. M**., & Khan, H. A. (2019). Performance comparison of CdTe thin film modules with c-Si modules under low irradiance. *IET Renewable Power Generation*, *13*(11), 1920-1926.

[Paper B] **Ahsan, S**., Niazi, K. A. K., Khan, H. A., & Yang, Y. (2018). Hotspots and performance evaluation of crystalline-silicon and thin-film photovoltaic modules. *Microelectronics Reliability*, *88*, 1014-1018.

[Paper C] **Ahsan, S. M**., Khan, H. A., Hassan, N. U., Arif, S. M., & Lie, T. T. (2020). Optimized power dispatch for solar photovoltaic-storage system with multiple buildings in bilateral contracts. *Applied Energy*, *273*, 115253.

[Paper D] **Ahsan, S. M.**, Khan, H. A., Ayyadi, S., Arif, S. M., & Lie, T. T. (2021, October). Optimized Power Dispatch for Solar-Storage System and Electric Vehicles with Multiple Buildings in Bilateral Contracts. In *2021 IEEE PES Innovative Smart Grid Technologies Europe (ISGT Europe)* (pp. 1-5). IEEE.

[Paper E] **S. M. Ahsan**, H. A. Khan, N.-u. Hassan, and S. Ayyadi," Optimized Power Dispatch for Smart Building(s) and Electric Vehicles with V2X Operation," *(Submitted in Energy Reports)*

[Paper F] **Ahsan, S. M**., Khan, H. A., Hussain, A., Tariq, S., & Zaffar, N. A. (2021). Harmonic Analysis of Grid-Connected Solar PV Systems with Nonlinear Household Loads in Low-Voltage Distribution Networks. *Sustainability*, *13*(7), 3709.

Nomenclature

[Chapter 3] A Novel Rooftop Solar PV Architecture for Profit Maximization

Sets

d days (1-365)

t hours (1-24)

Parameters

$S\ (t,d)$	Power generated by the solar PV at any time step and day (kW)
$B_1(t,d)$	Power demand by building 1 at any time step and day (kW)
$B_2(t,d)$	Power demand by building 2 at any time step and day (kW)
$B_3(t,d)$	Power demand by building 3 at any time step and day (kW)
$P_{B_2}\ (t,d)$	Contracted power demand by building 2 at each time step
$P_{B_3}\ (t,d)$	Contracted power demand by building 3 at each time step
$R_{\text{pur}}\ (t,d)$	Purchase rate of electricity from grid ($/kWh)
$R_{\text{sell}}\ (t,d)$	Sale rate of electricity to grid ($/kWh)
$R_{cont_2}\ (t,d)$	Contracted rate of electricity from solar/battery to building 2 ($/kWh)
$R_{cont_3}\ (t,d)$	Contracted rate of electricity from solar/battery to building 3 ($/kWh)
SOP_{Max}	Maximum power attainable from the battery during each time step (kW)
SOP_{Min}	Minimum power attainable from the battery during each time step (kW)
η_{ch}	Charging efficiency of the battery
η_{dis}	Discharging efficiency of the battery
Δt	Optimization time step (one-hour)

Variables

$P_{\text{ESS2G}}\ (t,d)$	Battery-to-grid power transfer (kW)
$P_{\text{G2ESS}}\ (t,d)$	Grid-to-battery power transfer (kW)
$P_{\text{RE2ESS}}\ (t,d)$	Solar PV to battery power transfer (kW)

$P_{\text{RE2G}}\ (t,d)$ Solar PV to grid power transfer (kW)

$P_{RE2B_1}\ (t,d)$ Solar PV to building 1 power transfer (kW)

$P_{RE2B_2}\ (t,d)$ Solar PV to building 2 power transfer (kW)

$P_{RE2B_3}\ (t,d)$ Solar PV to building 3 power transfer (kW)

$P_{ESS2B_1}\ (t,d)$ Battery to building 1 power transfer (kW)

$P_{ESS2B_2}\ (t,d)$ Battery to building 2 power transfer (kW)

$P_{ESS2B_3}\ (t,d)$ Battery to building 3 power transfer (kW)

$P_{G2B_1}\ (t,d)$ Grid to building 1 power transfer (kW)

$P_{G2B_2}\ (t,d)$ Grid to building 2 power transfer (kW)

$P_{G2B_3}\ (t,d)$ Grid to building 3 power transfer (kW)

$X\ (t,d)$ a binary variable corresponding to the battery's charging

$Y\ (t,d)$ a binary variable corresponding to the battery's discharging

$SOP\ (t,d)$ Power state of the battery (kW)

[Chapter 4] Optimized Charging and Discharging of Electric Vehicles in Smart Building with Bilateral Contracts

Sets

t hours (1-24)

i number of buildings (1-3)

n number of electric vehicles

Parameters

$S\ (t)$ Power generated by the solar PV (kW)

$B_i(t)$ Power demand by i^{th} building (kW)

$P_{B_2}(t)$ Contracted power demand by building 2

$P_{B_3}(t)$ Contracted power demand by building 3

$R_{\text{pur}}\ (t)$ Purchase rate of electricity from grid ($/kWh)

$R_{\text{sell}}\ (t)$ Sale rate of electricity to grid ($/kWh)

$R_{\text{EV}}\ (t)$ Sale rate of electricity to all EVs ($/kWh)

$R_{cont_2}(t)$ Contracted rate of electricity from solar/battery to building 2 ($/kWh)

$R_{cont_3}(t)$ Contracted rate of electricity from solar/battery to building 3 ($/kWh)

$SOP_{ESS^{Max}}$ Maximum power attainable from the battery (kW)

$SOP_{ESS^{Min}}$ Minimum power attainable from the battery (kW)

$SOP_{EV_n{}^{Max}}$ Maximum power state of the n^{th} EV (kW)

$SOP_{EV_n{}^{Min}}$ Minimum power state of the n^{th} EV (kW)

$R_{EV_{SG}}(t)$ Sale rate of electricity from grid to all EVs ($/kWh)

$R_{EV_{SB_1}}(t)$ Sale rate of electricity from B_1 to all EVs ($/kWh)

$R_{EV_{pur}}(t)$ Purchase rate of electricity from all EVs ($/kWh)

$\eta_{ESS_{ch}}$ Charging efficiency of the storage

$\eta_{ESS_{dis}}$ Discharging efficiency of the storage

$\eta_{EV_{ch}}$ Charging efficiency of all EVs

$\eta_{EV_{dis}}$ Discharging efficiency of all EVs

Δt Optimization time step (one-hour)

Variables

$P_{\text{ESS2G}}(t)$ Battery-to-grid power transfer (kW)

$P_{\text{G2ESS}}(t)$ Grid-to-battery power transfer (kW)

$P_{\text{RE2ESS}}(t)$ Solar PV to battery power transfer (kW)

$P_{\text{RE2G}}(t)$ Solar PV to grid power transfer (kW)

$P_{RE2B_1}(t)$ Solar PV to building 1 power transfer (kW)

$P_{RE2B_2}(t)$ Solar PV to building 2 power transfer (kW)

$P_{RE2B_3}(t)$ Solar PV to building 3 power transfer (kW)

$P_{ESS2B_1}(t)$ Battery to building 1 power transfer (kW)

$P_{ESS2B_2}(t)$ Battery to building 2 power transfer (kW)

$P_{ESS2B_3}(t)$ Battery to building 3 power transfer (kW)

$P_{G2B_1}(t)$ Grid to building 1 power transfer (kW)

$P_{G2B_2}(t)$ Grid to building 2 power transfer (kW)

$P_{G2B_3}(t)$ Grid to building 3 power transfer (kW)

$P_{G2EV_n}(t)$ Grid to n^{th} EV power transfer (kW)

$P_{ESS2EV_n}(t)$ Battery to n^{th} EV power transfer (kW)

$P_{RE2EV_n}(t)$ Solar PV to n^{th} EV power transfer (kW)

$P_{EV_n2G}(t)$ n^{th} EV to grid power transfer (kW)

$P_{EV_n2ESS}(t)$ n^{th} EV to battery power transfer (kW)

$P_{EV_n2B_1}(t)$ n^{th} EV to building 1 power transfer (kW)

$P_{EV_n2B_2}(t)$ n^{th} EV to building 2 power transfer (kW)

$P_{EV_n2B_3}(t)$ n^{th} EV to building 3 power transfer (kW)

$X_{ESS}(t)$ Binary variable linked with the charging of storage

$Y_{ESS}(t)$ Binary variable linked with discharging of storage

$X_{EV_n}(t)$ Binary variable linked with the charging of the n^{th} EV

$Y_{EV_n}(t)$ Binary variable linked with discharging of the n^{th} EV

$SOP_{ESS}(t)$ The power state of the storage (kW)

$SOP_{EV_n}(t)$ The power state of n^{th} EV (kW)

Abstract

Smart urban buildings are being built as a synergetic deployment of renewable energy sources and electric vehicles. These buildings employ rooftop solar (depending on space constraints) to reduce grid dependence and as per our assessment have high profit margins by either contributing to the grid stability and/or having local aggregation for optimum routing of power. A large influx of rooftop solar photovoltaics (PV) deployments has been seen in buildings over the past decade due to lucrative net-metering schemes introduced by the various governments, including Pakistan. However, the selection of optimum technology for large-scale rooftop PV installations and the introduction of a comprehensive profitable architecture in smart buildings has remained an open question for the PV and smart grid research community, respectively, primarily due to the evolving space of the technology as well as changing regulations around feed-in tariffs (FiTs). Precisely, in the context of profit maximization and operational viability (technical) for smart buildings, it is needed to assess the a) optimum solar PV technology for rooftop deployments under constraints (low irradiance and partial shading conditions), b) lucrative business propositions for smart building (with solar PV, storage and/or charging infrastructure) and c)total harmonic distortion (THD) in current and voltage as a power quality parameter to gauge the stability of low voltage distribution network. Therefore, in this thesis all these research areas are explored leading to a novel and comprehensive framework for the profitable electricity sharing mechanism among multiple buildings.

Firstly, it is examined that under low irradiance and partial shade, the performance of thin film (TF) PV outshines the power output from crystalline silicon (c-Si) PV. However, due to the relatively low efficiency of TF PV modules, larger rooftop area is required to extract similar amount of power compared to c-Si. Henceforth, given the facts that TF PV panels are lower cost and perform well under low irradiance and partial shading conditions these modules are optimum for localities without significant space constraints.

Secondly, to cope with the challenge of lowering the overall electricity tariff for the consumers, a novel business model is proposed for multiple buildings having bilateral contracts and

connected with the grid, simultaneously. The proposed business architecture caters for the profit margins of each participating building, whether it has rooftop solar PV or not. The detailed results from the model signify that smart building (with solar and storage) earn up to 43 % of annual profits after incorporating installation costs of photovoltaic-battery system. Further, secondary buildings (without solar or storage) achieve 3 - 16 % of savings in the electricity costs based on different contracted loads and agreement tariffs. This work can further enhance the utilization of solar energy resources via rooftop solar photovoltaic to help mitigate the per capita carbon dioxide emissions in countries like Pakistan with high dependency on fossil fuel for electricity generation.

Thirdly, the integration of electric vehicles in smart building enables added options of electricity trade for the prosumer (smart building) along with the optimized charging of electric vehicles. It allows the smart building to earn up to 87 % profit and secondary buildings electricity cost saving goes up to 41 %. To further facilitate the charging station integration in smart building, vehicle-to-everything (V2X) concept is introduced. The optimized charging and discharging of electric vehicles in the parking station of smart building enables the fleet of electric vehicles to earn savings up to 66 %. In addition, primary building (smart building) earns profit up to 62 % whereas the electricity cost savings of secondary buildings ranges from 2- 20%. Resultantly, the objective of lowering overall electricity cost with the introduction of profit maximization framework for the smart building, secondary buildings and electric vehicles on a local level is successfully achieved in this thesis.

Lastly, the technical evaluation of rooftop grid-connected PV systems with high diffusion of non-linear loads facilitates the integration of rooftop solar PV as a distributed energy resource in the low voltage networks. The results reveal that the installation of solar PV at alternate buses allows to operate within the limits for total harmonic distortion in voltage and current. Overall, this thesis presents a detailed techno-economic model for smart building(s) having bilateral contracts with secondary buildings and charging infrastructure for electric vehicles, along with a detailed assessment of the power quality parameters for grid-connected rooftop solar PV in low voltage networks.

Chapter 1

Introduction

1.1 Context and Motivation

Pakistan's circular debt in the energy market has become an inevitable challenge for the government. At the end of the previous fiscal year, FY2020-21, the circular debt in the power sector reached PKR 2.33 trillion [1]. The amount of financial shortfall that the central power purchasing agency (CPPA) cannot pay to power supply industries is known as circular debt [2]. This gap is due to (a) the disparity between the actual cost of providing electricity and the revenues collected by power distribution companies (DISCOs) from sales to customers plus subsidies; and (b) insufficient payments to CPPA from collected income by the DISCOs [2, 3]. This revenue shortfall ripples through the entire energy supply chain, from electricity generators to fuel suppliers, refiners, and producers, resulting in a fuel shortage for public sector thermal generating companies (GENCOs), a reduction in power generated by Independent Power Producers (IPPs), and increased load shedding. Also, due to higher end consumer tariff, the customers that do not able to pay their electricity bills to distribution companies cause a liquidity crisis, preventing power companies from making payments to transmission companies, which then default on oil and gas payments to suppliers [4].

On the other hand, the implementation of competitive electricity markets in Pakistan's power industry has the potential to lower electricity rates. In his context, central power purchasing agency - guarantee (CPPA-G) has developed a model known as competitive trading bilateral contract market (CTBCM) [2, 5]. The CTBCM is created with the goal of creating a competitive wholesale market. Bulk power consumers (BPCs) are the ones who can buy directly from the

market. This form of contract can be particularly beneficial in the wholesale power market to integrate current energy purchase agreements (EPAs) and/or power purchase agreements (PPAs) into several contracts between a generator and different purchasers [3, 5]. This strategy will bring competition to the electricity sector and promote the energy sector's long-term financial viability through procedures that will remain successful despite political shifts. The CPPA-G, which presently purchases power from power companies, will cease to exist, and distribution companies (DISCOs) will purchase power directly from power companies. The CPPA-G will serve as a market operator, handling settlements, balancing, and invoicing, as well as managing independent auctions for additional capacity procurements. Indeed, this will increase the efficiency of the power market and, in the long run, lower the consumer end electricity tariff [6].

However, there is still a lot of attention and efforts required to establish and integrate the local electricity markets in the power sector of Pakistan. Local electricity markets generally operate without market operator with the provision of peer-to-peer (P2P) power sharing/trading at a local level [7-10]. This challenging issue of transformation to local electricity markets in Pakistan can be handled with the introduction of aggregation model with bilateral contracts in solar assisted smart building. Usage of local resources to generate electricity by the large consumers such as industries, commercial and residential buildings and bilateral contracts among the buildings helps to achieve the goal of shifting and implementing comprehensive local electricity market model in Pakistan. The proposed model has been tested in New Zealand settings; however, it is entirely adaptable to Pakistan's electricity sector.

Rooftop solar PV coupled with storage at smart building in bilateral contracts with the secondary buildings helps to achieve the lucrative profits for each entity. Optimized charging of electric vehicles and vehicle-to-everything (V2X) technologies are seen as a way forward in this context in terms of achieving economical, technological, and environmental advantages. Electric vehicles earn savings from local optimized charging and trade with the smart building and grid. Grid congestion can resultantly be avoided with the applicability of this profit model which will contribute towards the adoption of local electricity market and resultantly lowering the electricity tariff in the coming years in a country like Pakistan.

1.2 Research Challenges

1.2.1 Research Direction

The thesis work is structured following two research directions. The first line of research identifies the optimum PV technology for large-scale installations on the rooftop of buildings to extract the maximum power from the solar PV under low irradiance and partial shading conditions. Depending upon the performance of PV system under low irradiance and partial shade, ideal candidate for rooftop solar PV installations is identified. The second line of research focuses on the profit maximization of multiple buildings with bilateral contracts along with the optimized charging and discharging of electric vehicles in smart building allows to achieve the maximum profit for each participating building and fleet of electric vehicles. Last, the technical power quality assessment of grid-connected PV systems under high diffusion of non-linear loads facilitates the integration of distributed energy resource into the low voltage network.

1.2.2 Scientific Contribution

This thesis first contributes by the detailed performance assessment of two types rooftop solar PV technologies through **[Paper A]-[Paper B]**. The optimum type of solar PV technology under low irradiance and partial shading conditions for large-scale rooftop deployments is identified.

Performance of PV panels under low irradiance. Low irradiance, which is common in the mornings, evenings, and on overcast days, reduces the efficiency of solar panels from their rated (standard testing circumstances) value. Due to their growing market share, **[Paper A]** assesses cadmium telluride (CdTe) thin film panels (TFP) and compares their low irradiance performance to traditional crystalline-Silicon (c-Si) panels. The performance of both material systems is examined over a four-year period in order to assess their respective changes in efficiency and energy production.

Performance of PV panel under partial shade. The creation of hotspots in active operation under partial shade has a substantial impact on the dependability of solar photovoltaic (PV) panels. In **[Paper B]**, hotspots in traditional crystalline-silicon (c-Si) and developing thin-film (TF) PV modules are investigated, as well as the impact of shade on their performance. In various shadow

circumstances, both module technologies respond differently, with the TF panel technology providing superior outcomes in terms of hotspots and power output.

The second line of work contributes to the proposition of novel architecture for profit maximization of multiple buildings (in bilateral contracts) and electric vehicles through **[Paper C]-[Paper F].**

Optimized power dispatch for multiple buildings in bilateral contracts. [Paper C] presents a grid-interactive photovoltaic-storage system in a multi building scenario with net-metering. A simulation model is developed for an interconnected multi building environment with a primary building owning the photovoltaic-battery system. Multiple secondary buildings can procure power from the primary building based on suitable bilateral contracts. The applicability of the model is demonstrated through real-time load demand of three buildings along with actual time-of-use pricing data from the utility in the city of Auckland, New Zealand.

Optimized charging of electric vehicles in smart building. The integration of renewable energy sources with specific energy storage systems in buildings is becoming feasible, and there are multiple well-documented benefits. Allowing electric vehicles (EVs) in these smart building provides more choices for optimizing power flows and lowering electricity costs. In **[Paper D],** a mixed-integer linear programme (MILP) is devised to optimize the profitability of the smart building, as well as the financial gains to secondary buildings (without solar and storage) and an EV fleet. The smart building's charging system also helps EVs load by taking into consideration elements including feeder time-of-use (TOU) tariffs, negotiated rates between buildings, and EV charging pricing.

Optimized charging and V2X operation in smart building. Smart buildings are being built as a synergetic deployment of electric vehicles (EVs) and renewable energy sources. Smart charging of electric vehicles and vehicle-to-everything (V2X) technologies are seen as a way forward in this context in terms of achieving economic, technological, and environmental advantages. **[Paper E]** proposes a framework for the multi-objective techno-economic optimization for profit maximization of multiple inter-connected buildings (with bilateral contracts) and scheduling of EVs. The primary building owns the photovoltaic system coupled with storage and charging

infrastructure for electric vehicles. Based on appropriate bilateral contracts, several secondary buildings can purchase power from the primary building. The optimized charging of electric vehicles at affordable rates using local resources at the primary building assists the grid in managing the EVs load during peak hours. Real load profiles for three buildings, actual time-of-use tariff and stochastic information of EVs (initial state-of-power, arrival and departure times) are used to validate the model in Auckland, New Zealand.

Technical evaluation of rooftop grid-connected PV systems. Grid voltage levels and total harmonic distortion (*THD*) at the low voltage (LV) distribution feeder are affected by the high penetration of grid-connected PVs, non-linear loads, and bidirectional power flows. **[Paper F]** evaluates LV power quality issues with high non-linear loads at the point of common coupling (PCC). Various examples of PV penetration (0 % to 100 %) are tested at the radial modified IEEE-34 bus system to assess total harmonic distortion in the current (THD_i) and voltage (THD_v) at PCC for practical feeder data in a weak grid environment.

1.3 Thesis Outline

In addition to Chapter 1, there are five other chapters in the thesis.

Chapter 2 presents the contribution towards the comprehensive qualitative and quantitative assessment of two types of PV technology for rooftop spaces under low irradiance and partial shade. In the 1st part, chapter discusses the performance of crystalline silicon and CdTe thin film PV modules under low irradiance. The 2nd part discusses the formation of hotspots and performance evaluation of crystalline silicon and thin-film PV modules under partial shading conditions.

Chapter 3 presents thesis contribution to profit maximization of building with solar photovoltaic-storage system having bilateral contracts with multiple buildings. The 1st part discusses the literature review for the grid-connected rooftop solar PV topologies. The 2nd and 3rd parts present the contribution to the thesis and proposed system architecture for the rooftop PV systems, respectively. In the 4th part, detailed mathematical modeling with objective function and system constraints is presented. The results of two case studies and three scenarios for the evaluation

of proposed framework is presented in 5th part. The 6th and last part of the chapter discusses the detailed financial analysis for multiple building involved in the trade.

Chapter 4 entails the contribution towards the integration of electric vehicles in smart building with bilateral contracts. The 1st part discusses the comprehensive literature review for the smart buildings with the integration of electric vehicles. The contribution to the thesis with the enablement of V2X capability in smart buildings is discussed in 2nd part. The 3rd part presents the system overview for the profitable electricity trade among smart building and fleet of electric vehicles with optimized charging. The mathematical model for the optimized charging of electric vehicles with objective functions and optimization constraints are presented in 4th part. In the 5th part, the detailed results of optimized power dispatch and financial gains of multiple buildings under two different cases are discussed. In the 6th part, a detailed optimization problem is formulated for the profitability of each participating entity with V2X concept embedded into the system. The 5th part of the chapter discusses the results of optimized power dispatch for each building and fleet of electric vehicles with V2X capability. The 7th and last part presents a comprehensive financial analysis for the multiple buildings and fleet of electric vehicles.

Chapter 5 contributes to the thesis with the detailed harmonic analysis of rooftop grid-connected PV systems. The 1st part presents the comprehensive literature review for the harmonic analysis of rooftop PV systems. The 2nd part outlines the contributions towards the thesis for the grid-connected PV systems. The 3rd, 4th and 5th parts of the chapter present the methodology opted for the harmonic evaluation of rooftop PV systems, the total harmonic distortion introduced due to non-linear household loads and characteristics of solar PV system deployed, respectively.

Chapter 6 summarizes the major findings from thesis and suggests future study directions.

1.4 List of Publications

The following are the papers that are crucial to this thesis:

[Paper A] **Ahsan, S. M.**, & Khan, H. A. (2019). Performance comparison of CdTe thin film modules with c-Si modules under low irradiance. *IET Renewable Power Generation*, *13*(11),

1920-1926.
https://ietresearch.onlinelibrary.wiley.com/doi/pdf/10.1049/iet-rpg.2018.5479

[Paper B] **Ahsan, S**., Niazi, K. A. K., Khan, H. A., & Yang, Y. (2018). Hotspots and performance evaluation of crystalline-silicon and thin-film photovoltaic modules. *Microelectronics Reliability*, *88*, 1014-1018.
https://doi.org/10.1016/j.microrel.2018.06.097

[Paper C] **Ahsan, S. M**., Khan, H. A., Hassan, N. U., Arif, S. M., & Lie, T. T. (2020). Optimized power dispatch for solar photovoltaic-storage system with multiple buildings in bilateral contracts. *Applied Energy*, *273*, 115253.
https://doi.org/10.1016/j.apenergy.2020.115253

[Paper D] **Ahsan, S. M.**, Khan, H. A., Ayyadi, S., Arif, S. M., & Lie, T. T. (2021, October). Optimized Power Dispatch for Solar-Storage System and Electric Vehicles with Multiple Buildings in Bilateral Contracts. In *2021 IEEE PES Innovative Smart Grid Technologies Europe (ISGT Europe)* (pp. 1-5). IEEE.
https://doi.org/10.1109/ISGTEurope52324.2021.9640116

[Paper E] **S. M. Ahsan**, H. A. Khan, N.-u. Hassan, and S. Ayyadi," Optimized Power Dispatch for Smart Building(s) and Electric Vehicles with V2X Operation," *(Submitted in Energy Reports)*

[Paper F] **Ahsan, S. M**., Khan, H. A., Hussain, A., Tariq, S., & Zaffar, N. A. (2021). Harmonic Analysis of Grid-Connected Solar PV Systems with Nonlinear Household Loads in Low-Voltage Distribution Networks. *Sustainability*, *13*(7), 3709.
https://doi.org/10.3390/su13073709

The following papers were written during Ph.D. studies, although they are not included in this thesis:

[Paper G] Baig, M. Q., Khan, H. A., & **Ahsan, S. M**. (2020). Evaluation of solar module equivalent models under real operating conditions—A review. *Journal of Renewable and Sustainable Energy*, *12*(1), 012701. https://doi.org/10.1063/1.5099557

[Paper H] Arif, S. M., Lie, T. T., Seet, B. C., **Ahsan, S. M**., & Khan, H. A. (2020). Plug-In Electric Bus Depot Charging with PV and ESS and Their Impact on LV Feeder. *Energies*, *13*(9), 2139. https://doi.org/10.3390/en13092139

[Paper I] Arif, S. M., Hussain, A., Lie, T. T., **Ahsan, S. M.**, & Khan, H. A. (2020). Analytical Hybrid Particle Swarm Optimization Algorithm for Optimal Siting and Sizing of Distributed Generation in Smart Grid. *Journal of Modern Power Systems and Clean Energy*, *8*(6), 1221-1230. *https://doi.org/10.35833/MPCE.2019.000143*

[Paper J] Tahir, M. U., **Ahsan, S. M**., Arif, S. M., & Abdullah, M. (2018, November). GSM Based Advanced Water Quality Monitoring System Powered by Solar Photovoltaic System. In *2018 Australasian Universities Power Engineering Conference (AUPEC)* (pp. 1-5). IEEE. https://doi.org/10.1109/AUPEC.2018.8757904

[Paper K] Siraj, K., **Ahsan, S. M.**, & Khan, H. A. (2021, June). Techno-economic Evaluation of Residential DC Power System for Multiple Distribution Voltages. In *2021 IEEE 48th Photovoltaic Specialists Conference (PVSC)* (pp. 0858-0862). IEEE. https://doi.org/10.1109/PVSC43889.2021.9518862

[Paper L] **Ahsan, S. M.**, & Khan, H. A. (2022, March). LV Harmonic Analysis of Single-Phase Rooftop Solar PV Systems with Non-Linear Loads. In *2022 IEEE Green Technologies Conference (GreenTech)* (pp. 1-6). IEEE. https://doi.org/10.1109/GreenTech52845.2022.9772022

[Paper M] S. Ayyadi, **S. M. Ahsan**, S. M. Arif, H. Abououbaida, and H. A. Khan "Cost-effective Fast Charging Station Integrated with Solar Photovoltaics and Storage" *(To be Submitted)*

[Paper N] H. A. Khan, Syed S. Tariq, and **S. M. Ahsan** " Climate Change Adaptation through Solar Interventions for Vulnerable Communities in Developing Regions," *(To be Submitted)*

Chapter 2

Performance Evaluation of c-Si and Thin Film PV

2.1 Performance Comparison between c-Si and Thin Film PV under Low Irradiance

This chapter identifies the optimum solar PV technology under low irradiance and partial shading conditions for large scale rooftop solar PV installations. Solar energy has the highest potential (for electricity generation) among all the renewable technologies and has seen a large growth in recent years [11] primarily due to lowering solar panel costs which have decreased from 4.0 $/W to 0.3 $/Wp in the last decade [12, 13]. Therefore, the photovoltaic technology is now competitive and in many cases a cheaper alternative to conventional fossil fuel based electricity production [14]. Traditionally, crystalline Silicon (c-Si) has been commonly used for photovoltaic (PV) applications due to low costs and mature technology with over 93 % of the market share [15, 16]. However, due to low temperature processing [17] and maturing technology of thin film panels (TFP), their share in the PV industry is increasing and is likely to grow at an annual rate of around 12.9 % till 2030 [18-20]. While TFP has a potential to be considerable cheaper than c-Si, their lower efficiency (compared with c-Si technology) will require larger deployment area for equivalent energy production. This can be a deterrent in domestic/residential rooftop installations in certain regions where space constraint is an important issue. However, with utility scale deployments in deserts or large barren lands, where space is typically not a constraint, TFP is becoming an increasingly popular choice [21].

2.1.1 Performance Ratio Assessment and Spectral Response of Solar Panels

For any commercial PV deployment, the ultimate goal is to maximize the power output of the system and in turn maximize the performance ratio (PR) [22]. PR is the ratio between produced energy to the ideal energy available [23]. Various losses such as temperature [24], shading and mismatch effects [25, 26], wiring losses [27], inverter losses [28] affect the PR of a PV plant and numerous remedies have been discussed in the literature. However, another important aspect, i.e., the effect of low irradiance on the performance of solar panels is largely limited in the literature. Several studies discuss the low irradiance loss in solar PV panels but the analysis is largely limited to c-Si panels [29-32]. For TFPs, various studies mainly analyze system PRs in practical environmental conditions. For instance, Schweiger et al. [33] discusses the impact of various losses on the energy yield in different climate zones. Ozden et al. [34] also compared outdoor performance of TFP with Si and analyzed the relative PRs for operation in Turkey. Further, Huld et al. [35] presented a method for estimating the PV energy yield in large geographical area. Several other studies [36-39] also present PR and energy output variations of TFP and assess related aspect for performance enhancement. While all these papers assess PR and factors that affect the PR, the explicit quantification of low irradiance loss for TFP has not been reported in the literature. Therefore, in this chapter, this loss due to varying irradiance on CdTe TFP (the highest used thin film technology with more than 50% share in thin film PV market [13, 40]) is quantified. The energy produced from a typical CdTe panel setup is analyzed and compared with that of c-Si system for four years through the hourly data available through National Renewable Energy Laboratory (NREL) [41]. This analysis is then extended to measured high-granularity (15-min interval) irradiance data for eight days and comparison is made between CdTe TFP and conventional c-Si panels based upon specific energy yield on per day basis. This work will therefore be very useful in making technological assessment of panel technology in future deployments particularly in areas with high irradiance variations.

For evaluating the performance of solar panels, it is critical to analyze the material performance in terms of their spectral responses. SR is the ratio of photo-generated short circuit current at a given wavelength to the incident power density or photon flux [24]. Alternatively, it is also given

as the ratio of current generated by the solar cell to the power incident on the solar cell. Lower bandgap materials have a peak spectral response in the infrared, while greater band gap materials have a maximum spectral response in the visible or higher energy area. The relationship between spectral response and a material's quantum efficiency (QE) at a specific wavelength is given by (2.1) [42]. c-Si and CdTe have different bandgaps at room temperature which results in different cut-off wavelengths (λ_g) given by (2.2).

$$SR(\lambda) = \frac{q * \lambda}{hc} * QE(\lambda) \tag{2.1}$$

$$\lambda_g = \frac{1240}{E_g\,(eV)}\ (n) \tag{2.2}$$

A higher cut-off wavelength of 1100 nm lies in infrared region where low energy photons are absorbed. Therefore, spectral sensitivity of c-Si peaks at this value of wavelength, (adapted from [43]) whereas CdTe based cells having bandgap of 1.54 eV at STC correspond to a cut-off wavelength of 800 nm with spectral sensitivity peaking between 650-800 nm of the incoming spectrum shown in Figure 2.1.

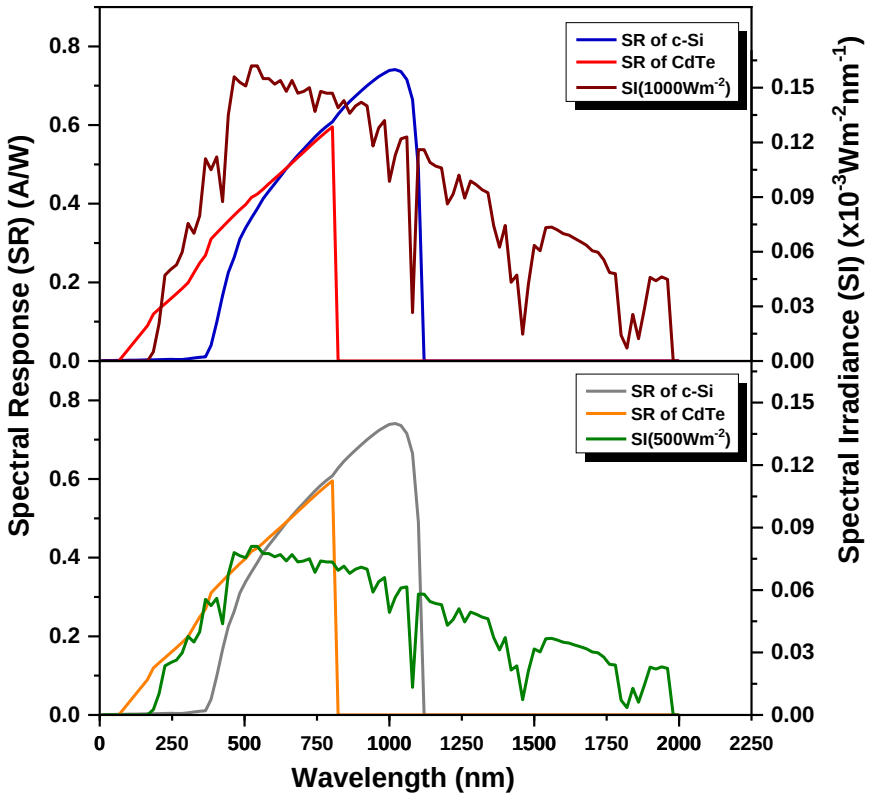

Figure 2.1 Spectral response of c-Si and CdTe under spectral irradiance of 1000 Wm^{-2} and 500 Wm^{-2}, respectively.

2.2 Solar Panel Modeling and Low Irradiance Results

In order to quantify the effects of low irradiance, it is important to analyze the parameters which affect the panel output. The short circuit current density (J_{SC}) for any material system is given by (2.3).

$$J_{sc} = \int_{E_g}^{\infty} G(\lambda) * SR(\lambda) * d(\lambda) \tag{2.3}$$

Here G (λ) and SR(λ) are the input irradiance and spectral response respectively at a specific wavelength [44]. J_{SC} is calculated under varying irradiance conditions by integrating the product of aforementioned quantities over available range of given wavelengths. The short circuit current decreases as input irradiance declines depending upon on the solar insolation as well as the

spectral response of the material being employed for absorptions [37]. The reverse saturation current density (J_o) is given by (2.4).

$$J_o = CT^3 * exp\ (-\frac{E_g}{k.T}) \tag{2.4}$$

where C is a constant that varies based on the material type and doping, and T is the temperature in Kelvin. The value of C used in the analysis is 17.90 mA/cm^{2}K^3, both for CdTe and c-Si [45]. Further, the open circuit voltage (V_{oc}) and fill factor (FF) and the efficiency (η) of a solar panel can be calculated using (2.5) - (2.7), respectively [31].

$$V_{oc} = \frac{kT}{q} * ln\ (\frac{J_{sc}}{J_o} + 1) \tag{2.5}$$

$$FF = \frac{v_{oc} - ln\ (v_{oc} + 0.72)}{v_{oc}\ + 1} \tag{2.6}$$

$$\eta = \frac{V_{oc}\ J_{sc} FF}{P_{in}} \tag{2.7}$$

where $v_{oc} = \frac{V_{oc}}{k.T/q}$, k is the Boltzmann's constant, T is cell temperature, q is the charge on an electron and P_{in} is the incident power given in W/m^2. The low irradiance performance of CdTe is better as compared to c-Si due to the fact that the peak of spectral response of CdTe lies in the visible region of the incoming spectrum whereas the peak of spectral response of c-Si lies in the infrared region. It is however important to analyze this effect and quantify the gains in terms of CdTe deployment. A 4 year beam irradiance data at 1-hr internal, acquired from NREL [41] is analyzed for the location in Lahore which shows an enhancement of energy production through CdTe for the year 2011-2012 and 2013-2014. A comparison of annual energy yield from c-Si and CdTe for four years is listed in Appendix A2. Figure 2.2 shows the comparison of the ideal energy available to the annual yield for c-Si and CdTe for year 2011-2012. It is evident that over multiple

years' same nature of variations is observed with respect to specific energy yield. In order to obtain the percentage loss in efficiency under low levels of irradiance, the difference between the efficiency at STC and non-standard irradiance values is computed. Under STC the rated efficiency (η_{STC}) can be given as (2.8).

$$\eta_{STC} = \frac{V_{oc(r)} J_{sc(r)} FF_{(r)}}{P_{in(STC)}} = \frac{\frac{kT}{q} ln\left(\frac{J_{sc(r)}}{J_o} + 1\right) J_{sc(r)} FF_r}{P_{in(STC)}} \quad (2.8)$$

where $V_{oc(r)}$, $J_{sc(r)}$ and $FF_{(r)}$ are the rated values of open circuit voltage, short circuit current density and fill factor at 1-sun condition (P_{in} = 1000 Wm^{-2}), respectively. The value of efficiency at lower insolation levels represented by η' can be written as (2.9).

$$\eta' = \frac{V'_{oc} J'_{sc} FF'}{P'_{in}} = \frac{\frac{kT}{q} ln\left(\frac{J'_{sc}}{J_o} + 1\right) J'_{sc} FF'}{P'_{in}} \quad (2.9)$$

where P'_{in} is the input power at low irradiance (typically varying throughout the day). The percentage decrease in efficiency of solar PV panel to calculate the difference in energy outputs from rated energy values can be written as (2.10).

$$\frac{\Delta\eta}{\eta_{STC}}(\%) = \frac{\eta' - \eta_r}{\eta_{STC}} * 100 \tag{2.10}$$

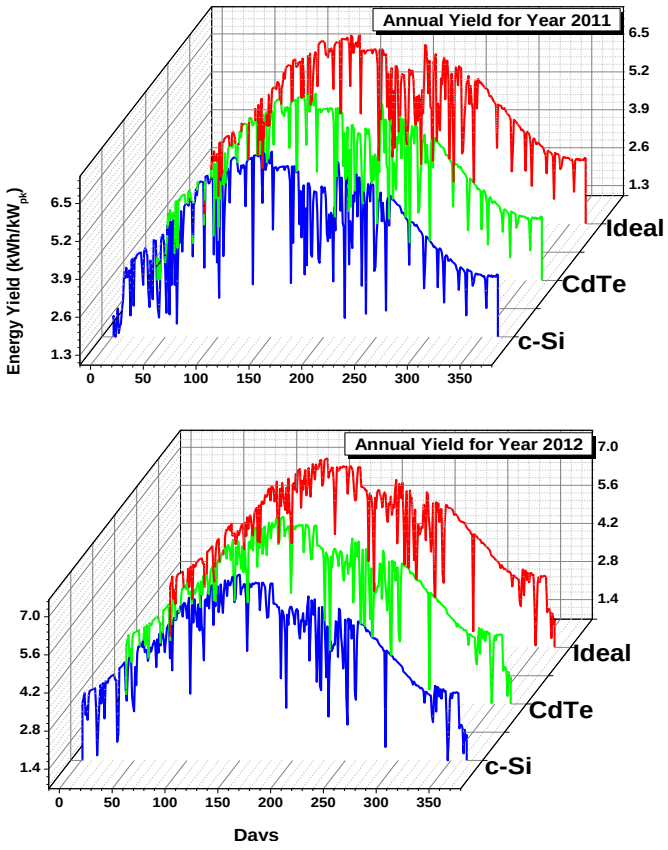

Figure 2.2 Comparison of ideal energy available to the energy produced by c-Si and CdTe for year 2011-2012 under non-standard conditions.

In order to further evaluate the performance of two panel systems based on real data, a high granularity 8-day measured data (4 summer and 4 winter days) has been analyzed for practical rooftop deployment of PV panels at Lahore University of Management Sciences [46]. The data for winter season and summer has been measured through an installed irradiance monitoring station (SMA Sunny Sensor Box), shown in Appendix A1. For the analysis, standard 1 kW_{pk} PV systems for each technology is considered and analyzed for energy yield per 15-min granularity. Results of c-Si and CdTe for 4 days of winter season are shown in Figure 2.3.

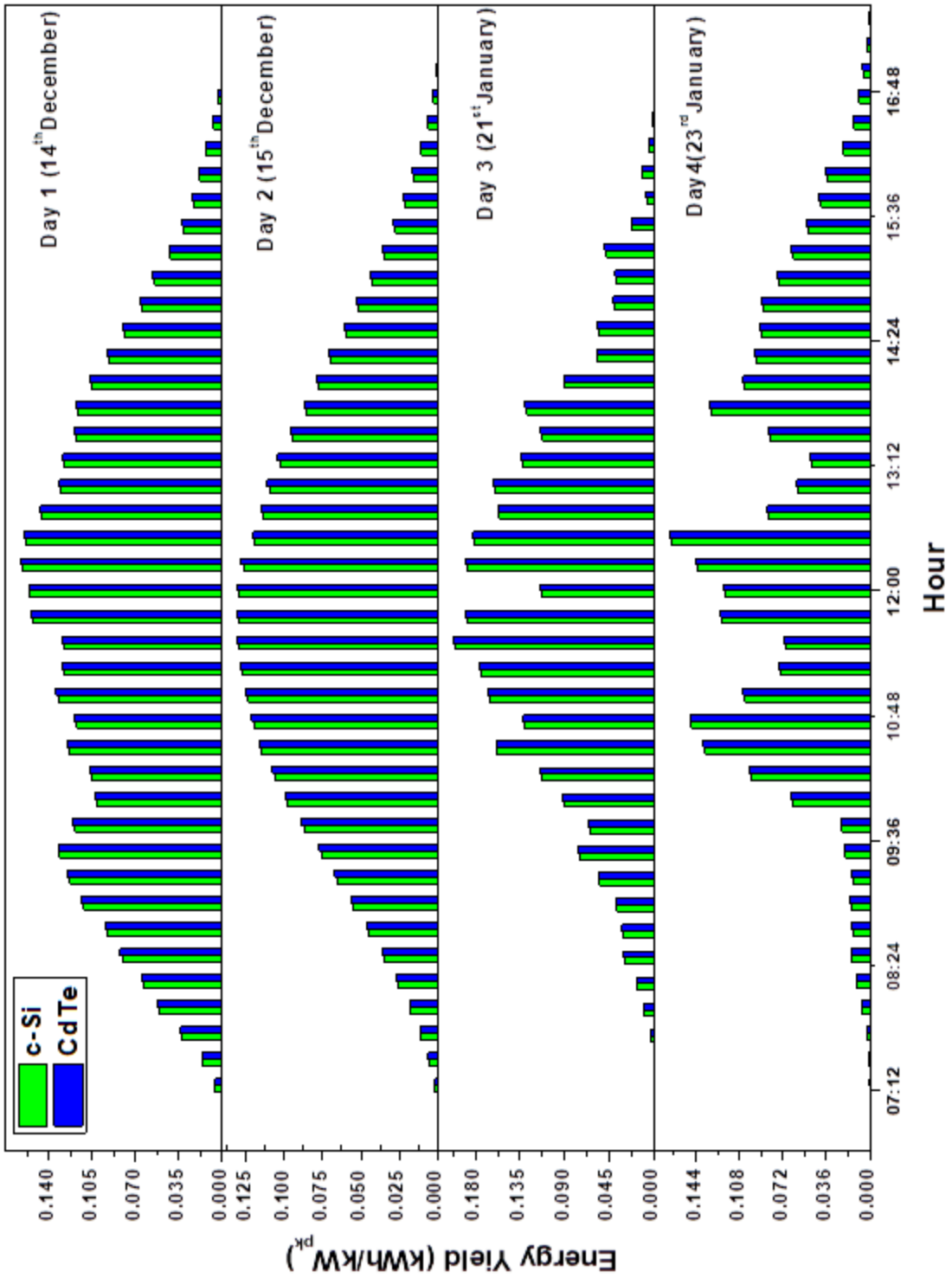

Figure 2.3 Comparison of energy yield by c-Si and CdTe for 4 winter days under varying irradiance.

It can be observed from Figure 2.3 that the energy yield from CdTe panels is higher compared to c-Si and the overall results are summarized in Table 2.1. Typically, in winter days, when the

insolation levels are significantly lower than the standard values, the energy difference between the c-Si and CdTe TFP is comparatively higher than the energy variability during summer days where high insolation days are more prevalent. It can be observed from Table 2.1 that for day 2 where high variation in insolation levels are seen, the additional energy yield of CdTe TFP is highest among all winter days.

Table 2.1 Energy output by c-Si and CdTe for four days of winter and four days of summer under low irradiance.

Day	Specific Energy Yield of Si ($kWhr/kW_{pk}$)	Specific Energy Yield of CdTe ($kWhr/kW_{pk}$)	Additional Production Output of CdTe (%)
Winter			
1	2.46	2.50	1.62
2	0.53	0.56	5.66
3	3.09	3.13	1.29
4	2.68	2.73	1.87
Summer			
5	5.48	5.53	0.91
6	5.95	5.99	0.67
7	5.12	5.17	0.97
8	6.73	6.78	0.74
Total	32.04	32.39	1.09(Weighted average)

This is primarily due to higher change (reduction) in efficiency of c-Si panel as compared to TFP under quite low light conditions. The temperature coefficients both for c-Si and CdTe have distinct effects on the overall energy yield of the PV modules and it sometimes dominate the irradiance effect [33, 47]. Therefore, this chapter primarily targets to present a rationale under merely low irradiance or overcast conditions without taking into account the temperature or partial shading effects. Overall, CdTe produced 1.09 % higher specific energy yield which would lead to higher PR. In order to further analyze the relative gains in CdTe, it is important to evaluate its performance for short circuit current, open circuit voltage and fill factor under low irradiance. The current increases during the day time as irradiance is increasing and vice versa. However, the

magnitude of current increase is different for c-Si and CdTe primarily due to the difference in bandgap, which results in different overall current contribution. This directly affects the open circuit voltage value, which in turns affects in FF as well as efficiency.

Therefore, it is important to analyze the variations in relative efficiency under varying insolation levels for all eight days during winters and summers. The resulting plots of relative efficiency (η_{rel}) given by (2.11) [33] are shown in Figure 2.3 which clearly show that a higher relative decline in efficiency is observed for c-Si compared to CdTe during the winter period in comparison to summer season where largely insolation levels are closer to standard values. Thus, the effect of lower irradiance is more obvious in winter days compared to summer days with CdTe TF panels showing an overall superior performance.

$$\eta_{rel} = 100 - \frac{\Delta\eta}{\eta_{STC}}(\%) \tag{2.11}$$

The percentage change in efficiency as a function of insolation intensity can be expressed as (2.12) [48].

$$\frac{\Delta\eta}{\eta_{STC}}(\%) = \left[\frac{kT}{q} * \frac{ln(n)}{V_{oc}}\right] * 100 \tag{2.12}$$

Where "n" corresponds to the number of suns under which solar PV module is operated. For c-Si and thin film (CdTe) under low irradiance, (2.12) takes the form as (2.13) and (2.14), respectively.

$$\frac{\Delta\eta(Si)}{\eta_{STC}}(\%) = 3.95 * ln(n) \quad (2.13)$$

$$\frac{\Delta\eta(CdTe)}{\eta_{STC}}(\%) = 2.31 * ln(n) \quad (2.14)$$

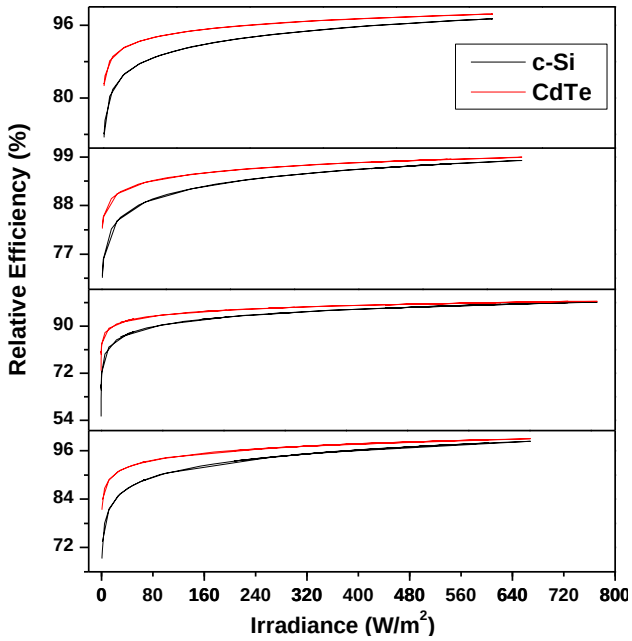

Figure 2.3 Variation in relative efficiency of c-Si and CdTe for 4 days of winter w.r.t. varying irradiance.

From Figure 2.3, it can be inferred that the daily results acquired though the analysis of c-Si and thin film correlates with the relationships given in (2.13) and (2.14), respectively. The uniformity in the results for 1-hr interval and 15-min interval is an interesting outcome of the analysis and suggests that 1-hr granularity is proving sufficient for reasonably accurate solar energy predictions. Further, higher variations in the energy yield are expected for winter months due to lower irradiances or equivalent peak sunlight hours. This is already established for c-Si in our earlier work that energy harvested through the course of whole year mainly depends upon the equivalent peak sunlight hours (EPSH) available for the whole day [31]. This generally means that the decline with respect to varying irradiance in the performance of CdTe TFP (as well as c-Si) would be lower in summer compared to winters with overall 1% relative gains in CdTe.

2.3 Performance Comparison between c-Si and Thin Film PV under Partial Shade

A larger number of thin film (TF) implementations are seen due to lower costs of production, where high temperature processing in the TF module manufacturing is not required unlike the conventional c-Si technology [15, 49, 50]. In recent years, the efficiency of TF panels has also increased, moving its utilization from laboratory to commercialization [20, 51]. Therefore, it is also important to evaluate the performance and reliability of these panels compared with the c-Si modules. The performance of conventional c-Si PV panels under partial shading conditions is deteriorated due to series cell connections, where a small amount of shade on any part of the panel can severely affects the output power of the module [52, 53]. This effect is quantified as mismatch losses [54], which can be reduced by using bypass diode(s) across a module. In addition, these bypass diodes also minimize hotspots which may accelerate the aging of panels and, in severe cases, result in irreversible malfunctioning. Partial shading also affects the performance of TF modules and this should be analyzed as well compared to the conventional c-Si panel technology.

Hotspots appear due to the series arrangement of solar cells. This results in the shaded region of the panel operating in the reverse-biased condition dissipating power as heat. Large uniform shading is generally less problematic for panels. However, under a high ambient temperature, uneven cell level shading significantly increases the possibility of hotspots [55]. Hotspots affect the PV modules in terms of reliability and may result in accelerated aging affecting the long term performance [56, 57], as aforementioned. Solar PV panels typically has a manufacturer warranty of more than 25 years for consistent operation under rated conditions. However, the occurrence of hotspots in practice affects the overall operation and under severe hotspots, cell encapsulate, joints and metal contact or the glass cover can break, subsequently resulting in module downtime [58]. Furthermore, the number of bypass diodes and their orientation also affect the performance of these panels [59]. TF module technologies are becoming more competitive due to increasing efficiencies and better module performance than c-Si PV modules in high-shade scenarios [47, 60]. This is primarily due to the monolithic cell orientation within a panel, where

cells with a long rectangular structure are uniformly integrated, resulting in lower hotspots [55, 61]. However, it is necessary to evaluate these hotspots and resultant temperatures to compare the two panel technologies. This is performed in this chapter on the system installed at Lahore University of Management Sciences (LUMS). In addition, the power production performance of the two in the same orientation to quantify the performance of the two systems (i.e., TF and c-Si panels) with varying shade conditions is benchmarked in this chapter.

2.3.1 c-Si PV and Thin Film PV Panels Construction

It is well known that in conventional c-Si solar panels, a number of cells are connected in series. Each cell behaves as an individual power source and for optimum power production, each must produce similar currents. TF PV modules, on the other hand, have long, narrow, and rectangular cells connected in series. The current flow is two-dimension (2D) due to the internal structure of series-connected cells, as shown in Figure 2.4 [61]. While each solar cell has an intrinsic layer of semiconductor in between the *p*- and *n*-type regions which creates an appreciable distance between these layers. This separation allows high tolerances against larger reverse voltage stresses during extreme partial shading conditions [62].

The 2D current-flow nature can be explained: each cell consists of multiple sub-cells connected in parallel, $N_{parallel}$. The total number of sub-cells connected in parallel per each cell depends upon the width and area of the module. The number of series-connected cells, $N_{series,}$ depending on the panel length, can also be observed. This unique geometrical orientation and inherent internal structure of TF solar cells enable high tolerance levels against high reverse break-down voltages. As a result, the probability of the occurrence of hot spot damages within a module is minimized. The electrical model for each individual sub-cell of CIS based TF can be depicted, as shown in Figure 2.5 [61], where I_{ph} is the light-generated current, I_D is the diode current, I_{sh} is the current flowing through the shunt resistance, and $I_{rec,G}$ is the conduction band offset also known as generation enhanced recombination [61]. It can be given as (2.15).

$$I_{rec,G} = I_{rec0} V exp\left(\frac{q}{kT}\sqrt{\frac{V}{m}}\right) \tag{2.15}$$

in which I_{rec0} is the Poole-Frenkel parameter known as the breakdown current prefactor ($mA/V.cm^{-2}$) depending upon the defect level, E_T ($I_{rec0} \sim E_T$), V is the terminal voltage (V), and m is the break down current index ($V^{-0.5}$) [63].

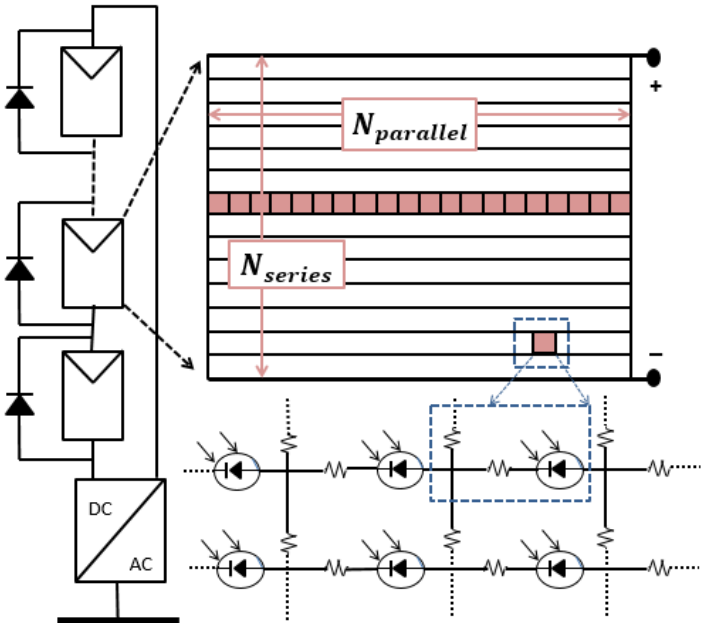

Figure 2.4 Monolithic integration of cells in TF modules.

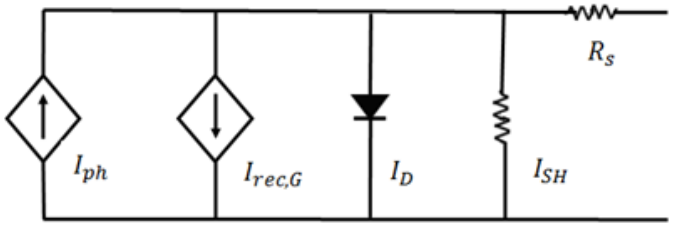

Figure 2.5 Internal structure of a TF sub-cell.

The rest of the electrical model for TF sub-cells is similar to the well-known c-Si models with respect to the diode current, short circuit current and open circuit voltage represented as (2.16)-(2.18), respectively [64].

$$I_D = I_0(exp\left(\frac{qV}{kT}\right) - 1) \tag{2.16}$$

$$I = I_{ph} - I_D - I_{rec0}\, Vexp\left(\frac{q}{kT}\sqrt{\frac{V}{m}}\right) \tag{2.17}$$

$$V_{oc} = \frac{kT}{q} ln\ (\frac{I_{ph}}{I_0} + 1) \tag{2.18}$$

Furthermore, Figure 2.4 illustrates the fact that for each TF module, only one bypass diode is connected unlike a typical c-Si module. The system under consideration mainly consists of three modules connected in series to form a string, across which a single DC to AC inverter is connected. For the entire string, three bypass diodes are employed.

2.4 Partial Shading Results for both c-Si and Thin Film PV

Thermal images to evaluate hotspots for the c-Si modules connected in series, obtained from the thermal camera (FLIR Vue 640 pro), are shown in Figure 2.6. Under no-shading (Figure 2.6(a)), the panels are completely uniform with no bright spots in the image (other than the junction box, which is close to the top of each panel). The temperature of the entire PV module is measured to be the same as approx. 49°C at 860-Wm^{-2} input irradiance. Furthermore, without shading, none of the bypass diodes are ON, and thus all cells are contributing to power production. The thermal image for the c-Si module with a bottom left cell half-shaded by a thick sheet is shown in Figure 2.6 (b) . As a cell in series orientation is shaded, this bypasses the sub-module through the bypass diode in ON-state. Therefore, the substring is now completely bypassed and it does not contribute to the power output. Hence, the power produced by cells is dissipated, as heat, which is manifested through the glowing of the cell or hotspot in the sub-module in Figure 2.6(b). Resultant hotspot temperature is measured to be 86°C, while the shaded part reduces to 33°C (due to the thick shade). The temperature of other two un-bypass sub-modules remain at 49°C measured using a temperature gun. For TF PV modules, due to the 2D current-flow nature, their performance is improved under shading conditions. The panels evaluated for the TF case are CIS-

based panels (WRG1005) [65]. Using a thick sheet to create shading, when the individual long and rectangular cell is not completely shaded, the shaded part appears as a darker area having a low temperature at 44°C. While the un-shaded sub-cell has a slightly higher temperature at 48°C in comparison to the shaded part. The current produced by the un-shaded portion of the cell can contribute to the module current since the current has more than one direction to flow. For symmetric shading, when the cells are partially shaded, the thermal images are shown in Figure 2.7.

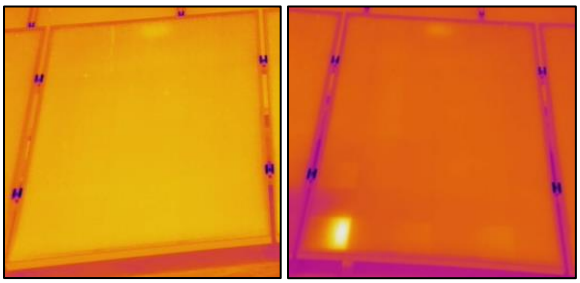

(a) (b)

Figure 2.6 Thermal images of a c-Si PV module (a) no shading with all cells contributing to the overall panel output and (b) hotspot at the partially-shaded left bottom cell.

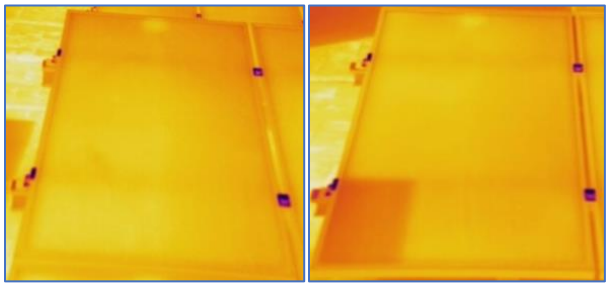

(a) (b)

Figure 2.7 Thermal images of a TF PV module under (a) no shading and (b) partial shading on the bottom part of the panel.

Figure 2.8 shows the measured temperatures of the shaded cells in both PV panels with reference to the shading percentage of the PV panel. It can be observed that in normal condition (when there is no shading) both c-Si and TF are working almost at the same temperature (ambient temperatures could be different as measurements were not simultaneously made). However, the

important fact remains that the hotspots in c-Si are significantly higher, which may affect the long-term reliability of the panel. Another reason for higher hotspots in c-Si is due to higher short-circuit currents, which increases the hotspot effect in shading [66, 67]. Typically, TF modules have higher open circuit voltages and lower short-circuit currents, which is also good for low manifestations of hotspots [65].

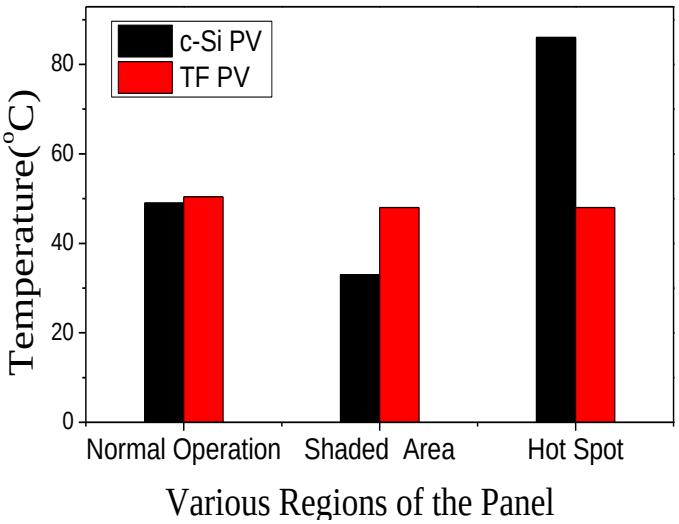

Figure 2.8 Effect of shading on the temperature of both types of PV Panels.

Further, to evaluate the power output from the two technologies a scaled down system with three series-connected panels is shown in Figure 2.9. The shade irradiance is also taken as 300 W/m^2 i.e., 30% of the standard irradiance at the Standard Test Condition (STC) [68]. The symmetric shading varies from no shading to 100 percent shading in a gradual manner. The half-module shading represents roughly 17 % of the string under partial shading. But it is important to mention that the orientations of series-connected cells and the number of bypass diodes connected across individual modules for both systems are different due to typical configurations [69]. For instance, for c-Si panel three bypass diodes, across each module of c-Si, are connected and the symmetric shading reduces the power output by bypassing each of the substrings in a gradual manner. On the other hand, only one bypass diode is connected across each TF module [65]. The power output varies proportionally due to symmetric shading and single module is

bypassed only when it is fully shaded, i.e., 100 % panel shading (33 % string under shade).

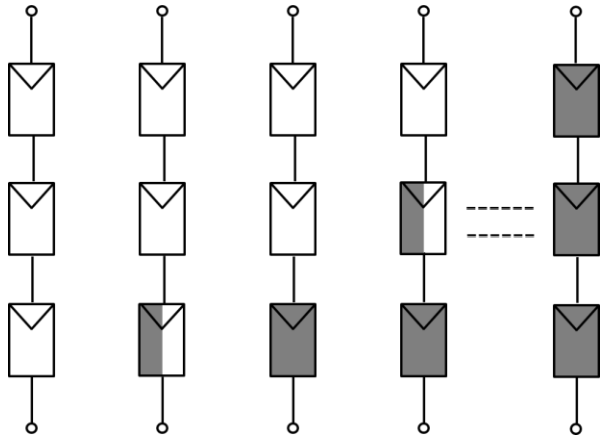

Figure 2.9 Incrementing shade from 0 to 100 % on a string of a PV system consisting of 3 series modules.

In Figure 2.10, the changes in the relative performance of the two systems under the same irradiance are shown. For each technology, the normalized power (with respect to the maximum for each technology) is shown for a fair comparison. PV panels for each technology are assumed to be under partial shading with an increasing shaded-percentage area of the string, as descried in Figure 2.9.

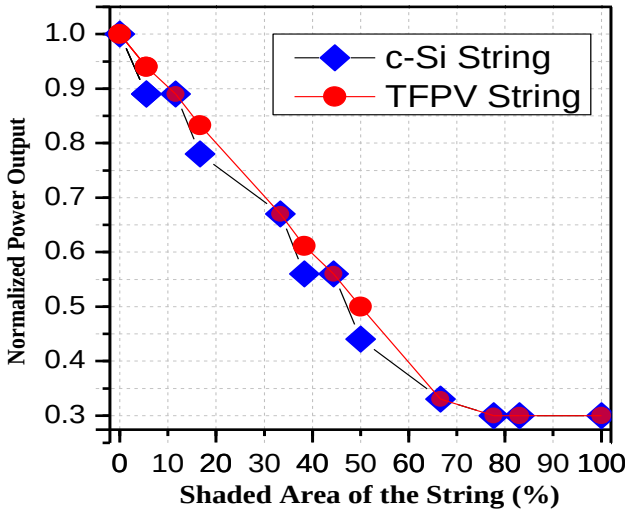

Figure 2.10 Effect of partial shading on the relative performance output of both technologies under partial shading.

The resultant variations in the relative power outputs can also be seen in Figure 2.10, where the production from the TF PV panels is higher than the c-Si panels under shading. The same trend in the power drop can be seen for both technologies at 11%, 33%, and 67% shading due to the bypass profile of the system at this level of system shading. Overall, the TF PV yields approximately 3.5% additional power output than the c-Si PV (on average) under the incrementing partial shading from 0 to 100 % (see Figure 2.9) on the entire string of both PV systems.

Chapter 3

A Novel Rooftop Solar PV Architecture for Profit Maximization

Following the identification of optimum solar PV technology for large scale rooftop installations under low irradiance and partial shade, this chapter proposes a novel rooftop solar PV architecture for profit maximization. Solar photovoltaics (PV) have seen a large influx over the past few years due to decreasing module costs making PV very competitive even in residential and commercial domestic settings [20, 70]. Two types of financial incentives are typically offered by utilities through either Feed-in tariffs (FiTs) or Net-metering. FiTs are government incentivized policies in which long-term power purchase agreements (PPAs) are signed with the utility for providing surplus electricity to the grid [71]. During last decade, FiT schemes have been frequently revised with addition of tax incentives, green certificates and subsidies to encourage large scale solar PV deployment [72]. The provision of net-metering with the national grid also encourages the installation of solar PV, giving prosumers an opportunity to sell the electricity back to the grid at the time of peak generation [73].

Net-metering tariffs vary in different regions or countries, however in developed countries, the compensation for distributed PV generation is typically about one third to one half of the retail electricity price [74]. This is where storage-based PV systems are becoming popular where surplus solar PV may be stored for peak time usage [75]. Various technologies are available in the market for energy storage including lead-acid, lithium-ion-iron-phosphate and lithium ion (Li-ion) [76]. Even though Lead-acid is most mature technology at prices of around US$150-200/kWh [77], their utility is low due to poor round trip efficiency and a low depth of discharge requirement (around 50%) [78, 79]. Li-ion based storage, on the other hand, has gained significant attention due to their higher energy density, higher depth of discharge, longer life and better high

temperature performance [80]. The prices of Li-ion batteries have significantly declined over last decade, providing the a more valuable alternative with recent costs as low as US$156/kWh in the market [81] with forecasts that Li-ion battery pack prices will fall to as little as 74 US$74/kWh in 2030 [82].

3.1 State-of-the Art Rooftop Solar PV Topologies

Various studies on rooftop solar PV with storage have been presented, however, the focus for vast majority of these papers is local optimization of a building considering grid integration or optimum sizing of system. For instance, Numbi et al. [83] established an optimal energy model of a 3 kW_p residential-grid interactive solar PV system under FiT. Further, Shaughnessy et al. [84] offered a solar plus model approach for wide-scale residential PV deployment paired with battery storage and time-of-use (TOU) tariff scheme. Several other contributions discussed the optimum storage-based solutions for individual buildings in interaction with grid for time-varying tariffs. For example, Jin et al. [85] studied the optimal operation of energy storage for an individual prosumer with intermittent renewable generation under time-varying electricity rates. In [86], Ke et al. proposed an optimal sizing of energy storage system for a university building installed with two different PV capacities (176 kW_p and 676 kW_p), considering two-phase and three-phase electricity pricing. Ratnam et al. [87] developed a linear program (LP) and quadratic program (QP) based algorithm to optimally schedule the battery storage coupled with solar PV and net-metering for a residential consumer. Anilkumar et al. [88] proposed a residential cost minimization model for grid-connected customers integrated with solar PV and energy storage system. Hartmann et al. developed an optimization algorithm to examine the profitability of installing energy storage units for an industrial and commercial consumer. Azim et al. [89] studied the optimal participation of prosumers in a peer-to-peer (P2P) trading network considering power losses in grid-connected mode.

However, the proposed assessment of multiple buildings with internal exchange as well as grid interaction is not evaluated in the literature before as a framework is developed for financial gain maximization of all buildings. Therefore, in this chapter taking the power sector of New Zealand as an illustration, a framework for profit maximization is proposed. The proposed model is

generic and homogeneously applicable to countries such as United States, Australia, Canada, Japan, Belgium, Netherlands, Italy, Turkey, Pakistan, India and other countries which heavily rely on fossil fuels for their electricity generation and provision of solar net-metering [90].

3.2 Overview and Mathematical Modeling of the System

Various commodities involved in the power trading (sharing) model are shown in Figure 3.1 with details given as follows:

- **Grid:** AC power source with time-of-use (TOU) pricing scheme with minimum disruption.
- **Primary Building:** Solar PV is installed locally and there is a provision for Energy Storage System (ESS).
- **Secondary Building(s):** Conventional nearby buildings without PV or storage. These secondary buildings agree to procure power from the primary building. In this chapter, two secondary buildings (B_2 and B_3) are considered having power purchase agreements with primary building (B_1).

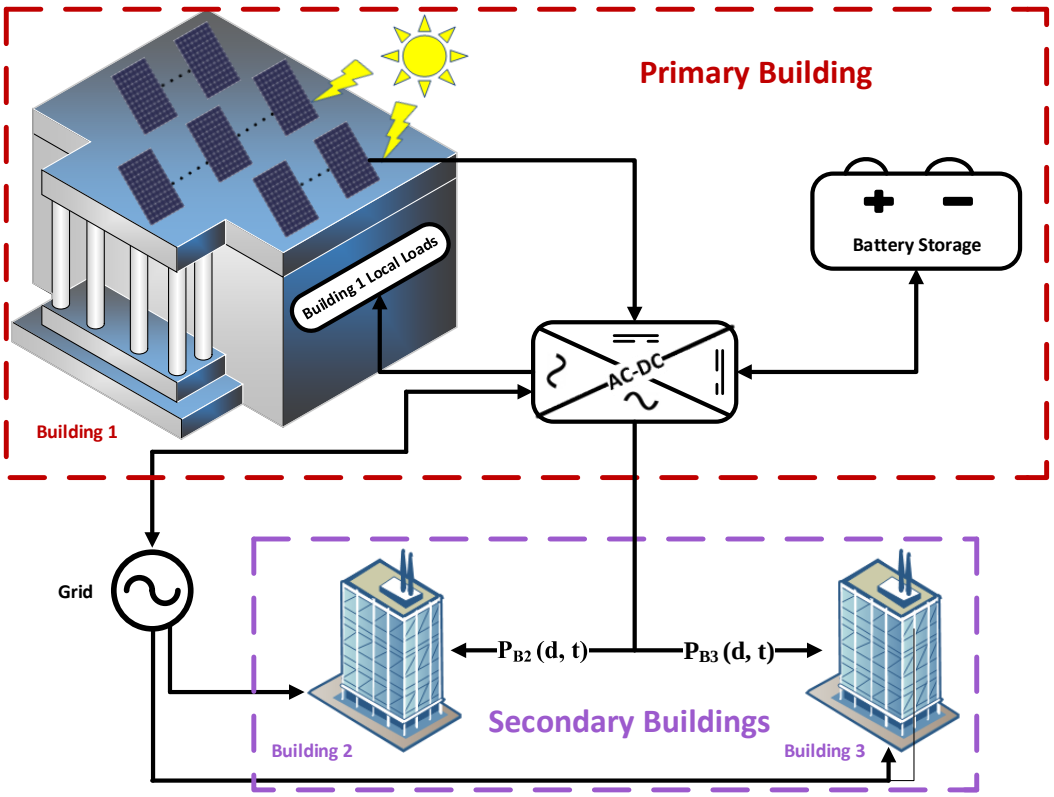

Figure 3.1 Architecture of proposed model, primary building (B_1) with rooftop PV-battery configuration with some contracted load with secondary buildings (B_2 and B_3).

The main technical aspects of this chapter as summarized follows:

- An optimization model is developed to assess the profit of the primary building (installed with rooftop solar PV and energy storage system) with power transactive interactions with secondary building(s).
- Each secondary building can have different contract prices with the primary building.
- Primary building can feed its own loads in addition to serving secondary buildings hence some portion of power from PV and ESS can be consumed by the primary building itself.
- Cost savings of secondary buildings are analyzed in terms of decrease in the electricity bills from the grid and payments to the primary building.
- Real-time (RT) load data from three commercial buildings in Auckland along with TOU rates from the utility are used to evaluate the profit of each building.

- Solar PV generation is incorporated for the primary building and is sized according to the space availability.

A mixed integer linear program (MILP) is developed in ILOG optimization studio to obtain the optimized dispatch and cost savings of each building owner. The power flows to secondary buildings and the grid by the primary building (solar PV and battery) at any interval is shown in Figure 3.1. It also shows that primary building can also sell the generated electricity back to the grid at somewhat reduced rates as compared to TOU tariff set by the grid. Figure 3.2 shows the state variables associated with the power flows, the optimized values of these state variables decide the maximum profit attainable for primary and secondary buildings, respectively.

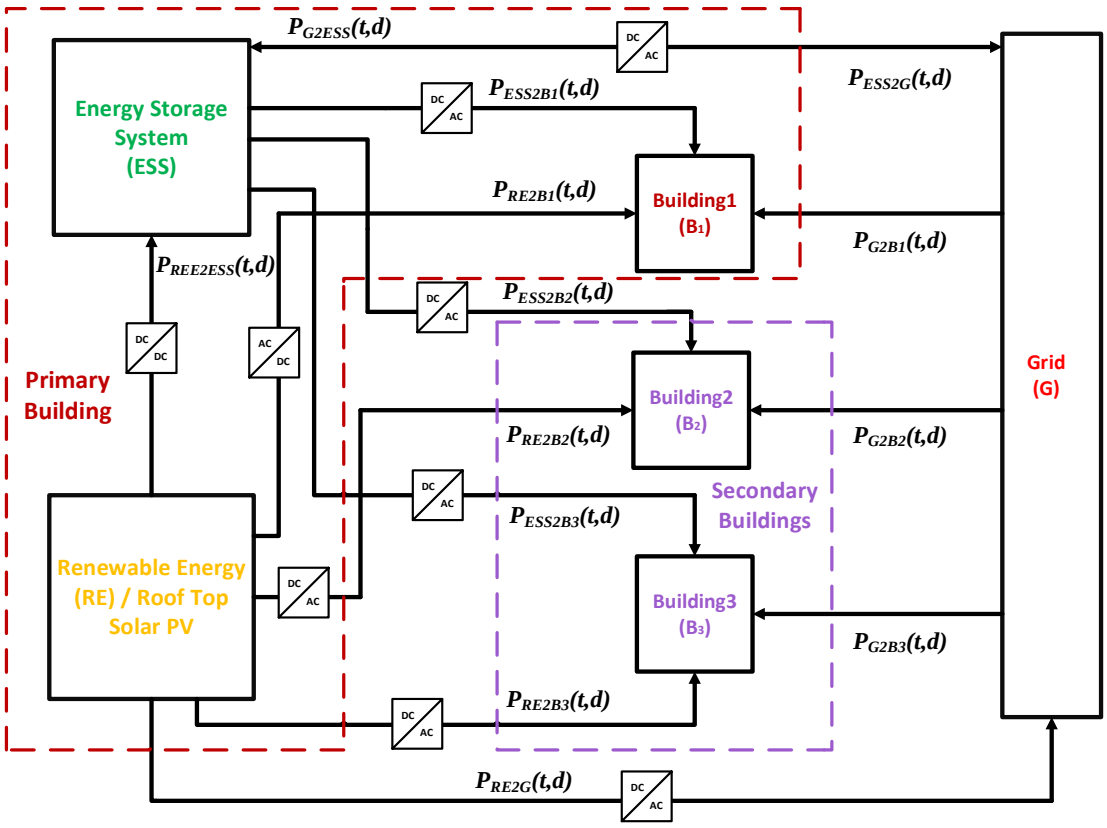

Figure 3.2 State variables associated with power flows. Secondary buildings (B_2 and B_3) only consume power and the primary building (B_1) supplies to local loads as well as secondary buildings along with bidirectional grid trade.

3.2.1 Objective Function and System Constraints

This profit model solves multi-objective optimization problem, ensuring the maximum profitability both for primary and secondary buildings. All associated/secondary buildings are connected to the primary building and have a specific load demand which can be met by the primary building as well as the grid. In the interest of secondary buildings engaged within procuring electricity from the primary building, it is guaranteed that a minimum contracted daily load demand of these buildings will always be met by the primary building with PV and storage or even import from the grid. Depending on the costs and tariffs, the grid may be utilized in the case where solar resources are not enough or profitable at the time. Therefore, in this case the primary building must buy the minimum contracted electricity from the grid and sell to the secondary building(s) at the specified rates. These rates can be decided upfront between buildings (primary and secondary), and these rates must be lower than the TOU rates available at the grid i.e., $R_{pur}\ (t,d) > R_{cont_3}\ (t,d)$ and $R_{pur}\ (t,d) > R_{cont_2}\ (t,d)$. The total revenue obtained each year by power trading between all the commodities can be written as annual cost functions, given by (3.1) subject to constraints for the optimization problem stated as (3.2)-(3.10).

$$\frac{Revenue^{Max}}{year} = Max \left\{ \begin{array}{c} \sum_{d=1}^{365}\sum_{t=1}^{24} \left(P_{RE2G}(t,d) * R_{sell}(t,d)\right) \\ + \\ \sum_{d=1}^{365}\sum_{t=1}^{24} \left(P_{ESS2G}(t,d)/\eta_{disch} * R_{sell}(t,d)\right) \\ + \\ \sum_{d=1}^{365}\sum_{t=1}^{24} \left(P_{RE2B_2}(t,d) * R_{cont_2}(t,d)\right) \\ + \\ \sum_{d=1}^{365}\sum_{t=1}^{24} \left(P_{ESS2B_2}(t,d)/\eta_{disch} * R_{cont_2}(t,d)\right) \\ + \\ \sum_{d=1}^{365}\sum_{t=1}^{24} \left(P_{RE2B_3}(t,d) * R_{cont_3}(t,d)\right) \\ + \\ \sum_{d=1}^{365}\sum_{t=1}^{24} \left(P_{ESS2B_3}(t,d)/\eta_{disch} * R_{cont_3}(t,d)\right) \\ + \\ \sum_{d=1}^{365}\sum_{t=1}^{24} P_{RE2B_1}(t,d) * \left(R_{pur}(t,d) - R_{sell}(t,d)\right) \\ + \\ \sum_{d=1}^{365}\sum_{t=1}^{24} P_{ESS2B_1}(t,d)/\eta_{disch} * \left(R_{pur}(t,d) - R_{sell}(t,d)\right) \\ - \\ \sum_{d=1}^{365}\sum_{t=1}^{24} \left(P_{G2ESS}(t,d) * \eta_{char}\right) * R_{pur}(t,d)\Big) \\ - \\ \sum_{d=1}^{365}\sum_{t=1}^{24} \left(P_{G2B_1}(t,d) * \left(R_{pur}(t,d)\right)\right) \\ - \\ \sum_{d=1}^{365}\sum_{t=1}^{24} \left(P_{G2B_2}(t,d) * \left(R_{pur}(t,d) - R_{cont_2}(t,d)\right)\right) \\ - \\ \sum_{d=1}^{365}\sum_{t=1}^{24} \left(P_{G2B_3}(t,d) * \left(R_{pur}(t,d) - R_{cont_3}(t,d)\right)\right) \end{array} \right\} * \Delta t \tag{3.1}$$

$$X(t,d) + Y(t,d) \leq 1 \qquad X(t,d), Y(t,d) \in \{0,1\}, \ \forall\ (t,d) \tag{3.2}$$

$$P_{G2ESS}(t,d) \ + P_{RE2ESS}(t,d) \leq \ SOP_{max} * X(t) \tag{3.3}$$

$$SOP_{min} \leq SOP\,(t,d) \leq SOP_{max} \tag{3.4}$$

$$P_{ESS2B_1}(t,d) + P_{ESS2B_2}(t,d) + P_{ESS2B_3}(t,d) + P_{ESS2G}(t,d) \leq (SOP_{max} - SOP_{min}) * Y(t,d) \tag{3.5}$$

$$\begin{aligned} SOP(t+1,d) = {} & SOP(t,d) + ((\eta_{char} * P_{G2ESS}(t,d) + ((\eta_{char} * P_{RE2ESS}(t,d))) * X(t,d) \\ & - \left(P_{ESS2G}(t,d)/\eta_{disch} + P_{ESS2B_1}(t,d)/\eta_{disch} + P_{ESS2B_2}(t,d)/\eta_{disch}\right. \\ & \left. + P_{ESS2B_3}(t,d)/\eta_{disch}\right) * Y(t,d) \end{aligned} \tag{3.6}$$

$$P_{RE2B_1}(t,d) + P_{RE2B_2}(t,d) + P_{RE2B_3}(t,d) + P_{RE2G}(t,d) + P_{RE2ESS}(t,d) = S(t,d) \tag{3.7}$$

$$P_{G2B_1}(t,d) + P_{ESS2B_1}(t,d)/\eta_{disch} + P_{RE2B_1}(t,d) \leq B_1(t,d) \tag{3.8}$$

$$P_{B_2}(t,d) \leq P_{G2B_2}(t,d) + P_{ESS2B_2}(t,d)/\eta_{disch} + P_{RE2B_2}(t,d) \leq B_2(t,d) \tag{3.9}$$

$$P_{B_3}(t,d) \leq P_{G2B3}(t,d) + P_{ESS2B3}(t,d)/\eta_{disch} + P_{RE2B3}(t,d) \leq B_3(t,d) \tag{3.10}$$

The objective function in (3.1) and related constrains maximize the revenue for primary building. The two binary variables $X(t,d)$ and $Y(t,d)$ in (3.2) are used for charging and discharging of the battery storage, respectively. It ensures that battery would not be charged and discharged simultaneously during any time interval. The charging of battery from solar PV and grid must be limited by its maximum achievable power given by (3.3). SOP_{min} and SOP_{max} are the minimum and maximum power available at each time step by the storage, respectively as stated by (3.4). The values used for SOP_{min} and SOP_{max} are 10% and 100% of the battery capacity, respectively. The maximum extractable power from the battery is shown as (3.5). The time step used in this chapter is always assumed to be one hour, and therefore, the terms energy and power are used interchangeably throughout the thesis. The amount of power available from the storage at the next time step is expressed as (3.6). The power balance i.e., the production from solar PV equals sums of the power flows towards B_1, B_2, B_3, grid and energy storage system (ESS), is specified as (3.7). The power supplied to B_1 by the grid, battery or solar PV should be less than or equal to its load demand given as (3.8). (3.9) and (3.10) signify that load demand of B_2 and B_3 will be supplied

by primary building in accordance with the contract ceiling amounts of power. In the above formulation, all the decision variables have non-negativity constraints. The objective function is developed to ensure that all contracted buildings will have lower electricity costs compared to grid only option (i.e., business as usual where all buildings have grid as the only source of power). Since, there are multiple agents, all available rooftop area of B_1 is utilized for solar due to its low levelized cost of electricity (LCOE) [91, 92].

Figure 3.3 shows the flow chart used for optimized solution of the profit model. The model is formulated as MILP in ILOG optimization studio with CPLEX solver. The input parameters into the profit model are assumed to be known upfront i.e., annual load demand of B_1, B_2 and B_3, solar PV production and tariff information are available. Therefore, this chapter primarily presents the deterministic model and can serve as a benchmark to confirm the optimal solutions from a stochastic model dealing with uncertainties.

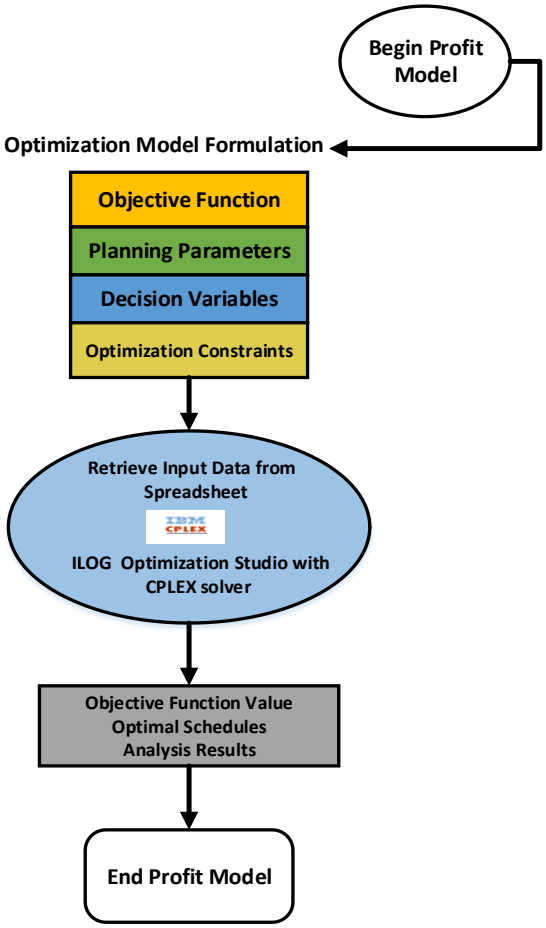

Figure 3.3 Flow chart for the optimized power dispatch from the profit model.

3.3 Results of Optimized Power Dispatch for Multiple Buildings

Three cases are performed with the proposed simulation model. A reference case is made in which no solar PV and storage is assumed at any of the buildings. Various system component sizes and prices are summarized in Table 3.1.

Table 3.1 Size of Solar PV and ESS along with the installation costs.

System Component Size and Cost	Rooftop Solar PV	Energy Storage System (ESS)
System size	400 kW_p	400 kWh
System technology	Monocrystalline Silicon	Li-Ion Battery
Price (NZ$) per Watt/kWh	0.411 [93]	260 [82]
Estimated life of the component (years)	25	8
Total price of the system (NZ$)	164,400	104,000

The peak and off-peak pricing schemes from grid with equal contract prices for B_2 and B_3 for a particular day are shown in Figure 3.4 [41]. It shows the per unit purchasing price (NZ$/kWh) from the grid for a particular day from a utility (Electra) in New Zealand, it is assumed that same TOU pricing scheme is followed annually. The rate (NZ$/kWh) at which electricity is exported/sold back to the grid (net-metering) is lower than the TOU rates provided by the grid. Based on the purchasing and selling price to the grid, a contracted tariff is decided between the primary and secondary building(s). This tariff is set in such a way that it allows the primary building to sell the electricity to the secondary building at the rates higher than the net-metering (utility price for selling to the grid). In addition, it facilitates the secondary building(s) to purchase electricity from the primary building at rates lower than the TOU.

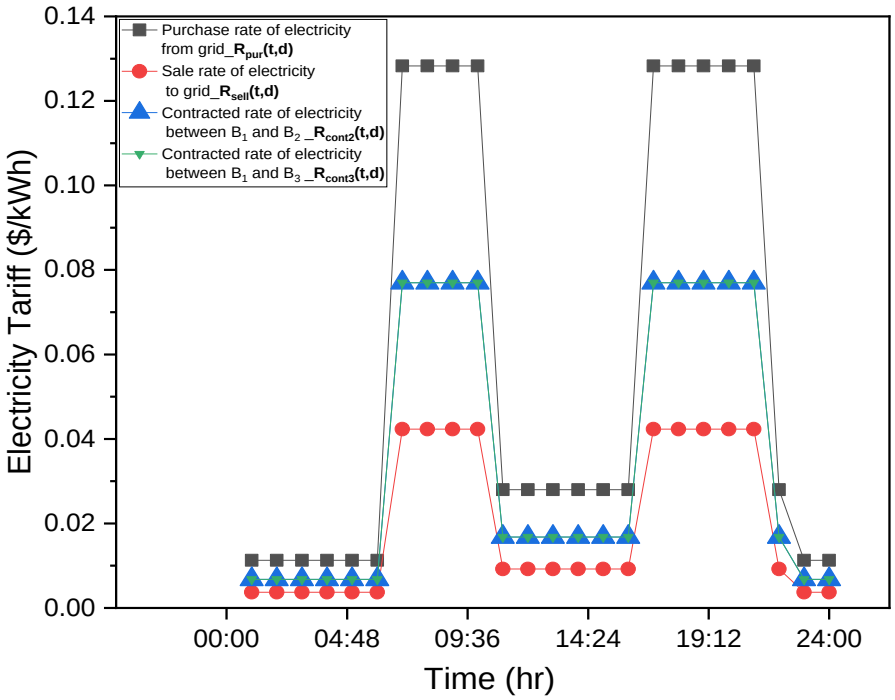

Figure 3.4 Time-of-use pricing during peak and off-peak hours with equal contract rates for a typical weekday.

The daily average kW load demand for the three commercial buildings in Auckland, New Zealand is shown in the Figure 3.5. The hourly actual load demands of three buildings for a complete year is shown in Appendix B1. Various load patterns are observed for different types of buildings, and usage diversity is key in optimizing the power flow from primary building (B_1) to secondary

buildings (B_2 and B_3). The values used for minimum contracted load with B_2 and B_3 ($P_{B_2}(t,d)$ and $P_{B_3}(t,d)$) are 10 kW and 20 kW, respectively (scenario 1).

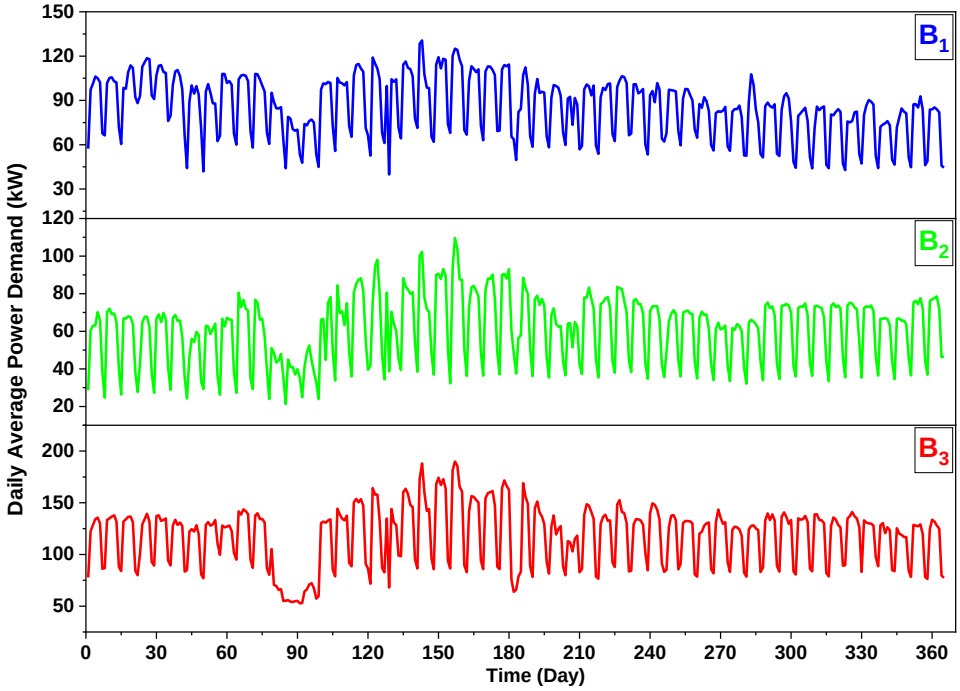

Figure 3.5 Daily average electricity load demand (kW) of building 1, 2 and 3, respectively for the whole year.

Two cases (case 1 and case 2) along with the reference case 0 (business as usual – no solar or storage) are simulated to evaluate the objective function of the optimization framework as discussed below. Further, the contract rates between primary and secondary buildings are taken as percentage of the actual TOU tariff to mimic real life scenario to gauge actual savings for multiple buildings. Therefore, three sub-cases (a, b, and c) for each case, respectively are studied to examine the effect of varying contracted rates between primary and secondary buildings.

Reference Case (Case 0): For the reference case, there is no rooftop solar PV or the ESS at any buildings (primary or secondary). The power procurement is entirely through the grid according to TOU pricing plan as established by the utility. Our analysis shows that the cost incurred annually by B_1, B_2 and B_3, for buying electricity from the grid at TOU rates is \$48,710, \$35,479, and \$69,434, respectively. These are the annual payments to the utility by B_1, B_2 and B_3, calculated as (3.11)-(3.13), respectively.

$$P_{B_1}^0 = \sum_{d=1}^{365} \sum_{t=1}^{24} \left(B_1(t,d) * R_{pur}(t,d) * \Delta t \right) \tag{3.11}$$

$$P_{B_2}^0 = \sum_{d=1}^{365} \sum_{t=1}^{24} \left(B_2(t,d) * R_{pur}(t,d) * \Delta t \right) \tag{3.12}$$

$$P_{B_3}^0 = \sum_{d=1}^{365} \sum_{t=1}^{24} \left(B_3(t,d) * R_{pur}(t,d) * \Delta t \right) \tag{3.13}$$

Case 1: In this case, the primary building has a rooftop solar PV system of 400 kW_p without storage provision. The solar power output from the PV system for whole year can be consumed by primary building, trade with the secondary building(s) at the decided agreement pricing scheme or sold back to the grid.

Case 2: In this case, the primary building has rooftop solar PV alongside ESS. The power from solar PV and storage can be used to meet the load demand of primary building partially or fully, sold to the grid or secondary buildings based on contracted rates to maximize the profit.

3.3.1 Optimized Power Flow without Storage (Case 1)

The power generated from solar PV can either be exported back to the grid or traded with the secondary building(s) as there is no ESS. Also, B_1 can supply its own load depending upon the dynamics of PV generation and contracted loads. As per policy in New Zealand, electricity can be sold to the grid at one-third of the utility price. In this case, the profit model is analyzed at varying contracted prices between secondary buildings ($R_{cont_2}(t,d)$ and $R_{cont_3}(t,d)$) with B_1. The effect of different pricing scheme is discussed in detail in the sub-cases of the case 1. The cost of rooftop solar PV modules at primary building is rationalized over a 25-year span.

3.3.1.1 Case 1(a)

The power generated by the primary building (B_1) is sold to both the secondary buildings (B_2 and B_3) at 60% of the TOU pricing set by the grid. The contracted rates are equivalent for this case ($R_{cont_2}(t,d) = R_{cont_3}(t,d)$) and the corresponding results of optimized dispatch for one day of summer and winter are shown in Figure 3.6 and Figure 3.7. Figure 3.6 shows that the buildings load (primary and secondary) fed through solar PV at B_1. It also shows that solar feeds some fraction or full load of B_1 in addition to partial load support to B_2 and B_3 depending upon the PV generation in the day-time.

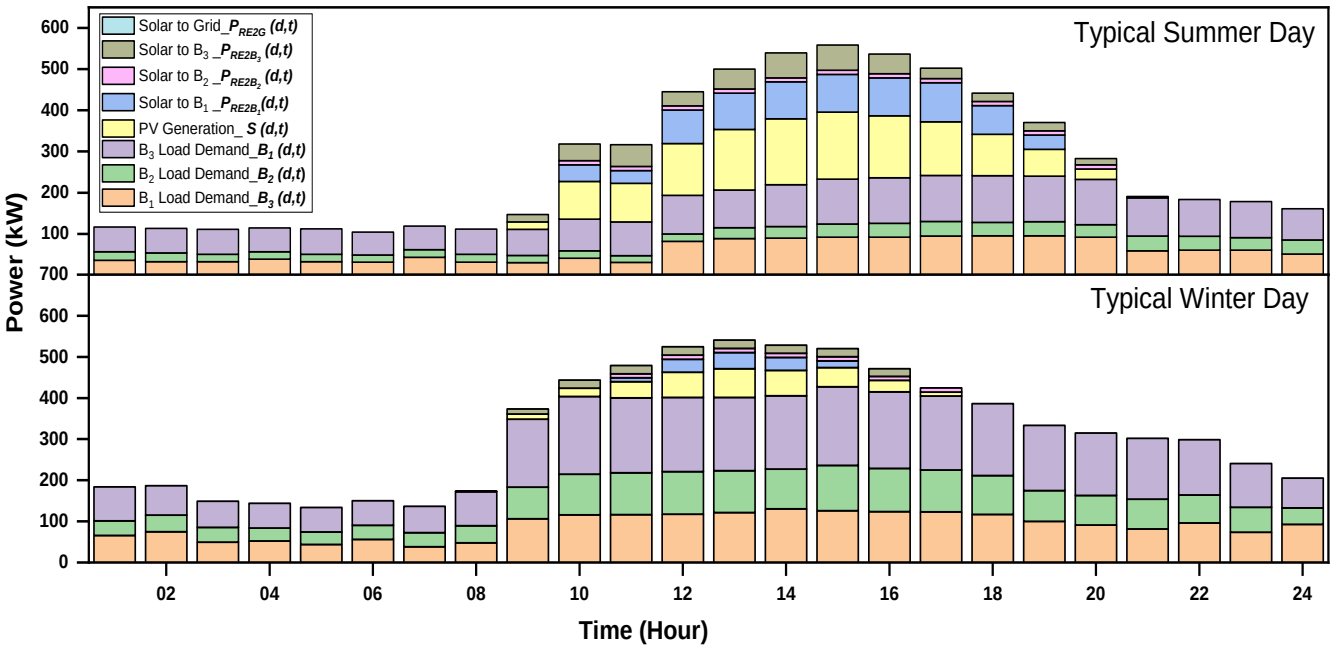

Figure 3.6 Real-time (RT) load demand of B_1, B_2 and B_3 along with hourly power dispatch of solar PV for a typical summer and winter day, respectively.

The hourly power flows among grid, primary building (B_1) and secondary buildings (B_2 and B_3) is shown in Figure 3.7. It can be observed that when onsite PV generation is not available, the primary building B_1 procures electricity from the grid under TOU pricing scheme and sells at reduced rates to meet the minimum contracted load demand of the secondary buildings B_2 and B_3, respectively.

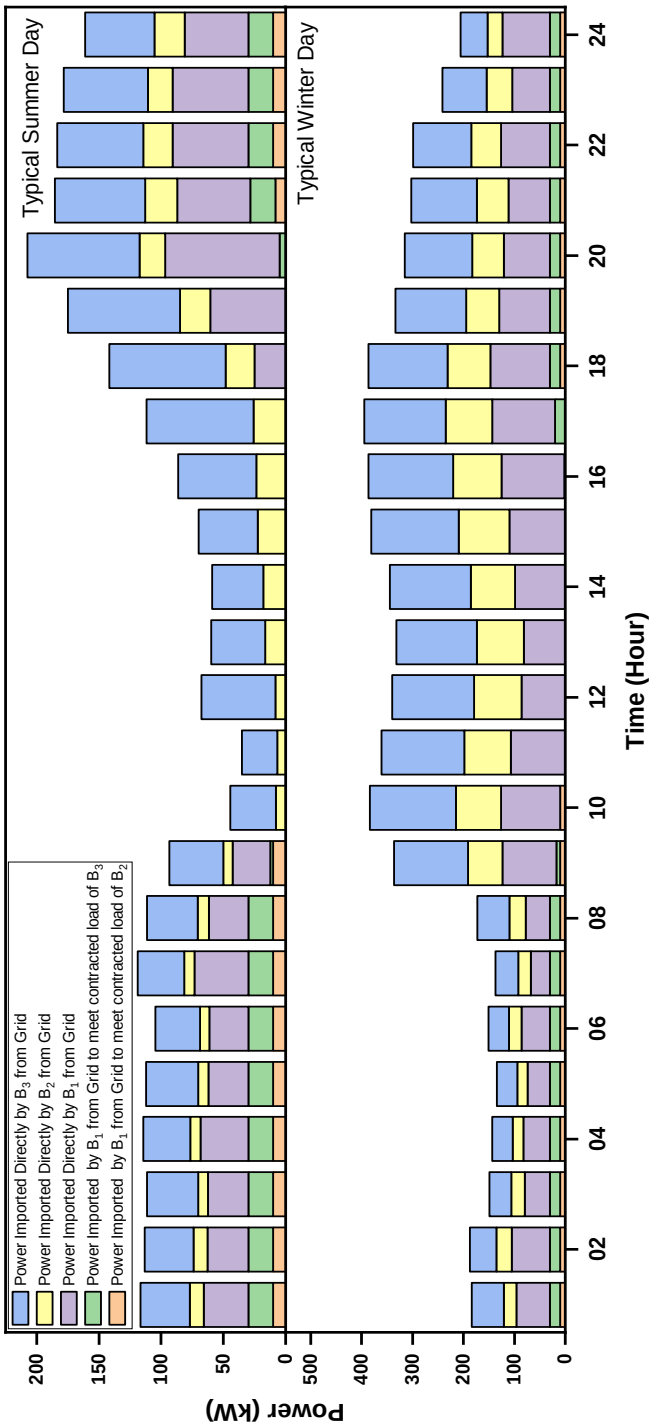

Figure 3.7 Hourly electricity trade between grid and B_1, B_2 and B_3 for a typical summer and winter day, respectively.

3.3.1.2 Case 1(b)

For this sub-case it is assumed that B_2 has higher contracted price in comparison to B_3 with the primary building ($R_{cont_2}(t,d) > R_{cont_3}(t,d)$) as shown in Figure 3.8. The contracted price for B_2 and B_3 are set to be 80% and 60%, respectively, of TOU rates of electricity from the grid. Figure 3.8 shows the solar PV generation and buildings load fed through grid and solar for a typical day of summer. It can be observed that B_3 overall has higher power procurement from B_1 (primary building with solar PV) due to higher amount of minimum contracted load. Beyond minimum contracted load, B_1 trades more frequently with B_2 due to higher contracted rates with B_2 (i.e., 80 % of the TOU grid price).

3.3.1.3 Case 1(c)

In this sub-case, the contracted rates of B_3 are assumed to be higher than B_2 ($R_{cont_3}(t,d) > R_{cont_2}(t,d)$). The sale rate from B_1 to B_2 and B_3 is configured at 60% and 80%, respectively of the grid TOU pricing. It is seen that the power sold to B_3 increases in comparison to case 1(b) due to the high contracted prices with B_3 (80 %). B_1 trades more often with B_3 beyond minimum contracted load due to higher tariff.

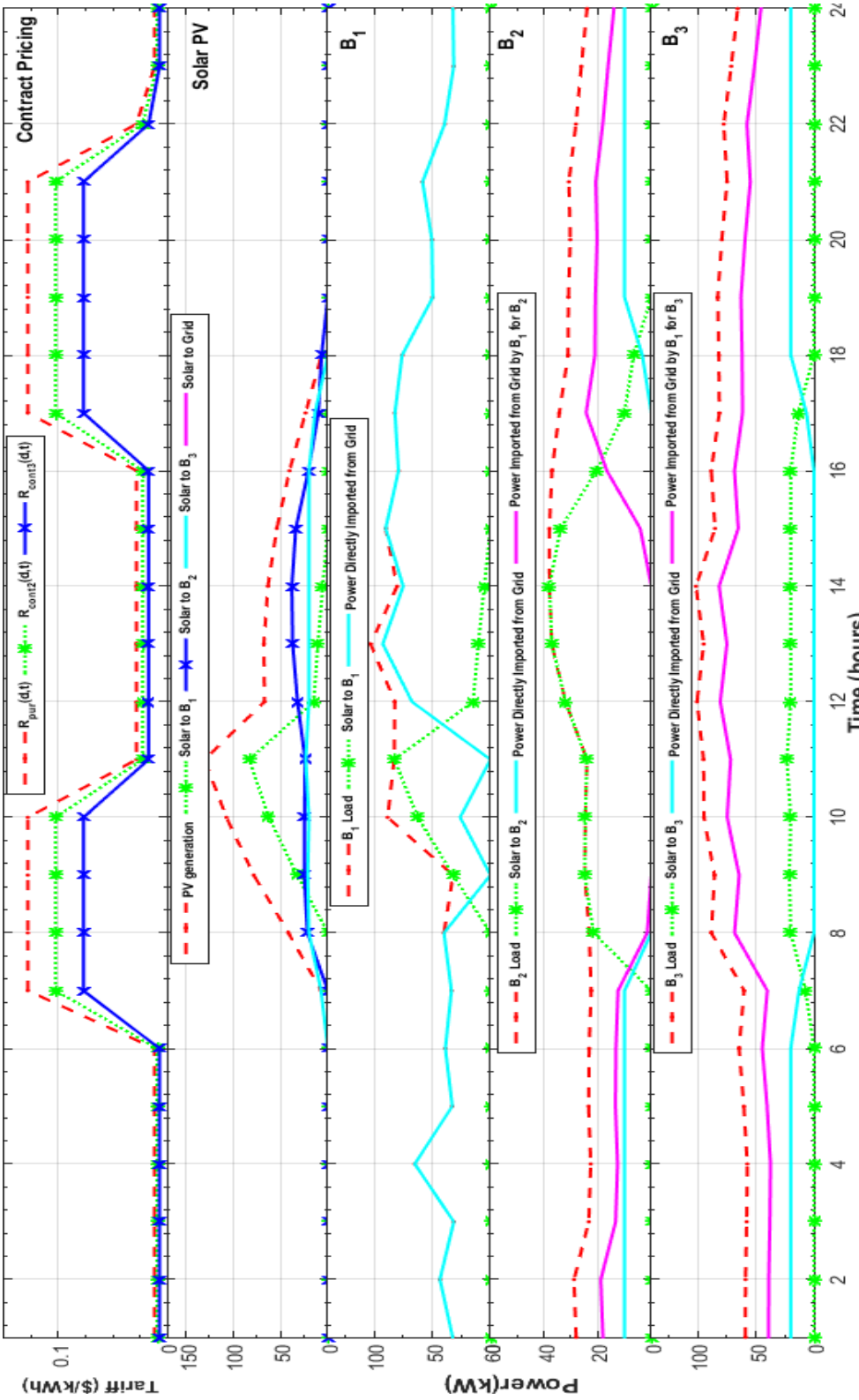

Figure 3.8 Hourly solar PV generation and consumption for B_1, B_2 and B_3, respectively at R_{cont2} (t,d)> R_{cont3} (t,d) for a typical summer day.

3.3.2 Optimized Power Flow with Solar and Storage (Case 2)

In this case the primary building has ESS available along with rooftop solar PV. A life span of 10 years is taken for Li-ion and the size and cost of ESS are already specified in Table 3.1. Additionally, the effect of varying contracted prices with B_1 ($R_{cont_2}(t,d)$ and $R_{cont_3}(t,d)$) is studied in detail in the sub-cases of this case.

3.3.2.1 Case 2(a)

In this sub-case, $R_{cont_2}(t,d) = R_{cont_3}(t,d)$ i.e., both the secondary buildings (B_2 and B_3) agree to buy the power generated by primary building (B_1) at 60% of the TOU pricing set by the grid. The corresponding results of optimized power dispatch for one day of summer and winter are shown in Figure 3.9 and Figure 3.10. Figure 3.9 shows the power generated by solar PV, building load demands, building load fed through solar PV and power flows from solar to grid for a typical day of winter and summer. The power flows from grid to buildings are shown in Figure 3.10. It can be observed that in intervals where PV generation is unavailable and storage SOP is low, the primary building B_1 procures electricity from the grid and sells at reduced rates to meet the minimum contracted load demand of the secondary buildings, B_2 and B_3, respectively. Further, Figure 3.10 shows that for summer day with peak solar generation during 9:00 AM-12:00 Noon, B_1 completely fulfils the load demand of primary as well as secondary building via solar PV or battery. Therefore, no power is imported either directly or through B_1 to supply the load of B_2 and B_3.

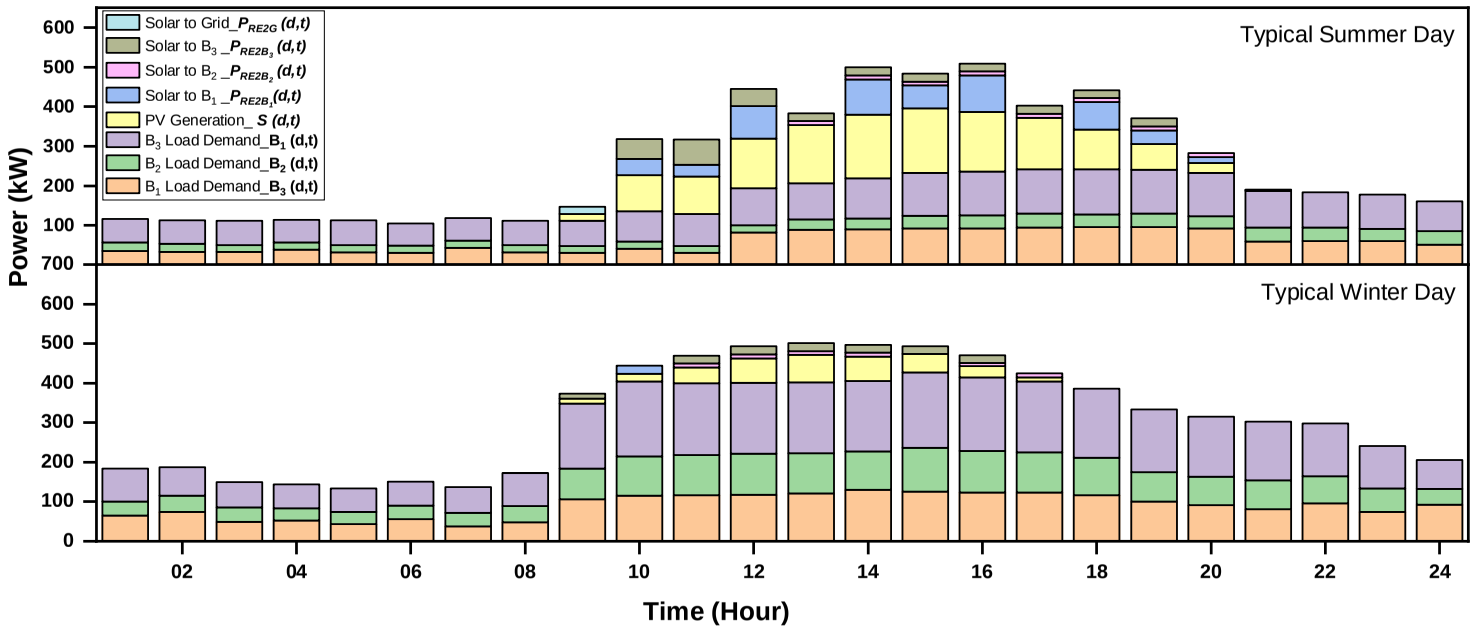

Figure 3.9 Real-time (RT) load demand of B_1, B_2 and B_3 along with hourly power dispatch of solar PV for a typical summer and winter day.

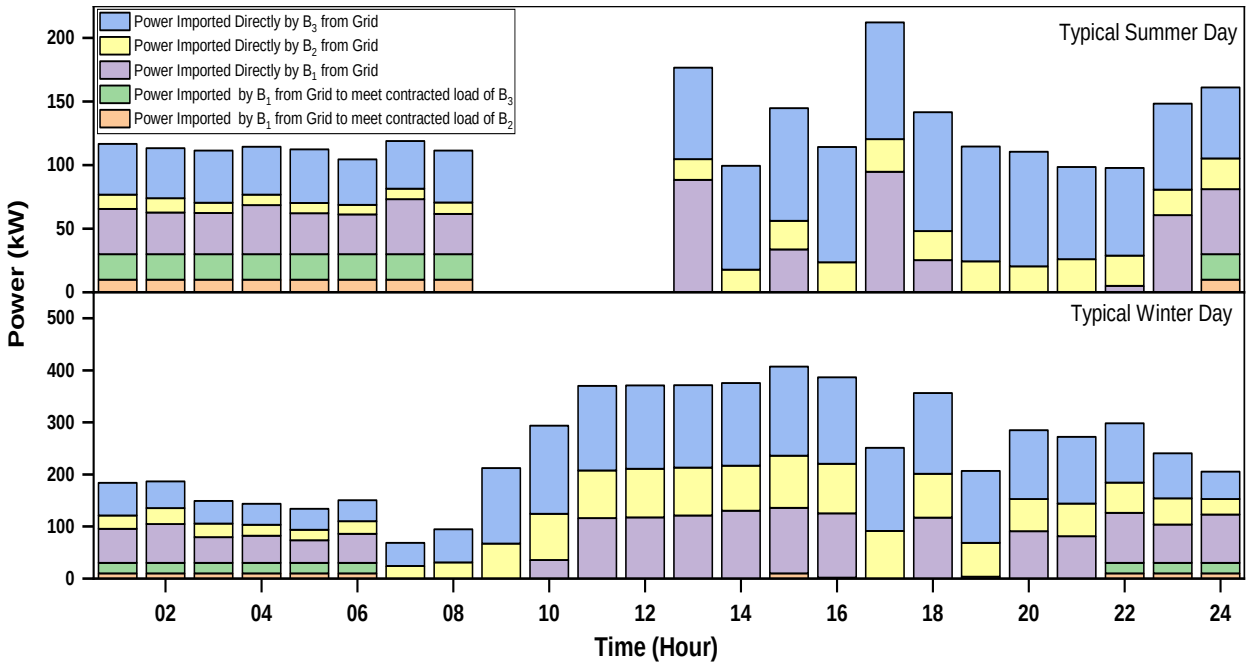

Figure 3.10 Hourly power exchange between grid and B_1, B_2 and B_3 for a typical summer and winter day.

The battery power states together with charging and discharging of the battery is shown in Figure 3.11. Results show that during summer days when on-site PV generation is higher during day-time, lower amounts of units are bought from the grid to meet the load demand of all buildings. With no storage, the incentives associated with peak and off-peak pricing were not utilized, since the PV generation was exported to the grid or sold to buildings as per availability of the solar resource. However, with the additional battery, it charges during off-peak hours either from solar or grid when the grid rates are relatively low and sells secondary buildings at peak hours to maximize the profit of both primary and secondary buildings.

Moreover, B_2 and B_3 also get the electricity at fairly reduced rates compared to the TOU rates. Figure 3.11 also shows that in a typical summer day, storage is mostly charged through solar PV during daylight hours due to availability of the resource. However, in a winter day, storage gets largely charged through the grid during off-peak hours due to low solar PV. For both seasons, storage contributes more during peak hours due to high TOU rates as established by the utility.

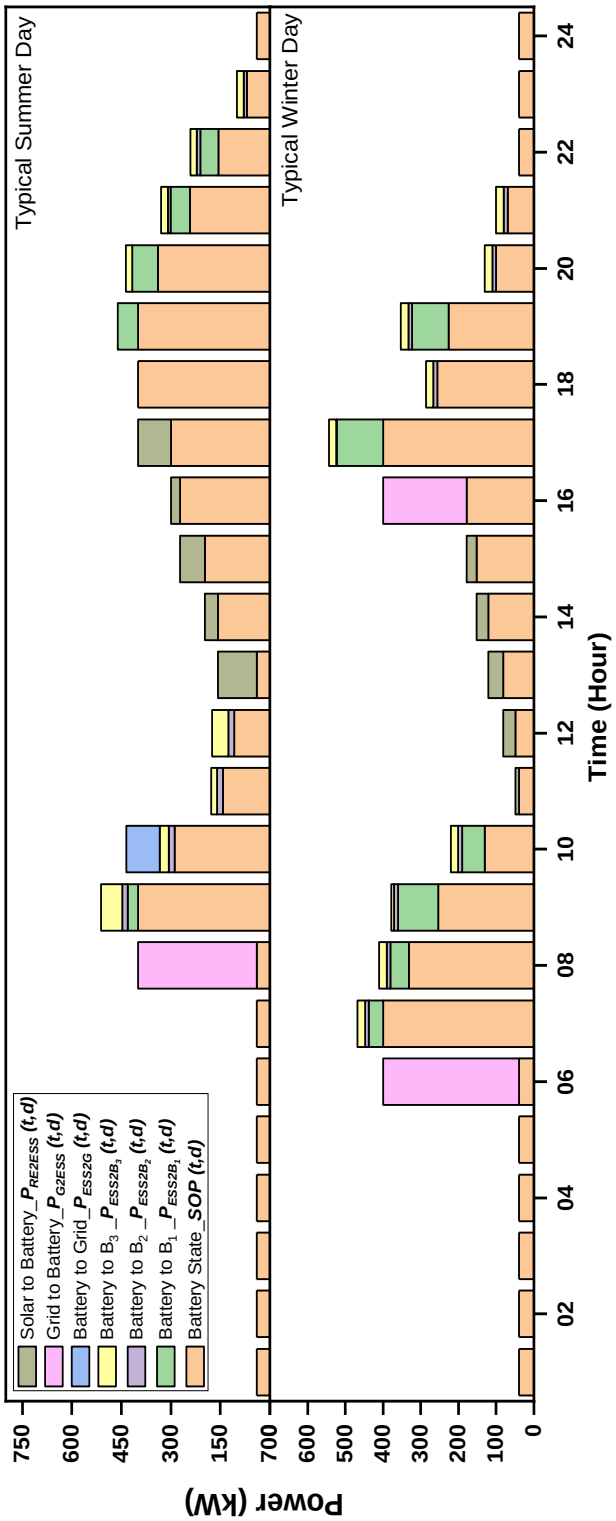

Figure 3.11 Hourly electricity trade among B_1, B_2, B_3, battery and grid for a typical summer and winter day.

3.3.2.2 Case 2(b)

In this sub-case where the contracted price of B_2 is set to be higher than B_3 i.e., $R_{cont_2}(t,d) > R_{cont_3}(t,d)$. The sale rates for B_2 and B_3 are taken as 80% and 60%, respectively of the grid price ($R_{pur}(t,d)$). Figure 3.12 shows the power transactions in primary and secondary buildings with loads fed through the grid, solar PV, and storage for a typical summer day. The power supplied to B_2 is increased through the involvement of ESS, due to high contract tariffs of B_1 with B_2 (i.e., 80 % of the TOU grid price). Further, the exports from B_1 to B_3 are largely confined to minimum contracted load due to low contract tariffs set with B_3 (at 60 %).

3.3.2.3 Case 2(c)

In this sub-case it is assumed that B_3 has higher contracted price in comparison to B_2 ($R_{cont_3}(t,d) > R_{cont_2}(t,d)$) with the primary building (B_1). The contracted price for B_2 and B_3, respectively are assumed to be 60% and 80% of the TOU rates as characterized by the utility grid. It is observed that B_3 procures higher quantity of electricity as compared to case 2(b) owing to the higher contract prices (80 %) with B_1. While the trade from B_1 with B_2 is limited mainly to minimum contracted load due to low contract rates.

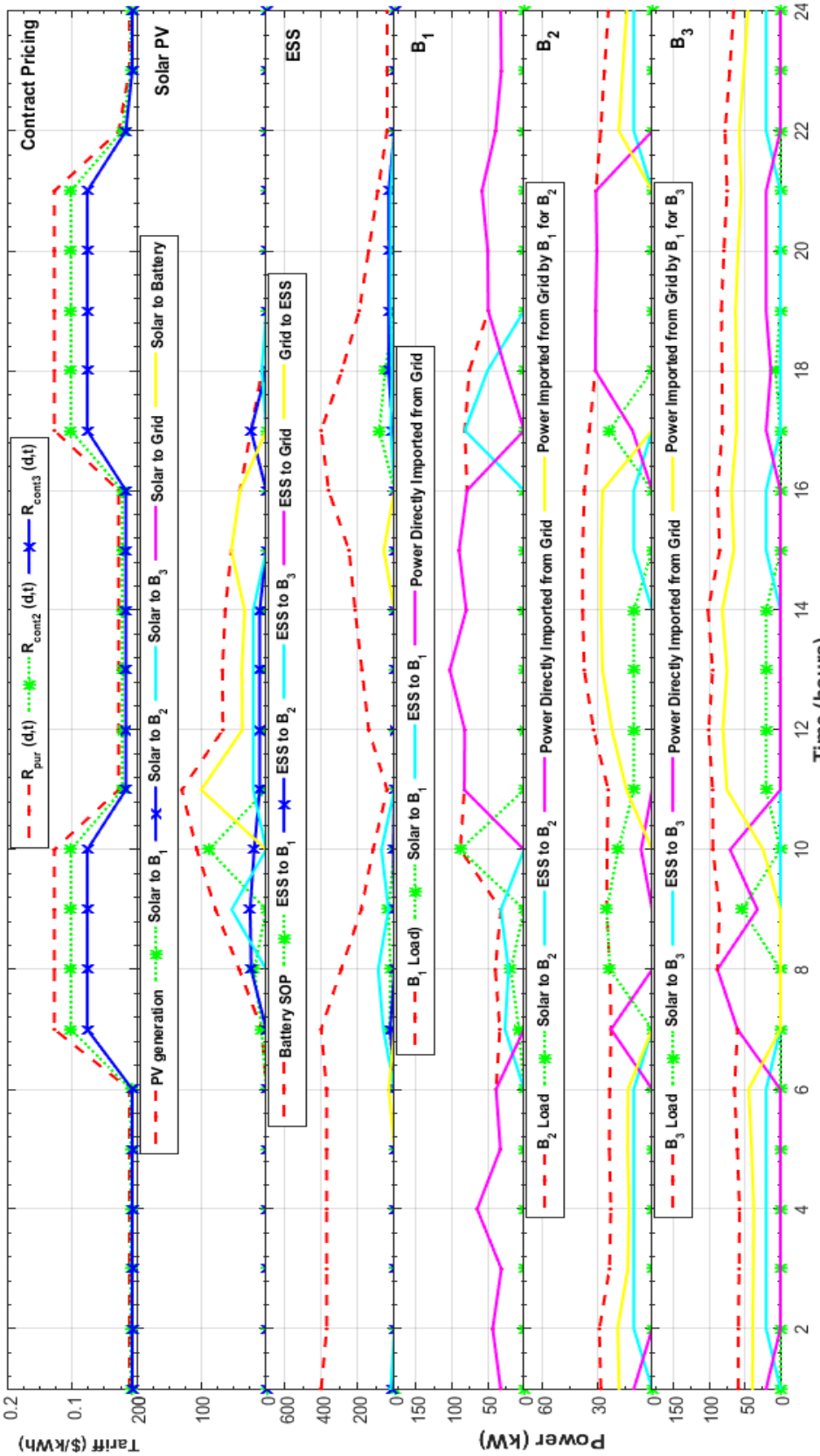

Figure 3.12 Optimized power dispatch from solar PV and battery to B_1, B_2 and B_3 respectively at R_{cont2} (t,d) > R_{cont3} (t,d) for a typical summer day.

3.4 Detailed Financial Analysis for Multiple Buildings

The detailed financial analysis is performed for the complete year and the costs associated with the sales and purchase of electricity for B_1, B_2 and B_3 is given in the Tables in Appendix B2. It is observed from the financial analysis that the profits of secondary buildings (B_2 and B_3) are comparatively less as compared to B_1. This can be explained on the basis of reduced contract tariffs with B_2 and B_3 as compared to TOU rates, which encourages secondary buildings to trade regularly with primary building. In addition, B_1 has more freedom to choose when to sell electricity either back to the grid or B_2 or B_3. Furthermore, considering practical load sites, the nature of load profiles of participating buildings will be distinct and can prove to be the essential parameter to help determine the profitability of primary as well as secondary buildings. Therefore, to help gauge the effect of variation of minimum contracted load between primary and secondary buildings, two more scenarios are considered. Primary building (B_1) having 15 kW and 10 kW of minimum contracted load with B_2 and B_3, respectively (scenario 2) and the amount of minimum contracted load for B_1 with B_2 and B_3 is set to 15 kW (scenario 3). Summarizing the results for each scenario, the annual net revenues earned by B_1 and annual savings received by B_2 and B_3 for cases 1 and 2 are listed in Table 3.2.

Table 3.2 Net Revenues (NZ$) and savings annually earned by B_1, B_2 and B_3 for scenario 1, 2 and 3.

Building	Case 1 (solar PV at B_1)			Case 2 (solar PV + ESS at B_1)		
	(a)	(b)	(c)	(a)	(b)	(c)
Scenario 1						
B_1	11,539	13,945	15,413	31,508	35,853	38,314
B_2	2,319	2,987	2,217	3,157	5,587	2,402
B_3	4,838	4,508	4,628	6,224	5,305	8,592
Scenario 2						
B_1	12,205	15,146	15,220	31,734	36,488	37,956
B_2	3,345	3,527	3,245	4,099	5,928	3,377
B_3	2,863	2,501	3,841	4,613	3,566	8,136
Scenario 3						
B_1	11,540	14,398	14,918	31,508	36,142	37,890
B_2	3,344	3,413	3,245	4,033	5,796	3,377
B_3	3,814	3,502	4,144	5,348	4,428	8,202

The proposed type of tariff settings encourages peer to peer (P2P) energy trading in a grid-connected mode. A mutually beneficial optimization framework enables the monetary benefits for each inter-connected building (B_1, B_2 and B_3). Due to local consumption of solar power by primary and secondary building and active participation in the net-metering scheme, the load on the utility grid gets shared. Additionally, local sharing of power in the vicinity (secondary buildings) helps with minimizing the line losses (I^2R), thereby aids to improve the stability of the grid. Various salient aspects and observations from each case and scenario can be summarized as follows:

- For case 0 (reference case), the purchasing price of electricity was higher due to increased prices during peak hours. It is found that $48,710, $35,480, and $69,434 incurred annually to meet the load demand of B_1, B_2 and B_3, respectively.

- For cases 1 and 2 of each scenario, B_1 attains the highest revenues in cases 1(c) and 2(c), respectively due to higher values of contracted price with B_3 and overall greater load demands of B_3.
- B_2 earns the maximum profit in 1(b) and 2(b) for each scenario. The higher contract price encourages B_1 to trade more frequently with B_2 as compared to B_3. Due to this higher energy trade in 1(b) and 2(b), B_2 receives relatively more monetary benefits in comparison to 1(c) and 2(c).
- For each scenario, B_3 earns the highest profit in 2(c). Due to higher contracted prices ($R_{cont_3}(t,d) > R_{cont_2}(t,d)$) and storage availability, B_1 sells more often to B_3, and highest profits are accordingly received.
- The earnings of B_2 and B_3 can be maximized via higher values of minimum contracted load with the primary building (with solar and storage). Results, summarized in Table 3.2, show that B_2 earns the lowest in the scenario 1 whereas B_3 earns minimum savings in the scenario 2 (both buildings have lowest power contracted quantities). In addition, the profits of secondary buildings raise with the higher contracted tariff between primary building (B_1) and secondary buildings (B_2 and B_3).
- Every participating building earns the highest savings in case 2 for each scenario, due to the higher contribution of storage during peak hours alongside solar PV.
- The revenues earned by primary building raised from 32% to 79%, 31% to 78% and 31 to 78% for scenario 1, 2 and 3, respectively after the addition of storage in case 2.
- The net present values (NPVs) are calculated using a discount rate of 5% [94], for all scenarios and sub-cases for primary building. The positive values of NPV indicate that the proposed framework is a viable business proposition for primary building. The formula for calculating NPV is given in Appendix B3.
- Similarly, with the application of battery storage and its utility during peak hours, the savings of B_2 increased from 8% to 15%, 10% to 16% and 9% to 16% for scenario 1, 2 and 3,

respectively and the B_3 raises its earning from 6% to 12%, 5% to 11% and 6% to 12% for scenario 1, 2 and 3, respectively.

- The financial gains of each participating building can be presented in terms of percentage decrease in electricity bill payments to the utility, computed through formulae given in Appendix B4. For all three scenarios, the monetary benefits of primary building ranges from 31-79% to 43% while the savings gained by B_2 and B_3 varies from 6–16% and 3-12%, respectively.

Chapter 4

Optimized Charging and Discharging of Electric Vehicles in Smart Building with Bilateral Contracts

Towards the integration of electric vehicles in the business architecture proposed in Chapter 3, this chapter discusses the techno-economic viability of incorporating the charging and discharging infrastructure in the smart building. The rise in electricity demand driven by electric vehicles (EVs) charging specifically during peak hours can be managed through smart charging infrastructures in a smart grid environment. EVs with zero emissions are considered an alternative transportation option. However, this type of new load (EVs) can introduce new challenges in the power grid operation when connected to the grid. Prosumers can help to improve the power systems operating in a smart grid with increasing penetration of EVs. Vehicle-to-Anything (V2X) technology advancement may be a solution to a serious problem that will occur in the future as EV penetration grows. V2X topologies include Vehicle-to-Grid (V2G), Vehicle-to-Building (V2B), Vehicle-to-Home (V2H), and Vehicle-to-Load (V2L) [95]. Through the induction of these technologies, prosumers can help to develop the utilities operate in a smart grid. The adoption of smart technologies in buildings is now considered critical to improving the overall energy efficiency, integrate renewable energy sources (RES), and reduce carbon footprint [96]. The power exchange agreements between the prosumers and consumers can help the utilities with the load shape during peak hours [97]. With the availability of more than one electricity resource for the consumers, there is an opportunity for a business model that allows both prosumers and consumers to earn benefits in a bilateral contract regime, particularly with the decreasing cost of distributed solar and maturing Li-ion battery technology.

4.1 State-of-the Art Charging and Discharging Business Architectures for EVs

Various studies on the profit maximization of large prosumers have been presented, but the emphasis has remained on the local optimization of buildings or charging stations (CS). Ma *et al*. [98] proposed a workplace car-park charging infrastructure model for plug-in hybrid electric vehicles (PHEVs), including a grid-connected dc system and renewable energy sources. To optimize the benefit of an EV CS, Wang *et al.* [99] proposed a joint admission and pricing system. A few other studies [100-102] looked at how to optimize EV charging to boost CSs or aggregator income. Shafiullah *et al*. [100] demonstrated how a load aggregator optimize benefits with many EVs by using efficient scheduling. Moghaddam *et al.* [101] explored a new organized competitive pricing model for charging electric vehicles (EVs) in the CS network, while Rabiee *et al.* [102] created a profit-maximizing economic-based queuing model for a CS.

Several other contributions explored an efficient energy management system for PV, batteries, and electric vehicles, taking into account the vehicle-to-grid (V2G) or vehicle-to-home (V2H) concepts. For instance, Khemakhem *et al.* [103] considered some residential customers under the vehicle-to-home V2H model, which aims to smooth each power demand through mutual energy management between plug-in electric vehicles (PEVs), houses, and neighbours. Gonçalves *et al.* [104] presented an automated home energy management system (AHEMS) for a unified grid optimization, local generation, and storage with time-varying tariffs. Chen *et al.* [105] investigated the energy utilization optimization strategies in a smart house with and without V2H and home distributed photovoltaic (HDPV) in Shanghai. Haq *et al.* [106] modelled a smart charging station for EVs powered by PV or grid with the implementation of V2G for improving the load shape during peak hours. Dai *et al*. [107] proposed a grid-connected photovoltaic, battery energy storage, electric vehicle charging station (PBES) optimization model for sizing PV, battery, and evaluating battery charging/discharging patterns. Luo *et al.* [108] proposed an optimization model for deploying electric vehicle charging stations and distributed generation services in tandem, taking into account the V2G role of electric vehicles.

4.2 System Overview for Optimized Charging of EVs

The different entities involved in the power trading network are shown in Figure 4.1. These include i) the grid with time-of-use (TOU) tariff scheme, ii) two types of buildings (primary and secondary as described in Chapter 3) and iii) a fleet of 30 EVs that can get charged at the parking station located in primary building. The summary for the system component sizes and costs associated with them are listed in Table 4.1.

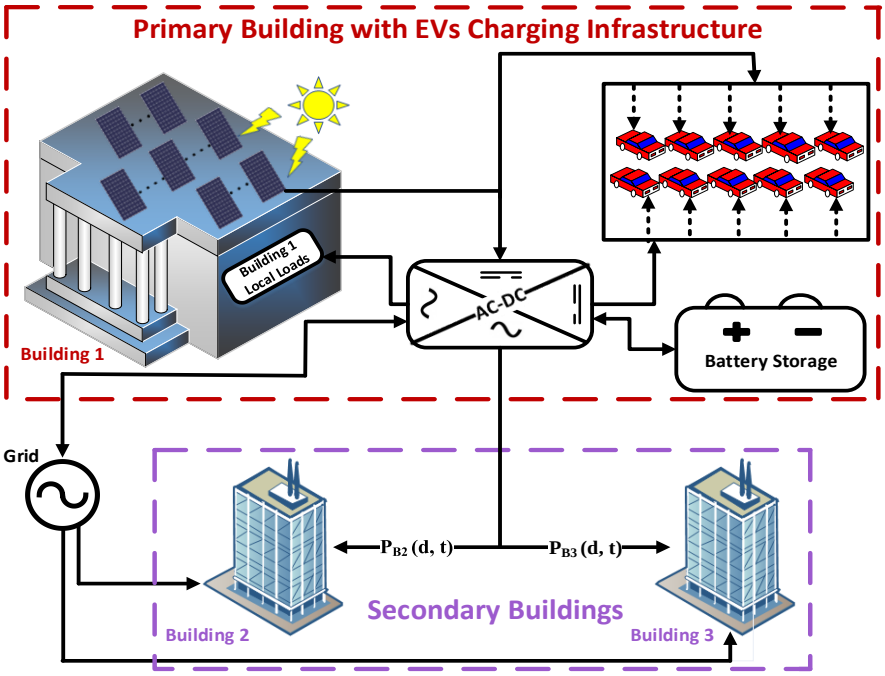

Figure 4.1 The proposed architecture, primary building (B_1) with rooftop PV-battery configuration and charging facilities for EVs with some contracted load with secondary buildings (B_2 and B_3).

Table 4.1 Size of Solar PV, ESS and Charger along with the installation costs.

System Component	Rooftop Solar PV	ESS	Charging Infrastructure
System size	400 kW_p	400 kWh	10 kW x 15
Price per unit	0.411 NZ$/W [93]	260 NZ$/kWh [82]	N/A
Estimated life of the component (yr)	25	8	25
Total price of the system (NZ$)	164,400	104,000	15,000 [109]

4.3 Problem Formulation for Optimized Charging of EVs

The problem is formulated as a multi-objective optimization problem targeting to maximize the profits for primary building and the savings for secondary buildings and a fleet of EVs. B_1 has a minimum contracted load agreement with B_2 and B_3 at reduced rates than the utility TOU pricing. The charging infrastructure at B_1 allows the EVs to get charged at reasonable rates during working hours for office-related trips. The time step for the optimization problem is taken as one hour (Δt).

4.3.1 Objective Function

The net revenue earned by B_1 can be maximized through (4.1). The earnings for the primary building comprise of revenue of B_1 from power exports to the grid (N_G), B_2 (D_{B_2}), B_3 (D_{B_3}) and EVs (D_{EV_n}). Also, the amount saved by B_1 through meeting its load demand (S_{B_1}) is added to its revenue. The costs incurred by B_1 consists of payments to the grid to meet the contracted load demands of B_2 (P_{B_2}) and B_3 (P_{B_3}), charge the battery banks (E_{B_1}), charge the EVs (P_{EV_n}), and the electricity units procured from the grid to meet the remaining load of B_1 (C_{B_1}).

$$\frac{Revenue^{Max}}{day} = Max\ (N_G + D_{B_2} + D_{B_3} + D_{EV_n} + S_{B_1} - C_{B_1} - E_{B_1} - P_{EV_n} - P_{B_2} - P_{B_3}) \tag{4.1}$$

The terms in (4.1) are further defined in the Appendix C1.

4.3.2 System Constraints

The optimization problem includes the system constraints on energy storage system, building loads, fleet of electric vehicles and solar PV.

4.3.2.1 Battery Storage Constraints

The battery storage constraints are given as (4.2) - (4.6). The two binary variables in (4.2) ensure that the battery must not be charged and discharged simultaneously; (4.3) limits the charging of the battery; (4.4) puts an upper and lower limit on the charging and discharging of the battery,

respectively. The maximum amount of power that can be extracted from the battery is given by (4.5). The power attainable at the next time slot is expressed as (4.6).

$$X(t) + Y(t) \leq 1 \qquad X(t), Y(t) \in \{0,1\}, \forall\, (t) \tag{4.2}$$

$$P_{G2ESS}(t) + P_{RE2ESS}(t) \leq SOP_{ESS^{Max}} * X(t) \tag{4.3}$$

$$SOP_{ESS^{Min}} \leq SOP\ (t) \leq SOP_{ESS^{Max}} \tag{4.4}$$

$$P_{ESS2B_1}(t) + P_{ESS2B_2}(t) + P_{ESS2B_3}(t) + P_{ESS2G}(t) + P_{ESS2EV_n}(t) \leq (SOP_{ESS^{Max}} - SOP_{ESS^{Min}}) * Y(t) \tag{4.5}$$

$$\begin{aligned} SOP_{ESS}\ (t+1) = {} & SOP_{ESS}\ (t) + ((\eta_{char} * P_{G2ESS}(t) + ((\eta_{char} * P_{RE2ESS}(t))) * X(t) \\ & - \left(P_{ESS2G}(t)/\eta_{disch} + P_{ESS2B_1}(t)/\eta_{disch} + P_{ESS2B_2}(t)/\eta_{disch} + P_{ESS2B_3}(t)/\eta_{disch}\right. \\ & \left. + (\eta_{char} * P_{ESS2EV_n}(t)/\eta_{disch}\right) * Y(t) \end{aligned} \tag{4.6}$$

4.3.2.2 Building Load and Power Trading Constraints

The load demand of B_1 can be supplied by the grid, battery, or solar PV, given as (4.7). The bilateral contracted power agreement ensures the supply of minimum contracted load to B_2 and B_3 specified as (4.8) and (4.9), respectively.

$$P_{G2B_1}(t) + P_{ESS2B_1}(t)/\eta_{disch} + P_{RE2B_1}(t) = B_1(t) \tag{4.7}$$

$$P_{B_2}(t) \leq P_{G2B_2}(t) + P_{ESS2B_2}(t)/\eta_{disch} + P_{RE2B_2}(t) \leq B_2(t) \tag{4.8}$$

$$P_{B_3}(t) \leq P_{G2B3}(t) + P_{ESS2B3}(t)/\eta_{disch} + P_{RE2B3}(t) \leq B_3(t) \tag{4.9}$$

4.3.2.3 Electric Vehicles Constraints

The EVs can be charged from the grid, solar, or ESS. For illustration purposes, a fleet of 30 EVs (Nissan Leaf) is taken with a nominal battery capacity of 24 kWh. Multiple types of EVs with

various battery sizes can also be used, but one manufacturer is used to minimize any inter-company comparisons for this chapter. It is further considered that 15 chargers (SAE-J1772, level 2, 208–240 VAC) [110] are available at the parking station located in the primary building and the charging efficiency is taken as 90 %. The usual working hours are taken as 8 am to 6 pm but they are not binding. The arrival time of EVs is obtained through t location-scale distribution [111].

The different generated arrival times for the EVs are correspondingly shown in Figure 4.2. The detention time (stay duration) of each EV is obtained as a normal distribution with a mean of 8.5h and variance of 4h i.e., N(8.5, 2^2). Monte Carlo simulations are performed to estimate the initial state-of-power (SOP) of each incoming EV. The framework serves as a model with upfront information of solar PV generation, TOU tariff, total load demand of buildings, and EVs stochastic information (initial SOP, arrival, and departure time). Eqs. (4.10) - (4.15) defines the charging process of EVs through the grid, solar PV, and ESS. The term "σ" signifies the charger capacity, taken as 10 kW for each level 2 charger.

$$P_{G2EV_n}(t) + P_{ESS2EV_n}(t) + P_{RE2EV_n}(t) \leq SOP_{EV_n}{}^{Max} \; ; \forall\,(n) \tag{4.10}$$

$$SOP_{EV_n}{}^{Min} \leq \; SOP_{EV_n}(t) \leq SOP_{EV_n}{}^{Max} \quad ; \forall\,(n) \tag{4.11}$$

$$SOP_{EV_n}(t+1) = SOP_{EV_n}(t) + (\eta_{char} * P_{G2EV_n}(t)) + (\eta_{char} * P_{ESS2EV_n}(t)/\eta_{disch}) + (\eta_{char} * P_{RE2EV_n}(t)) \quad ; \forall\,(n) \tag{4.12}$$

$$(\eta_{char} * P_{G2EV_n}(t)) \leq \sigma \quad ; \forall\,(n) \tag{4.13}$$

$$(\eta_{char} * P_{RE2EV_n}(t)) \leq \sigma \quad ; \forall\,(n) \tag{4.14}$$

$$(\eta_{char} * P_{ESS2EV_n}(t)/\eta_{disch}) \leq \sigma \quad ; \forall\,(n) \tag{4.15}$$

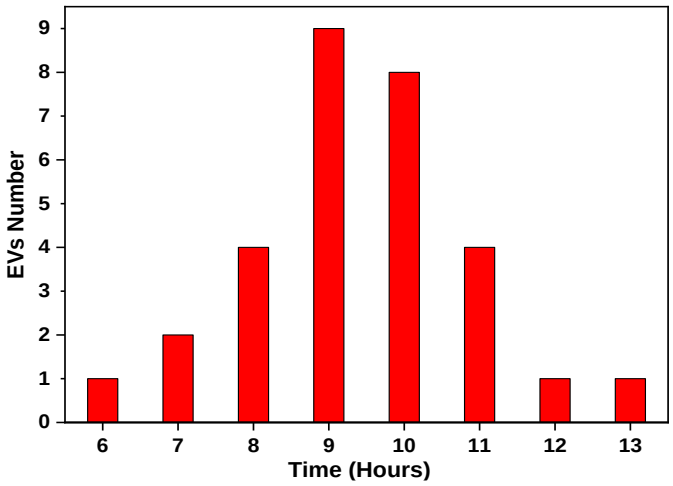

Figure 4.2 Number of EVs with different arrival times.

4.3.2.4 Solar PV Constraint

The solar PV generation equals the sum of power delivered to the grid, B_1, B_2, B_3, ESS and fleet of EVs, given as (4.16).

$$P_{RE2B_1}(t) + P_{RE2B_3}(t) + P_{RE2B_3}(t) + P_{RE2G}(t) + P_{RE2ESS}(t) + P_{RE2EV_n}(t) = S(t) \quad (4.16)$$

4.4 Results of the Optimized Charging of EVs

Three cases are evaluated for the daily profits and savings for primary and secondary buildings. The TOU pricing with contract rates for B_2 and B_3 and sales rates for EVs charging are shown in Figure 4.3, taken from [109, 112]. Equal contract rates (NZ$/kWh) of electricity (lower than the utility price) are taken for B_2 and B_3. The net-metering rate and charging cost of EVs is taken as one-third and 1.25 times the utility's electricity price (TOU tariff). Please note that these are typical numbers used and has been the case for Auckland, New Zealand [109, 112]. The minimum contracted load is 5 kW for each secondary building.

4.4.1 Reference Case/Business-as-Usual

For the reference (base) case, no solar, storage, and charging facilities are available at B_1. The total purchasing cost for a typical summer day incurred by B_1, B_2 and B_3 from the utility at TOU

rates is 85$, 41.4$, and 192$, respectively. The EVs also add to the peak load demand at the grid during peak hours if charged at some other charging station connected only to the grid.

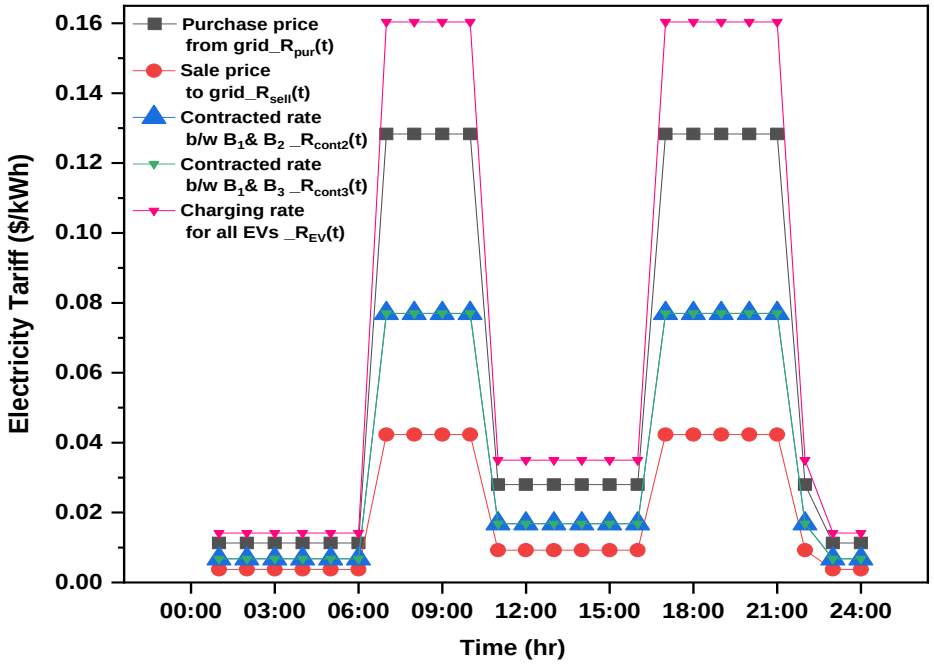

Figure 4.3 TOU pricing, contract, and charging rates of electricity along with net-metering tariff during peak and off-peak hours.

4.4.2 Optimized Charging of EVs with Solar and without Storage (Case 1)

A rooftop solar PV system of 400 kW_p without storage is installed at B_1. The solar PV generation and optimized results for power dispatch to each building, grid, and EVs through solar PV is shown in Figure 4.4. It can be observed that during the peak solar generation from 9:00 AM - 12:00 PM, all the EVs are charged through solar PV with a significant portion of solar being fed to the grid.

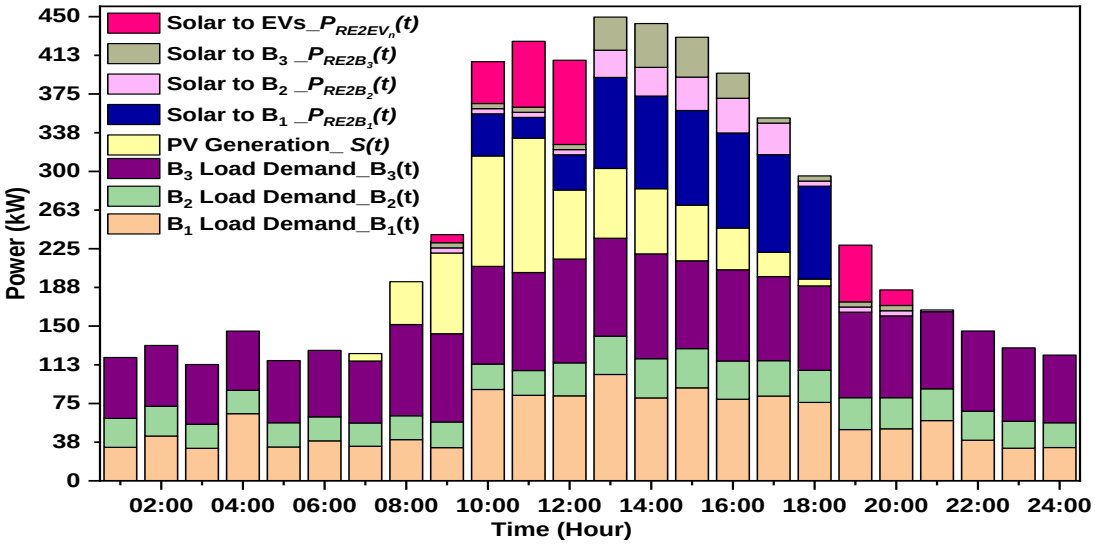

Figure 4.4 RT load demand of B_1, B_2, and B_3 and hourly power dispatch of solar PV (without ESS).

4.4.3 Optimized Charging of EVs with Solar and Storage (Case 2)

The provision of 400 kWh Li-ion battery banks alongside a 400 kWp solar PV system is available. The power flows towards B_1, B_2, B_3 and EVs via solar PV is shown in Figure 4.5. Further, the optimal cumulative charging pattern for 30 EVs from the battery (ESS) is shown in Figure 4.6. Both figures show that EVs are charged only through either battery banks or solar PV, reducing the overall peak demand of the utility. Results show that during high insolation hours (9:00 AM - 12:00 PM), solar PV partially supplies the load demands of EVs, B_1, B_2 and B_3. When solar is low or unavailable, storage contributes to meet the total load demand of B_1 and partial load support to B_2 and B_3.

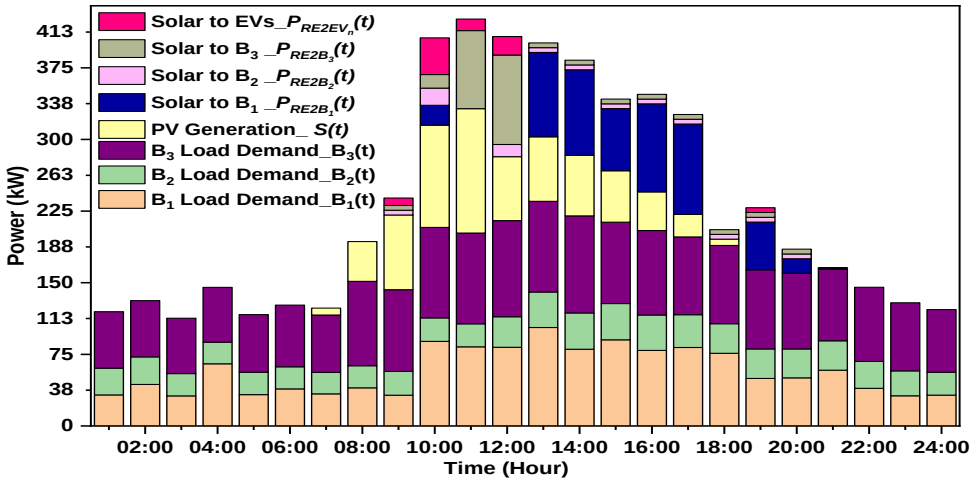

Figure 4.5 Hourly power dispatch of solar PV for a typical summer day (with ESS).

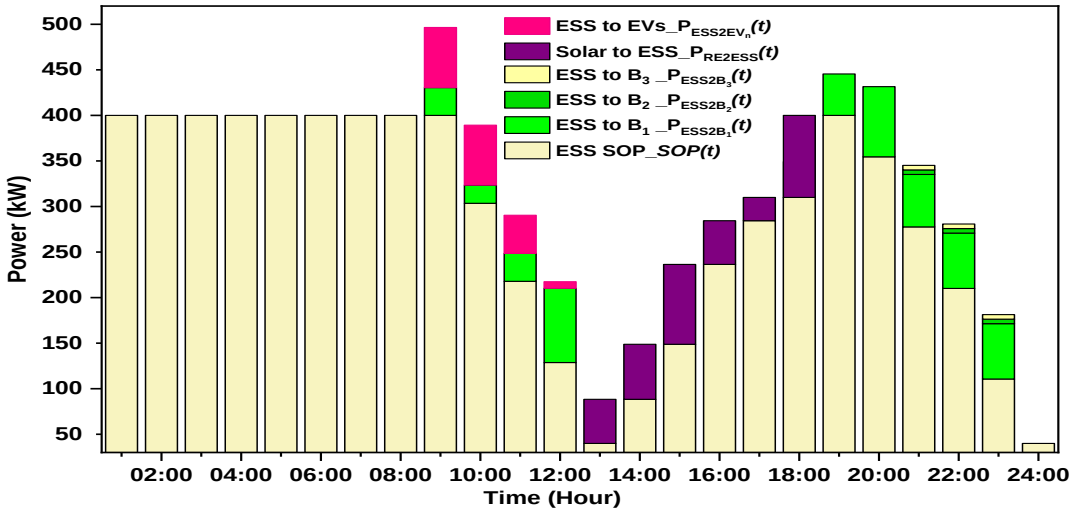

Figure 4.6 Hourly power flows among storage, B_1, B_2, B_3, grid and EVs.

4.4.4 Financial Results for Smart Building and Secondary Buildings

The net revenue earned by B_1 and the cost savings for B_2 and B_3 are listed in Table 4.2 for the typical summer day evaluated. It can be noted from Table 4.2 that each building is better off compared to the reference case (business as usual) and implying a suitable business proposition for each participating entity. For the two secondary buildings, a lower overall load demand of B_2 is seen, resulting in lower profits for B_2 compared to B_1 and B_3 for the specific day.

Table 4.2 Net revenues and cost savings (NZ$) for B_1, B_2 and B_3 for a typical summer day.

Building	Case 1	Case 2
B_1	68.6	94.6
B_2	5.3	4.1
B_3	52.3	79.2

4.5 System Overview for the Optimized Charging and Discharging of EVs

In order to facilitate the integration of vehicle to everything (V2X) services into the existing network as described in Section 4.3, a charging and discharging infrastructure is incorporated in the primary building. Several entities included in the techno-economic model are depicted in Figure 4.7.

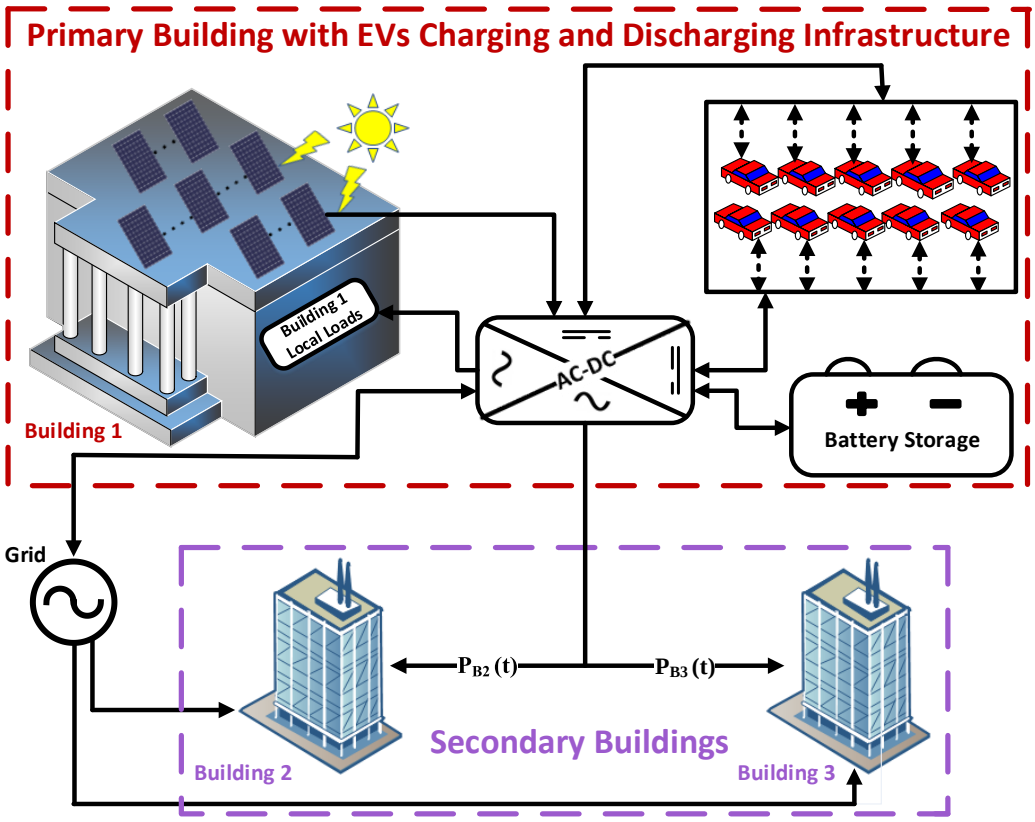

Figure 4.7 The architecture of the proposed profit model with the primary building (B_1) with charging/discharging infrastructure for EVs having some contracted load with secondary buildings (B_2 and B_3).

4.6 Mathematical Modeling for the Optimized Charging and Discharging of EVs

A mixed-integer linear program (MILP) is formulated in ILOG optimization studio to attain the optimized power delivery and cost savings for primary and secondary buildings and a fleet of EVs. The power flows from the primary building to secondary buildings, grid and EVs are shown in Figure 4.8. The selling rate of EVs to primary and secondary building is lower than TOU tariff i.e., $R_{EV_{pur}}(t) < R_{pur}(t)$.

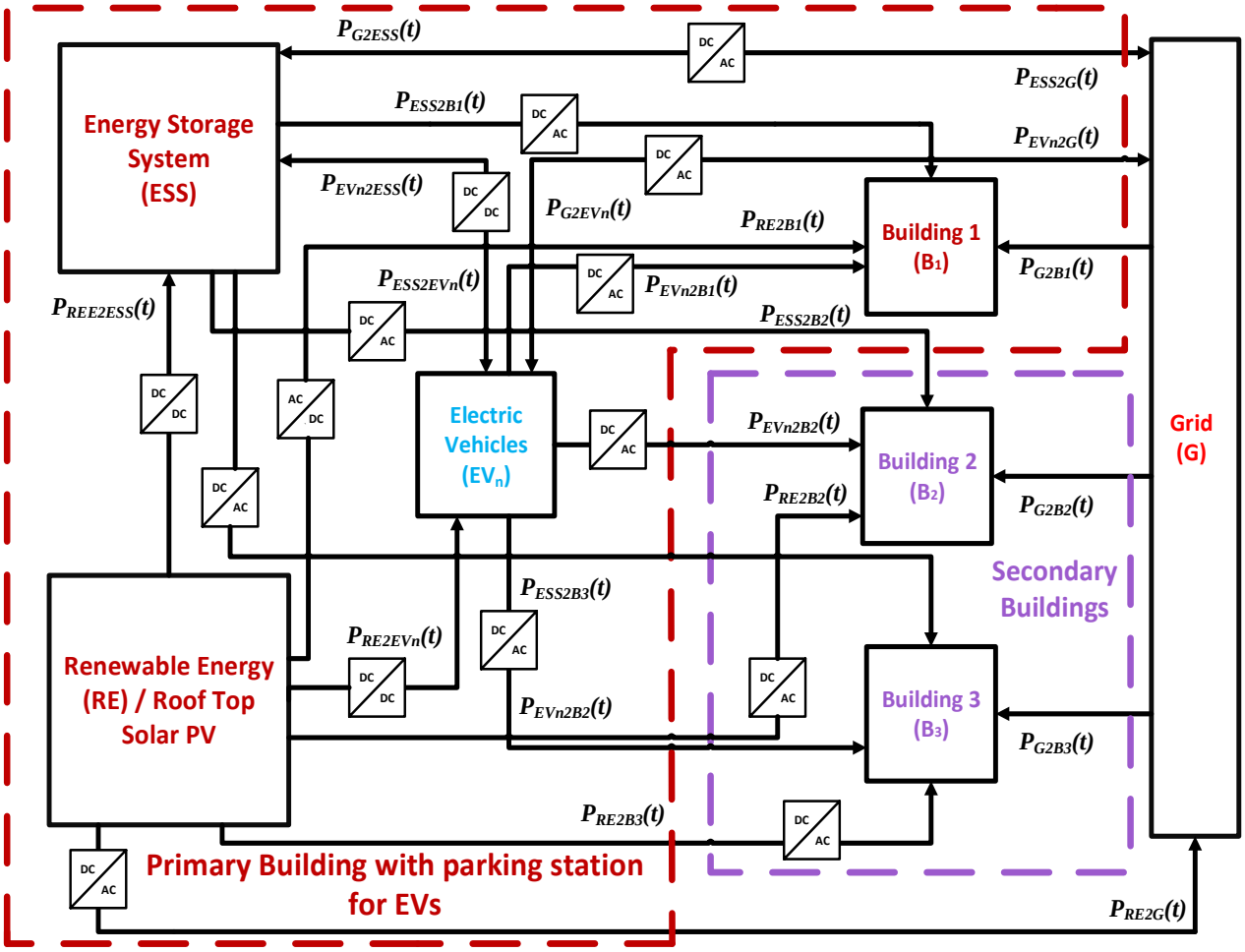

Figure4.8 State variables related to the power flows. Secondary buildings (B_2 and B_3) can be fed through grid, primary building (B_1) or EVs. B_1 provides power to local loads, secondary buildings and EVs as well as bidirectional grid exchange.

4.6.1 Objective Function

The primary building's daily revenue is maximized through the objective function in (4.17). The primary building's net profit is calculated by subtracting the solar PV, storage and charger costs per day from the gross revenue earned. The payments to the EVs by primary building for purchasing electricity ($C_{EV_{B_1}}$,$C_{EV_{ESS}}$) are included in (4.17).

$$\frac{Revenue^{Max}}{day} = Max\ (N_G + D_{B_2} + D_{B_3} + D_{EV_n} + S_{B_1} - C_{B_1} - E_{B_1} - P_{EV} - P_{B_2} - P_{B_3} - C_{EV_{B_1}} - C_{EV_{ESS}}) \quad (4.17)$$

The definitions of the additional terminologies used in (4.17) are given in the Appendix C2.

4.6.2 System Constraints

The optimization problem includes the system constraints on energy storage system, building loads, fleet of electric vehicles and solar PV.

4.6.2.1 Battery Storage Constraints

The constraints on battery storage are shown as (4.18) – (4.22).

$$X_{ESS}\ (t) + Y_{ESS}\ (t) \leq 1 \qquad (X_{ESS}\ (t), Y_{ESS}\ (t)) \in \{0,1\}, \forall\ (t) \quad (4.18)$$

$$(P_{G2ESS}(t)\ + P_{RE2ESS}(t) + P_{EV_n 2ESS}(t)) * X_{ESS}\ (t) \leq SOP_{ESS^{Max}} \quad (4.19)$$

$$SOP_{ESS^{Min}}\ \leq SOP\ (t) \leq SOP_{ESS^{Max}} \quad (4.20)$$

$$P_{ESS2B_1}(t)\ + P_{ESS2B_2}(t) + P_{ESS2B_3}(t) + P_{ESS2G}(t) + P_{ESS2EV_n}(t) * Y_{ESS}\ (t) \leq (SOP_{ESS^{Max}} - SOP_{ESS^{Min}}) \quad (4.21)$$

$$SOP_{ESS}(t+1) = SOP_{ESS}(t) + \big((\eta_{char} * P_{G2ESS}(t) + ((\eta_{char} * P_{RE2ESS}(t)\big) + ((\eta_{char} * P_{EV_n 2ESS}(t))) * X_{ESS} - \big((P_{ESS2G}(t)/\eta_{disch}) + (P_{ESS2B_1}(t)/\eta_{disch}) + (P_{ESS2B_3}(t)/\eta_{disch}) + (\eta_{char} * P_{ESS2EV_n}(t)/\eta_{disch})\big) * Y_{ESS}(t) \quad (4.22)$$

4.6.2.2 Building Load and Power Trading Constraints

B_1's load demand can be met by the grid, battery, solar PV, or EVs, specified as (4.23). (4.24) and (4.25) denote that the primary building will meet the load demand of B_2 and B_3 in compliance with the contracted power demand. Further, (4.26) and (4.27) shows that EVs can also supply power to B_2 and B_3 on top of the power contribution from the primary building.

$$0 \le P_{G2B_1}(t) + P_{ESS2B_1}(t)/\eta_{disch} + P_{RE2B_1}(t) + P_{EV_n 2B_1}(t)/\eta_{disch} \le B_1(t) \quad (4.23)$$

$$P_{B_2}(t) \le P_{G2B_2}(t) + P_{ESS2B_2}(t)/\eta_{disch} + P_{RE2B_2}(t) \le B_2(t) \quad (4.24)$$

$$P_{B_3}(t) \le P_{G2B3}(t) + P_{ESS2B3}(t)/\eta_{disch} + P_{RE2B3}(t) \le B_3(t) \quad (4.25)$$

$$0 \le P_{G2B_2}(t) + P_{ESS2B_2}(t)/\eta_{disch} + P_{RE2B_2}(t) + P_{EV_n 2B_2}(t)/\eta_{disch} \le B_2(t) - P_{B_2}(t) \quad (4.26)$$

$$0 \le P_{G2B3}(t) + P_{ESS2B3}(t)/\eta_{disch} + P_{RE2B3}(t) + P_{EV_n 2B_3}(t)/\eta_{disch} \le B_3(t) - P_{B_3}(t) \quad (4.27)$$

4.6.2.3 Electric Vehicles Constraints

Electric vehicles (EVs) can be charged using the grid, solar, or storage, with additional capacity to provide electricity to local loads at the primary and secondary buildings, battery and grid. A fleet of 15 electric vehicles (Nissan Leaf) with a nominal battery capacity of 24 kWh is used for illustration purposes. It is also assumed that 15 chargers (SAE-J1772, level 2, 208–240 VAC) [110] are accessible at the primary building's parking station, with a charging and discharging efficiency of 90%. The standard working hours are 9 a.m. to 5 p.m., although this is not mandatory.

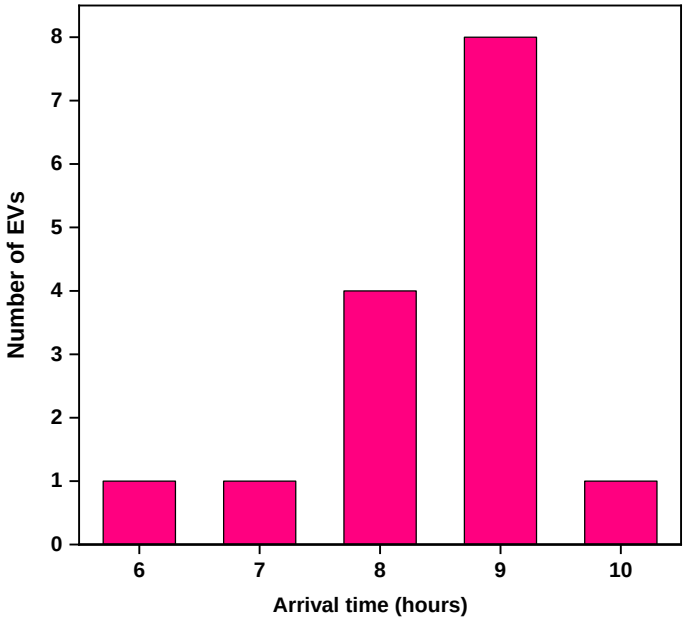

Figure 4.9 Number of EVs with different arrival times.

Eqs. (4.28)–(4.40) describe the charging and discharging of electric vehicles (EVs) involving the grid, solar PV, ESS, and primary and secondary building loads. Two binary variables for each EV ($X_{EV_n}(t)$ and $Y_{EV_n}(t)$) are used to avoid the simultaneous charging and discharging of EVs, stated as (4.28). Eq. (4.33) – (4.40) describe the charging and discharging of each EV, consistent with the charger capacity (σ). In this chapter, a capacity of 3.3 kW is taken for a typical level 2 charger.

$$X_{EV_n}(t) + Y_{EV_n}(t) \leq 1 \qquad (X_{EV_n}(t), Y_{EV_n}(t)) \in \{0,1\}, \forall (t), \forall (n) \tag{4.28}$$

$$\left(P_{G2EV_n}(t) + P_{ESS2EV_n}(t) + P_{RE2EV_n}(t)\right) * X_{EV_n}(t) \leq SOP_{EV_n Max}\ ; \forall (n) \tag{4.29}$$

$$SOP_{EV_n Min} \leq SOP_{EV_n}(t) \leq SOP_{EV_n Max} \quad ; \forall (n \tag{4.30}$$

$$(P_{EV_n 2B_1}(t) + P_{EV_n 2B_2}(t) + P_{EV_n 2B_3}(t) + P_{EV_n 2ESS}(t) + P_{EV_n 2G}(t)) * Y_{EV_n}(t) \leq (SOP_{EV_n Max} - SOP_{EV_n Min}) \ ; \forall (n) \tag{4.31}$$

$$SOP_{EV_n}(t+1) = SOP_{EV_n}(t) + (\eta_{char} * P_{G2EV_n}(t)) + (\eta_{char} * P_{ESS2EV_n}(t)/\eta_{disch}) + (\eta_{char} * P_{RE2EV_n}(t)) * X_{EV_n}(t) - ((\eta_{char} * P_{EV_n 2ESS}(t)/\eta_{disch}) + (P_{EV_n 2G}(t)/\eta_{disch}) + (P_{EV_n 2B_1}(t)/\eta_{disch}) + (P_{EV_n 2B_2}(t)/\eta_{disch}) + (P_{EV_n 2B_3}(t)/\eta_{disch})) * Y_{EV_n}(t) \quad ;\forall (n) \tag{4.32}$$

$$(\eta_{char} * P_{G2EV_n}(t)) \leq \sigma \quad ;\forall (n) \tag{4.33}$$

$$(\eta_{char} * P_{RE2EV_n}(t)) \leq \sigma \quad ;\forall (n) \tag{4.34}$$

$$(\eta_{char} * P_{ESS2EV_n}(t)/\eta_{disch}) \leq \sigma \quad ;\forall (n) \tag{4.35}$$

$$(P_{EV_n 2G}(t)/\eta_{disch}) \leq \sigma \quad ;\forall (n) \tag{4.36}$$

$$(\eta_{char} * P_{EV_n 2ESS}(t)/\eta_{disch}) \leq \sigma \quad ;\forall (n) \tag{4.37}$$

$$(P_{EV_n 2B_1}(t)/\eta_{disch}) \leq \sigma \quad ;\forall (n) \tag{4.38}$$

$$(P_{EV_n 2B_2}(t)/\eta_{disch}) \leq \sigma \quad ;\forall (n) \tag{4.39}$$

$$(P_{EV_n 2B_3}(t)/\eta_{disch}) \leq \sigma \quad ;\forall (n) \tag{4.40}$$

4.6.2.4 Solar PV Constraint

Solar PV generation is equal to the amount of power supplied to B_1, B_2, B_3, grid, ESS, and the fleet of electric vehicles, expressed earlier in the chapter as (4.16).

4.6.2.5 Solution Methodology

Non-negativity restrictions apply to each state variable. The flowchart for the optimized power delivery of the profit model is shown in Figure 4.10.

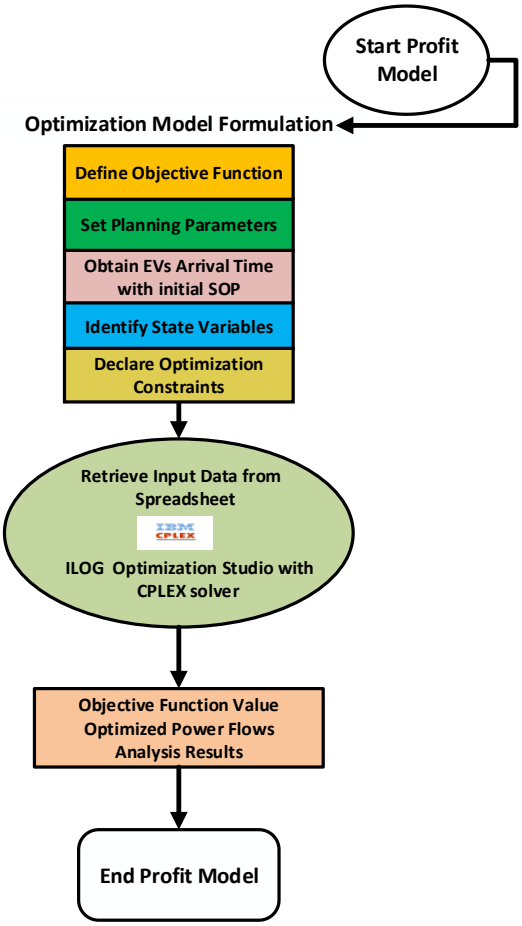

Figure 4.10 Flow chart for the optimized solution from the profit model.

4.7 Optimized Power Dispatch among Multiple Buildings and Electric Vehicles with V2X Capability

The proposed simulation model is used to run three cases. No solar PV, storage, or EVs are supposed in the primary building in the base case. Table 4.3 summarizes the sizes and prices of the different components.

Table 4.3 Size of Solar PV, storage and charging infrastructure along with the installation costs.

System Component	Rooftop Solar PV	Energy Storage System (ESS)	Charging Infrastructure
System size	400 kW_p	400 kWh	3.3 kW x 15
Price per unit	0.41 NZ$/W [93]	260 NZ$/kWh [82]	1,000 NZ$/charger
Estimated life (years)	25	8	25
Total price of the system (NZ$)	164,400	104,000	15,000 [109, 113]

Figure 4.11 [41] shows the peak and off-peak tariff schemes with equal contract rates for B_2 and B_3 for a given day. It indicates the per unit purchase price from the grid for a specific day from a New Zealand utility (Electra). Net-metering tariff is lower than the grid's TOU prices. The charging price for each EV from grid is higher as compared to the charging rates from primary building i.e., $R_{EV_{SG}}(t) > R_{EV_{SB_1}}(t)$. Further, the purchase price of electricity for primary and secondary buildings from EVs is lower than TOU tariff ($R_{EV_{pur}}(t) < R_{pur}(t)$), which encourages the buildings to purchase electricity from the EVs. This tariff arrangement guarantees profit for each commodity (primary and secondary buildings and fleet of electric vehicles) involved in the trade.

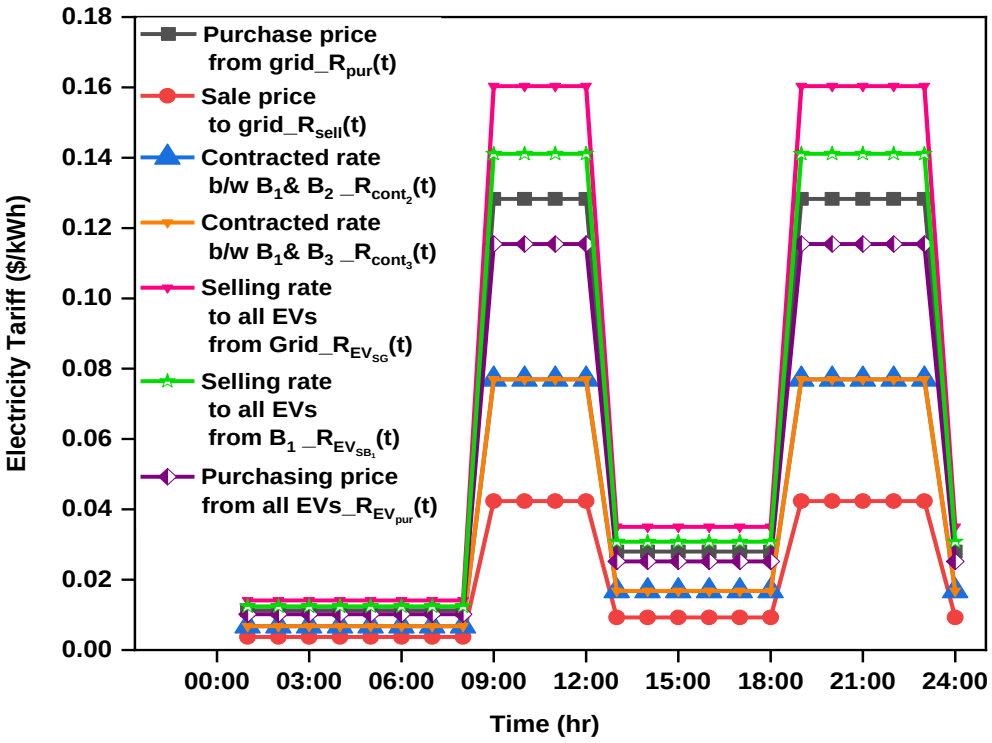

Figure 4.11 Time-of-use tariff design during peak and off-peak hours with equal contract rates.

Figure 4.12 illustrates the load demand of three commercial buildings on a typical summer day in Auckland, New Zealand. Furthermore, for scenario 1, the minimum contracted load from primary building is set as 5 kW with B_2 and B_3.

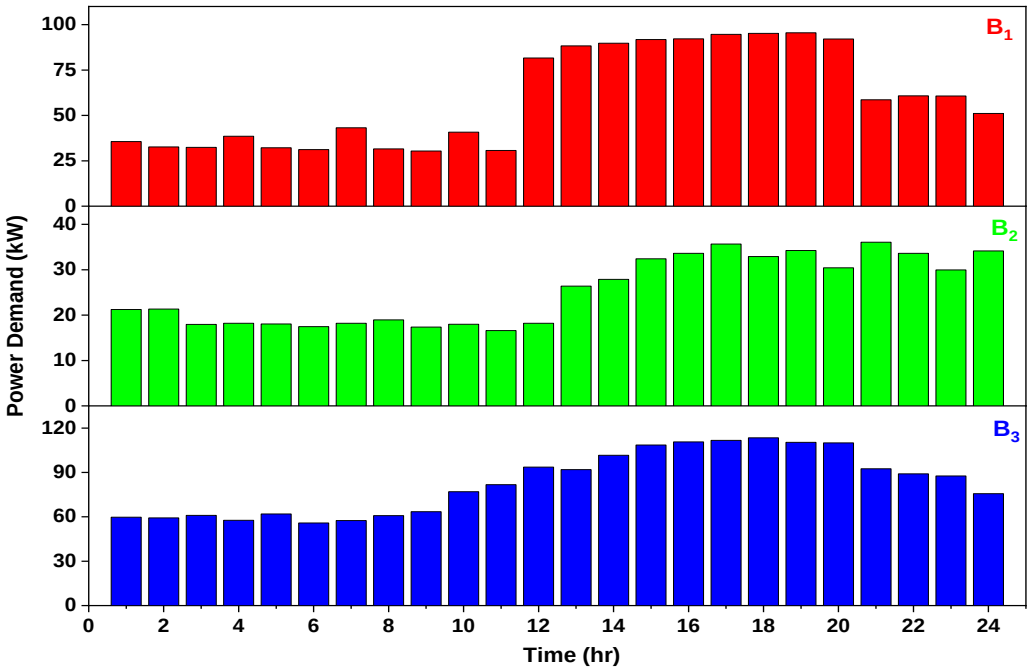

Figure 4.12 Real load demand (kW) of building 1, 2 and 3, respectively for a typical summer day.

Base Case or Business-as-usual (Case 0): In the base case, none of the buildings have rooftop solar PV, ESS, or charging infrastructure (EVs). B_1, B_2, and B_3 spend \$91, \$38, and \$129, respectively, on grid electricity purchases at TOU rates. Furthermore, depending on the initial SOP, arrival and departure times of each EV, the total cost to the grid for acquiring power from EVs is determined to be \$17 given as (4.41).

$$C_{EV}^{0} = \sum_{n=1}^{15} \sum_{t=1}^{24} \left(P_{G2EV_n}(t) * R_{EV_{SG}}(t) * \Delta t \right) \tag{4.41}$$

Case 1: In this case, the primary building includes a rooftop solar PV system with a capacity of 400 kWp and a parking station for charging and discharging a fleet of 15 electric vehicles, but there is no storage (ESS).

Case 2: In this case, the primary building features rooftop solar PV, electric vehicle charging infrastructure, and ESS.

4.7.1 Results with Solar and without Storage (Case 1)

The model is evaluated with different contracted rates between secondary buildings and B_1. The impact of various pricing tariff ($R_{cont_2}(t)$ and $R_{cont_3}(t)$) is examined in depth in the sub-cases.

4.7.1.1 Case 1(a)

The results for the optimized power flow among the buildings, solar PV, grid and EVs are shown in Figure 4.13 (a-c) at equal contract rates of 60% of TOU tariff. Figure 4.13 (a) shows that solar provides the most electricity to B_1, while also supplying power to B_2, B_3, and electric vehicles. Figure 4.13 (b) demonstrates how EVs are charged using solar PV or the grid directly. In addition, when onsite PV is insufficient, Figure 4.13 (c) illustrates that the primary building purchases electricity from the utility to meet the contracted load for B_2 and B_3.

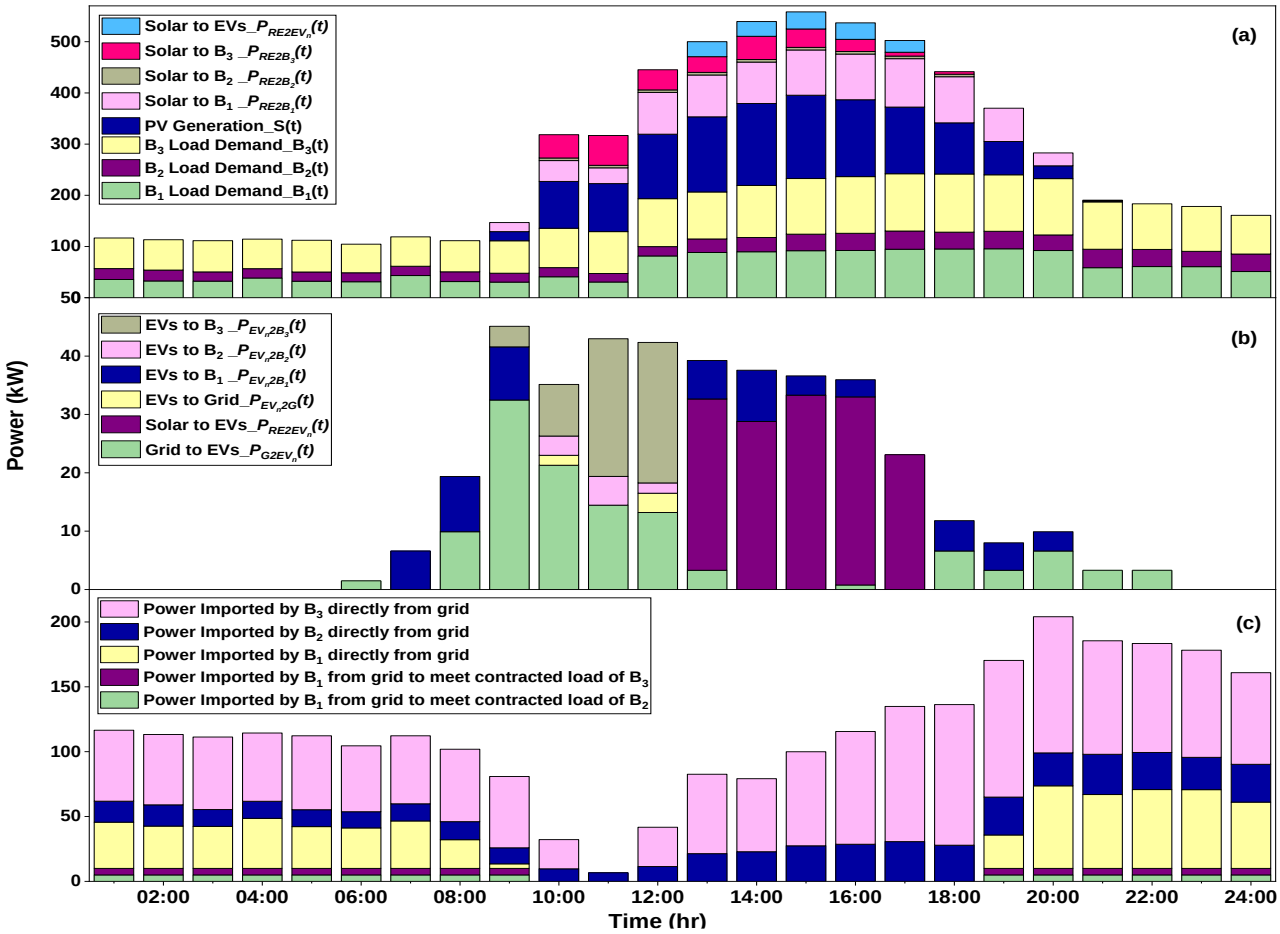

Figure 4.13 (a) Hourly power distribution of solar PV along with load demand of buildings (b) Optimized charging and discharging of EVs (c) Hourly electricity trade between grid and B_1, B_2 and B_3.

4.7.1.2 Case 1(b)

Secondary buildings (B_2 and B_3) receive power from the primary building (B_1) at a rate of 80% and 60% of the TOU tariff, respectively. Figure 4.14 depicts the contract pricing and hourly optimum solar power delivery to buildings and electric vehicles. To optimize the savings of both the primary building and the EVs, it has been noted that EVs deliver a larger amount of B_1 load.

4.7.1.3 Case 1(c)

The contract rated with B_2 and B_3 are set as 60% and 80% of TOU tariff i.e., $R_{cont_3}(t) > R_{cont_2}(t)$. It is observed that B_1 sells a higher amount of power to B_2 due to a) higher contracted tariff and b) higher load demand of B_2.

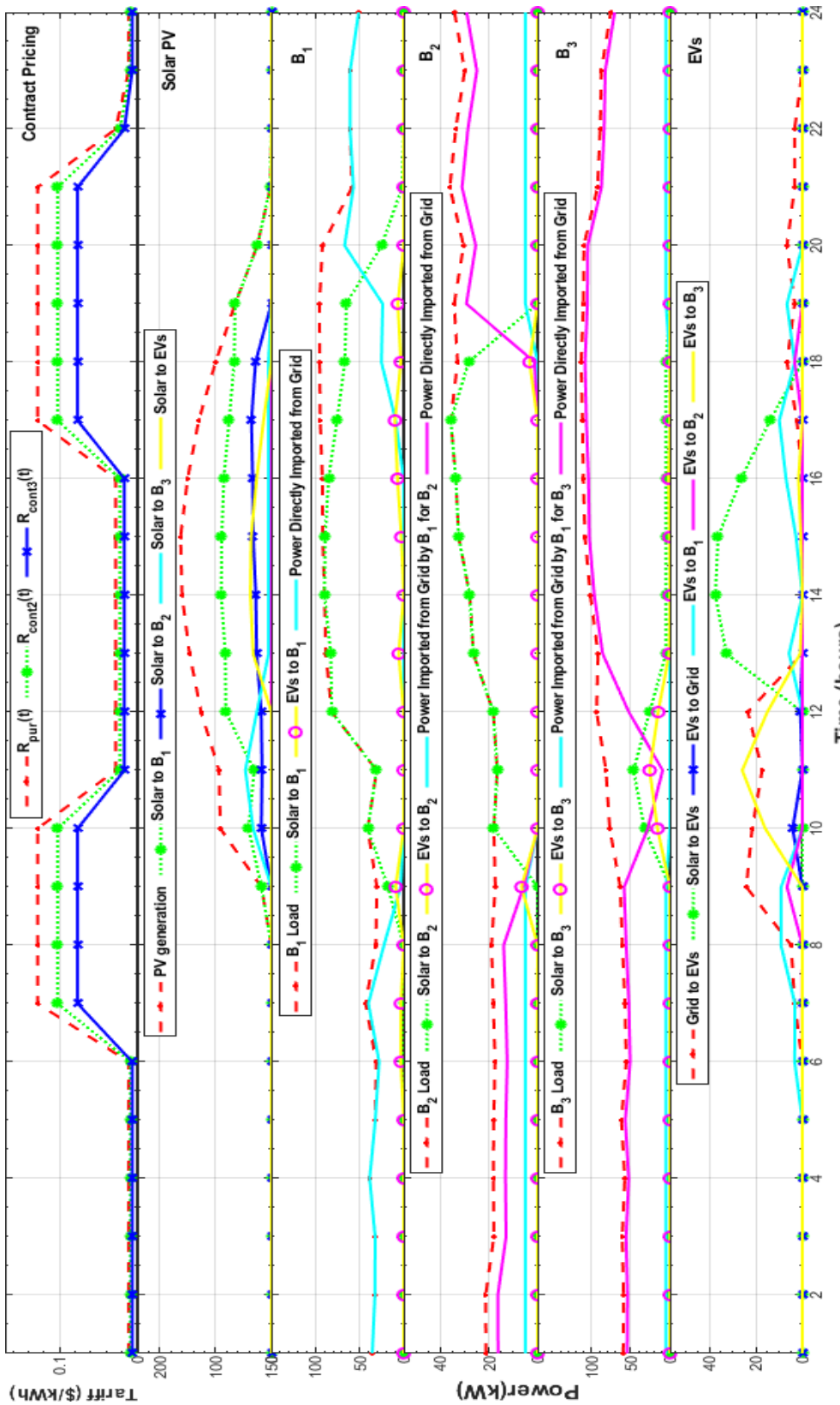

Figure 4.14 Hourly solar PV generation, consumption for B_1, B_2 and B_3 and charging and discharging of EVs, respectively at $R_{cont2}(t) > R_{cont3}(t)$.

4.7.2 Results with Solar and Storage (Case 2)

The primary building in this case has storage in addition to the availability of solar PV and parking station. The sub-cases discuss the effect of variable agreement prices with B_1.

4.7.2.1 Case 2(a)

Figure 4.15 (a) shows the optimal power flows from solar to B_1, B_2, B_3, EVs, and the grid at 60% of the grid's TOU tariff for both secondary buildings. In addition, Figure 4.15 (b) depicts the battery's changing power states. The battery is charged during off-peak hours (1:00 PM – 6:00 PM) and drained during peak hours (9:00 AM – 12:00 Noon) and (7:00 PM – 12:00 AM), demonstrating the benefit of storage during peak hours. Figure 4.16 (a) depicts the charging and discharging trends of 15 electric vehicles. It can be seen that a large amount of EV charging occurs during off-peak hours, i.e., 1:00 PM – 6:00 PM, using either solar or ESS. Figure 4.16 (b) shows the optimized power flows from grid towards primary and secondary buildings.

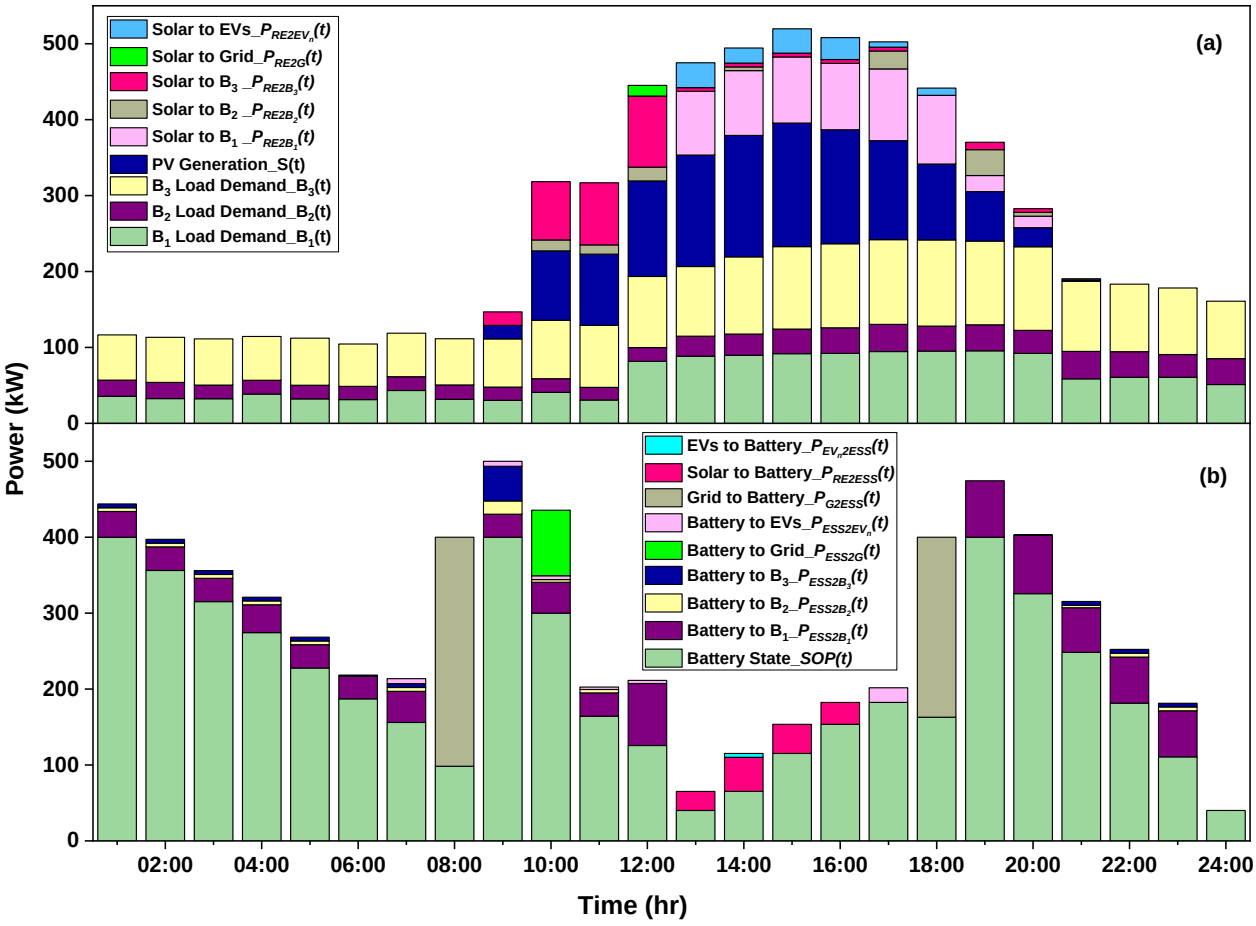

Figure 4.15 (a) Hourly electricity distribution of solar PV along with real time loads of buildings (b) Hourly power trade among storage, B_1, B_2, B_3, grid and fleet of EVs.

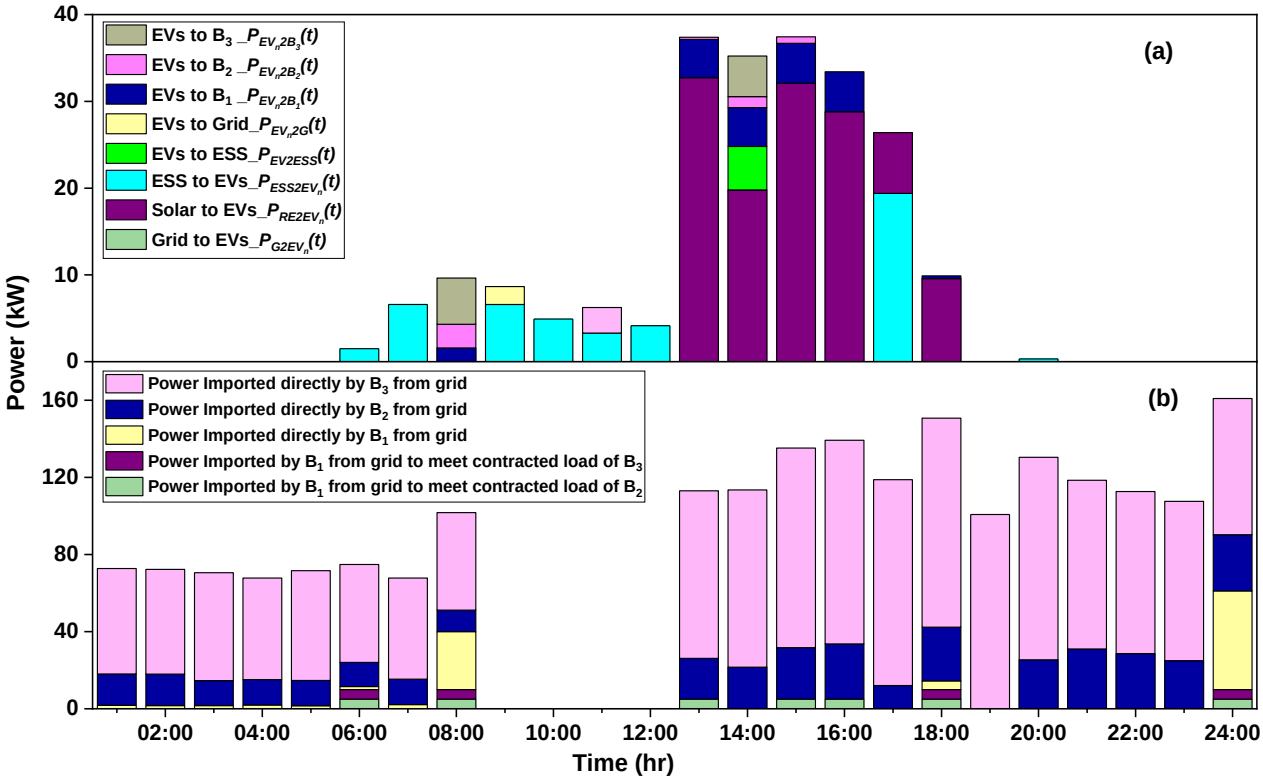

Figure 4.16 (a) Cumulative charging and discharging patterns of 15 EVs (b) Hourly power exchange between grid and B_1, B_2 and B_3.

4.7.2.2 Case 2(b)

Primary building trades with the B_2 and B_3 at an agreed-upon tariff of 80% and 60%, respectively. The contract pricing and optimal outcomes of power flows for solar PV, storage, primary and secondary buildings, and electric vehicles are shown in Figure 4.17.

4.7.2.3 Case 2(c)

Secondary buildings (B_2 and B_3) have contract tariffs of 60% and 80% of TOU pricing, respectively. The smart building's load demand is met to the greatest extent possible by local resources (solar PV and ESS), as well as power imported directly from the grid or from a fleet of electric vehicles.

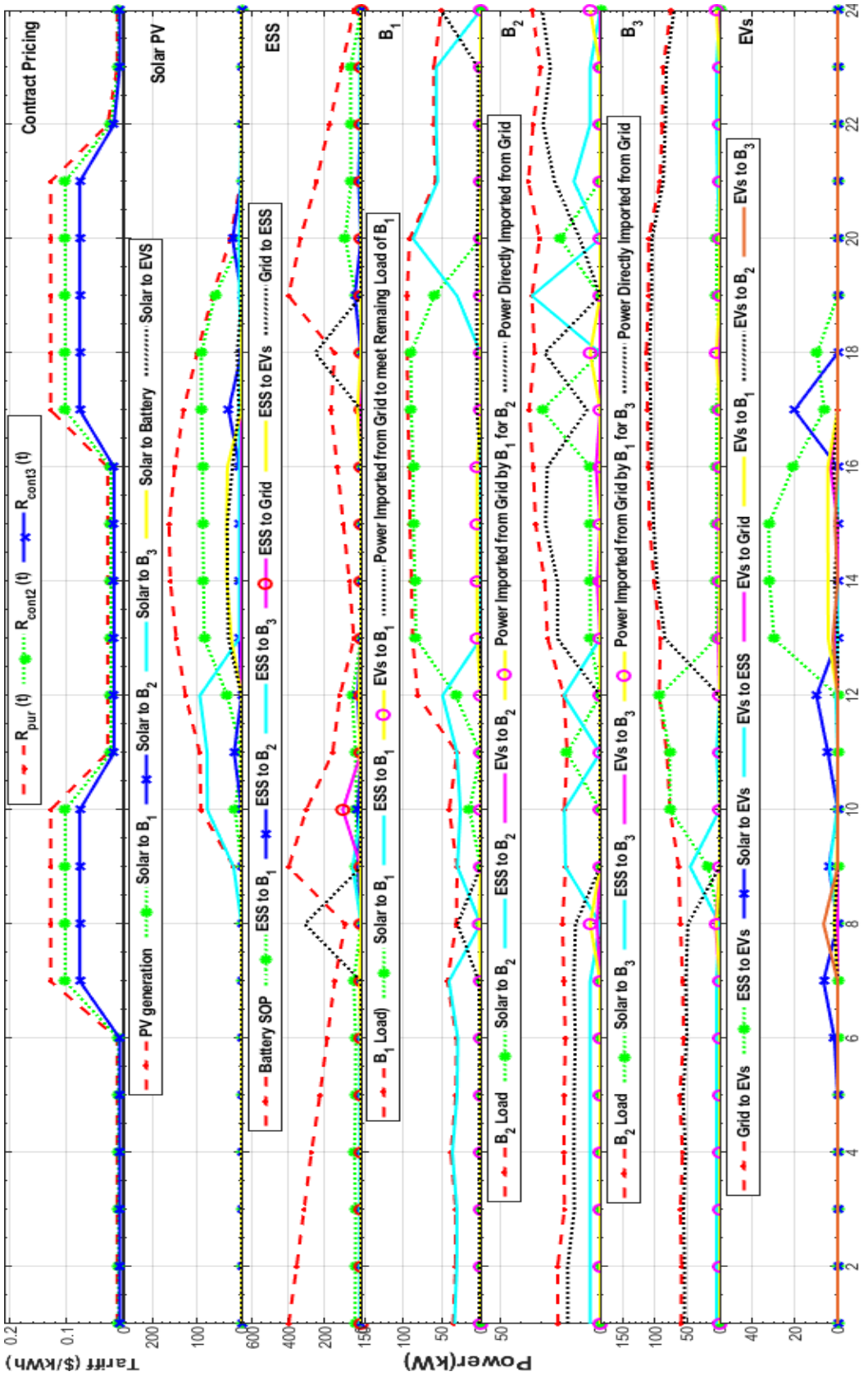

Figure 4.17 Hourly power flows among solar PV, battery, B_1, B_2, B_3 and fleet of EVs, respectively at R_{cont2} (t)> R_{cont3} (t).

4.8 Detailed Financial Analysis for Smart Building and Electric Vehicles with V2X capability

In Table 4.4, scenarios 2 and 3 analyze the modification of minimum contractual load. B_1's minimum bilateral contracted load with B_2 and B_3 is set to 5 kW and 10 kW, respectively (scenario 2), whereas B_2 and B_3's minimum bilateral contracted load with B_1 is set to 10 kW and 5 kW, respectively (scenario 3). Further, the cost of battery degradation associated with the charging and discharging of electric vehicles is incorporated in the savings of EVs. It is observed that up to 15% of EV's life is depreciated while performing V2X operations [114-116].

Table 4.4 Net revenues and savings (NZ$) daily earned by B_1, B_2, B_3 and fleet of EVs for scenarios 1, 2 and 3.

Building	Case 1 (solar PV + charging infrastructure at B_1)			Case 2 (solar PV + ESS + charging infrastructure at B_1)		
	(a)	(b)	(c)	(a)	(b)	(c)
Scenario 1						
B_1	24.1	27.6	28.3	95.4	99.4	105.6
B_2	4.2	3.4	3.0	3.6	4.2	5.5
B_3	3.0	3.4	8.6	3.6	18.0	11.3
EVs	6.5	5.4	6.3	9.4	9.4	9.4
Scenario 2						
B_1	21.8	25.4	27.4	94.9	98.2	105.4
B_2	3.2	3.3	3.3	3.04	3.6	5.7
B_3	13.1	10.4	9.5	9.9	19.9	11.6
EVs	6.5	5.7	6.3	9.4	9.5	9.4
Scenario 3						
B_1	22.7	26.8	26.4	94.9	99	104.5
B_2	6.3	4.2	6.2	3.9	4.5	7.6
B_3	9.9	8.3	8.1	9.1	18.1	10.6
EVs	5	5.4	6.9	9.4	9.4	9.5

- Table 4.4 shows that, when compared to the base case, all buildings and the fleet of 15 EVs gain revenue and save money, indicating that it is a viable business model for smart building with EV charging infrastructure. Furthermore, localized power-sharing in the neighborhood (secondary buildings) and charging of electric vehicles at the smart building's parking station help to reduce line losses and increase grid stability. The important characteristics and findings from each case and scenario are as follows:
- In case 2, the fleet of electric vehicles saves more money than in case 1 due to the use of storage for EV charging during peak hours.
- The financial advantages of each building and EVs' fleet may be computed using the formulae in Appendix C3, which can be stated as a percentage decrease in electricity bills.
- Revenues from primary buildings vary from 24% to 116%, while savings from B_2, B_3, and EVs range from 8% to 20%, 2% to 15%, and 29% to 56%, respectively.

Chapter 5

Harmonic Analysis of Grid-Connected Rooftop Solar PV Systems

Following the proposition of a novel business architecture for grid-connected solar PV in smart building in Chapters 3 and 4, technical evaluation is required for the optimal integration into the low voltage (LV) network. The large penetration of rooftop solar PV at the LV distribution grid has a significant effect on the harmonic pollution levels in the network. Power quality issues related to the low power factor of non-linear loads and high harmonic current emissions from solar PV inverters at LV network greatly affect the network's performance. The power electronic converters/inverters without producing pure sinewaves introduce harmonics into the system when connected to the LV grid. From the perspective of power quality, it is desired to obtain a pure sinusoidal waveform of current at the grid-connected PV inverter's output. However, due to the presence of power electronic inverters, harmonics may arise at the output of the inverter and travel through the distribution system's impedance and resultantly distorts the sinusoidal voltage waveform of the utility grid. Maximum power point tracking (MPPT), anti-islanding, grid fault conditions and energy measurement are the important characteristics of any grid-connected PV inverter [117]. Usually, the grid-connected residential PV systems have small to medium sizes (1 kW_p to 15 kW_p), compared to the high short circuit levels of the distribution grid. Therefore, the distortion in the system voltage is almost negligible when single PV system is connected to the grid, but when multiple connections are made at the same feeder or distribution grid, it may affect the system voltage at the point of common coupling (PCC).

5.1 State-of-the Art on the Harmonic Impacts Caused by Grid-Connected Solar PV Systems

For the power system's sustainable operation, harmonic analysis facilitates the integration of grid-connected solar PV into the system. To gauge the harmonic impacts triggered by grid-connected solar PV systems, several studies have been performed over the past few years [118-132]. Such as, Eltawil et al. [121] found that inverter failures are the most frequent incidents in grid-connected PV system. Authors recommended that PV inverters should be operated at unity power factor rather than variable power factors. [122] investigated the impact of grid-connected PV during low current flows, high values of THD_i were observed for a small-scale PV system installed at rooftop in Egypt. Harmonics are also introduced by the presence of non-linear loads and switching devices connected to the grid. The residential non-linear loads generally comprise of devices such as transformers, compact fluorescent lamps (CFL), light emitting diodes (LED), fluorescent tubes, air conditioners, inverters, mobile chargers, switch-mode power supplies (SMPS), TV, computers, and laptop chargers. SMPS are commonly present in laptops, computers, TV, and battery chargers for mobile phones.

Globally, non-linear loads in the residential settings comprise of 38-42 % of the utility loads and lighting loads vary from 40 to 70 %. Non-linear loads, when supplied with sinusoidal voltage sources, produces harmonics in the supply waveform and resultantly affect the operation of other linear devices connected to the distribution grid. Piccirilli et al. [133] considered the current distortion produced by Class-D full-wave rectifier to transfer wireless power. Corti et al. [134] proposed a precise methodology for the DC-DC converter simulation while considering the non-linear and dynamic nature of the photovoltaic device. Few studies also characterize the combined impacts of grid-connected solar PV along with the consideration of a few non-linear loads [16, 135]. However, none of the aforementioned studies characterize the potential harmonic impacts of grid-connected rooftop solar PV in the presence of diverse non-linear load profiles of residential devices. In this chapter, the load data (non-linear load penetration levels and THD_i) from a practical feeder in Lahore, Pakistan is taken as an illustration and tested on a modified IEEE-34 bus system. The utility, Lahore Electric Supply Company (LESCO), allows the residential

customers with three phase meters to install net-metering (rooftop solar PV). Therefore, in this chapter, different levels of total harmonic distortion (*THD*) produced at the point of common coupling (PCC) at LV network are investigated under the varying penetrations of three phase solar PV along with the existence of balanced single phase household non-linear loads. Various regulatory requirements and standards exist for the grid connected PV systems in terms of voltage and current distortions due to the presence of harmonics at PCC such as IEEE Std 519, IEEE Std P519a, ANSI C82.11, ANSI C82.14 and EN50160 [136]. However, in this chapter, IEEE 519-2014 standard is used as a reference for current distortion limits in the distribution grid rated from 120 V through 69 kV [137].

5.2 Adopted Methodology for the Evaluation of Three-Phase Systems

5.2.1 Typical Household Non-Linear Load with Total Harmonic Distortion

In this chapter, as discussed in the earlier section, a typical feeder of LESCO is taken as exemplification to help evaluate the total harmonic distortion in voltage (THD_v) and total harmonic distortion in current (THD_i), injected at LV network in the presence of non-linear residential loads along with grid-connected rooftop solar PV generation (net-metering). The average distribution (% age) of electricity consumption for a typical household in Lahore is characterized in Figure 5.1 [138]. Additionally, typical values of THD_i for various household appliances of a typical feeder in Lahore, along with the respective power factors and power ratings are presented in Appendix D1 [138].

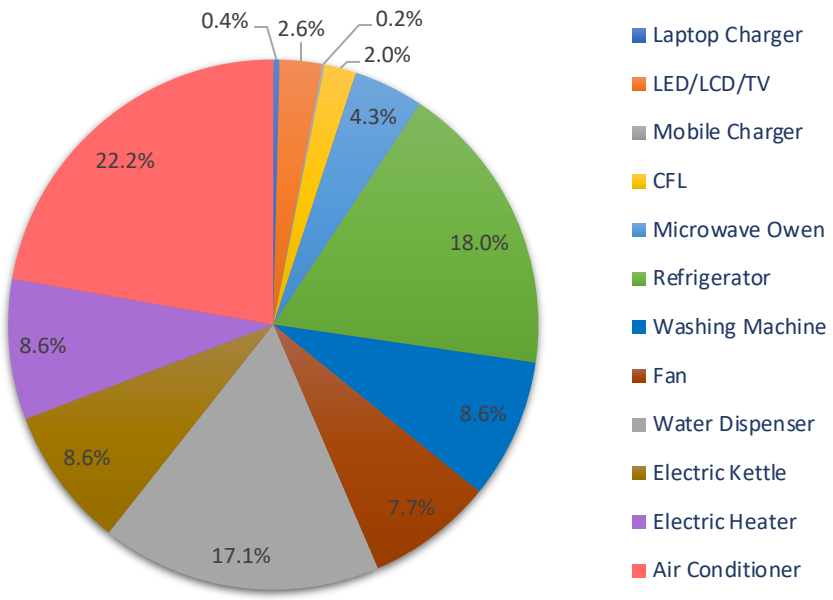

Figure 5.1 The distribution of electricity consumption for a typical (average) household in Lahore, Pakistan.

Moreover, in addition to non-linear loads, the non-linearity in the distribution grid can also be introduced by distributing harmonic sources such as non-sinusoidal waves at the output of solar PV inverters. As it stands, generally, inverters need to come with high-quality switching, producing pure sinusoidal waves. However, mostly modified sine waves of current and voltage at the output of substandard inverters pollute the LV grid. It is therefore required that the net-metering prosumers must insert the required reactive power along with the active power into the grid. Nevertheless, the residential customers do not meet the standard criterion of delivering the reactive power. Resultantly, capacitor banks or synchronous condensers are required to be installed by the utility for power factor correction at the LV grid.

5.2.2 Characteristics of Solar PV System

In order to accurately model and benchmark the harmonic pollution that can be produced due to the insertion of solar PV inverters, a real solar PV module along with the typical harmonic spectrum at the output of the inverter is used in this chapter. The specific parameters such as power rating (W), open-circuit voltage (V_{oc}), short circuit current (I_{sc}) and efficiency (η) of the solar PV module considered in the simulations at standard testing conditions (STC) are given in Table 5.1 along with the inverter specifications shown in Table 5.2.

Table 5.1 Specification of the solar PV module parameters according to manufacturer's datasheet at STC.

Parameters	Values
Manufacturer	Sharp
Type	Poly-crystalline
Model	ND-224UC1
Power (W)	224
V_{mp} (V)	29.58
I_{mp} (A)	7.45
V_{oc} (V)	36.44
I_{sc} (A)	8.25
Efficiency (η)	13.7 %
Fill Factor (FF)	73.3 %

Table 5.2 Specification of the inverter used for system evaluation.

Parameters	Values
Max. DC Power (kW)	10
Rated DC Voltage (V)	1000
Max. Input Current (A)	10
Max. AC Apparent Power (kVA)	9
Rated AC Voltage (V)	400
Max. Output Current (A)	12.9
Max. Efficiency (%)	90

Further, the *I-V* and *P-V* curves at STC for the respective module according to manufacturer's datasheet are shown in Figure 5.2. Depending upon the rooftop solar PV generation at different segments of the day and seasons of the year, distinct levels of THD_i are produced at the output of the PV inverter. Therefore, based on low and high PV generation in the winter and summer season, the harmonic spectrum of a typical PV inverter is taken from [130].

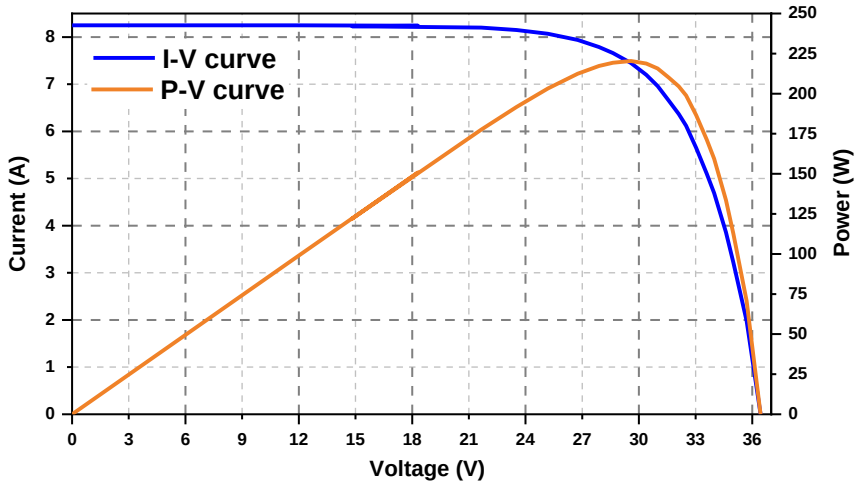

Figure 5.2 I-V and P-V curves of solar PV module at STC according to the manufacturer's datasheet.

The THD_i of the solar PV inverters with seasonal variations is given in Table 5.3. It can be observed from Table 5.3 that higher THD_i is produced for the period of low generation due to higher harmonic currents of the solar PV inverter. Further, it is considered that 4 kW_p (P_n) three-phase solar PV system (micro distributed generation, DG) can be installed at any node of a modified IEEE-34 bus distribution network. The maximum output (at non-STC) can be 3.3 kW_p and 3.1 kW_p in summers and winters, respectively. Additionally, the minimal production from solar PV during both summers and winters is taken as 0.6 kW_p.

Table 5.3 THDi (%) of solar PV inverter for each scenario based on current harmonic spectrum.

Scenario	***THD*$_i$ (%)**
Summer With High Overall Generation (S1)	7.8
Summer With Low Overall Generation (S2)	35.1
Winter With High Overall Generation (S3)	7.7
Winter With Low Overall Generation (S4)	43

5.3 Results of Voltage and Current Harmonic Spectrum for 3-Phase System

Three cases are considered in this chapter along with the base case with no rooftop solar PV installed at any of the residential houses. Simulations are performed in the 20.0.0 licensed version of the electrical transient analyzer program (ETAP). Four different cases of solar PV penetration levels are taken to compare the harmonic levels inserted at PCC.

a. Base Case: 0% solar PV
b. Case 1: 33% solar PV
c. Case 2: 50% solar PV
d. Case 3: 100% solar PV

For cases 1-3, four different scenarios are analyzed in this chapter. All the cases and scenarios are tested at single radial supply modified IEEE-34 bus distribution feeder. Additionally, to facilitate the benchmarking of *THD* limits at the LV network, high loading levels of non-linear loads are constantly assumed at each node. Further, it is assumed that the secondary side of the distribution transformer (11 kV/0.4 kV) serves as the point of common coupling (PCC). And the THD_v and THD_i of the system are observed as an overall index of harmonic pollution inserted into the LV network. The four scenarios considered are as follows:

1. Scenario 1 (S1): summer with high overall generation and high loading levels
2. Scenario 2 (S2): summer with low overall generation and high loading levels
3. Scenario 3 (S3): winter with high overall generation and high loading levels
4. Scenario 4 (S4): winter with low overall generation and high loading levels

5.3.1 0% PV Penetration (Base Case)

A reference case (base case) is taken to help evaluate the harmonic pollution with the increasing solar PV penetrations. It is assumed that no solar PV system is installed at any node in the base case as shown in Figure 5.3. The single line diagram (SLD*)* for the base case (Figure 5.3) shows

that each node has three single-phase connections with a cumulative balanced three-phase load of 6 kW.

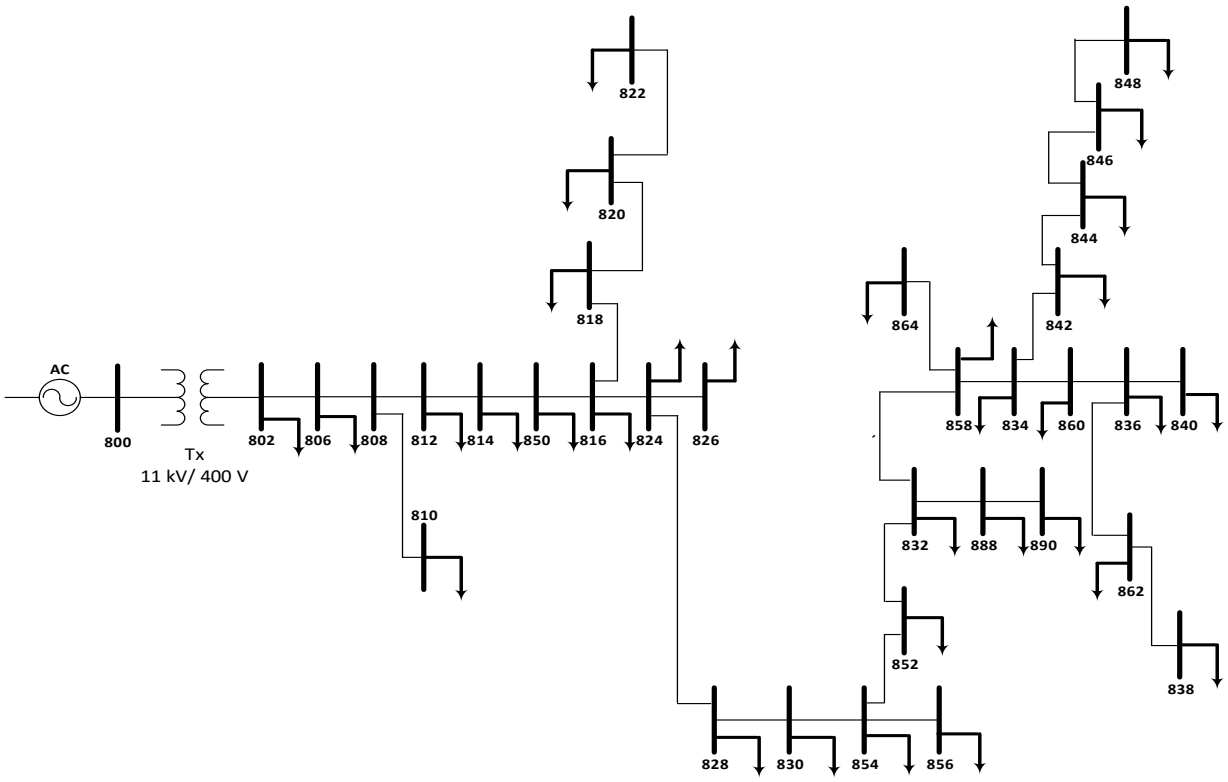

Figure 5.3 Single Line Diagram (SLD) of modified IEEE-34 bus distribution network with 0% PV penetration.

The modeling of a modified IEEE-34 bus distribution network composed of 34 sub-networks (buses) in ETAP is shown in Appendix D2. Further, Appendix D2 shows the details of each sub-network indicating the types and ratings of non-linear loads and PV panels connected. It illustrates that for each case and scenario, the loading levels are assumed to be constant i.e., loads remain in the ON-state throughout the simulations. However, only one of solar PV system out of four types (scenarios) can be assumed to be in ON-state for a particular scenario. The rest of the three PV panels are taken to be operated in the OFF-state depending upon the respective scenario. Also, depending upon the specific case, it is possible that all four PV systems may operate in the disconnected mode (OFF-state). For instance, each of the PV panels operates in OFF-state for the base case.

The per unit (p.u.) voltage profile at each bus for the reference case is shown in Figure 5.4 (a). It shows that the buses near the distribution transformer i.e., 802-830 operate as marginally loaded (p.u. voltage under 0.98) whereas the far end buses i.e., 832-890 except 850, are operating as critically loaded (p.u. voltage below 0.95). Also, the voltage and current spectrum of harmonics along with THD_v and THD_i inserted at the PCC is shown in Figure 5.4(b). It can be observed from the Fig. that THD_v level at PCC (6.6%) is well under safe operating standards (8.0%) when compared to the IEEE standards. However, the THD_i level at PCC (8.8%) is marginally above the IEEE benchmarks (8.0%) due to the high diffusion of non-linear household loads in the network. Additionally, the voltage and current waveforms at PCC for a complete cycle is shown in Figure 5.4 (c). It signifies that both the waveforms are distorted due to the high percentage of harmonic levels. Further, the percentage of active, reactive, and complex power losses in reference to total load in the distribution network is listed in Table 5.4. It signifies that reactive power losses (kVar) are almost double the of active power losses (kW) due to the poor power factor of some non-linear devices such as mobile and laptop chargers, CFL, LCD, refrigerator etc. Henceforth, it can be observed that there is a decent margin of improving the overall voltage profile along with a reduction of complex power losses through the integration of micro distributed generation (cases 1, 2 and 3).

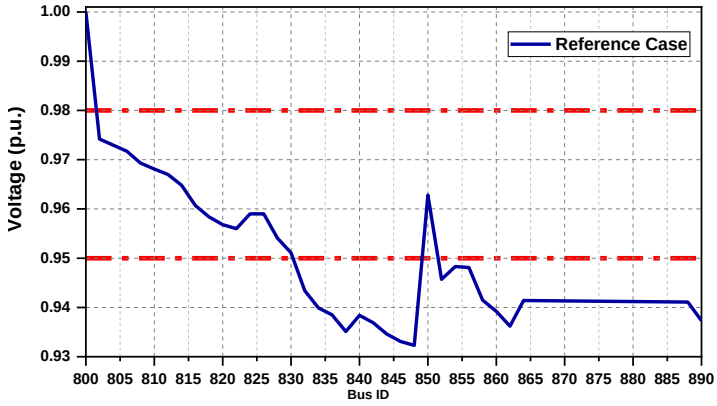

(a)

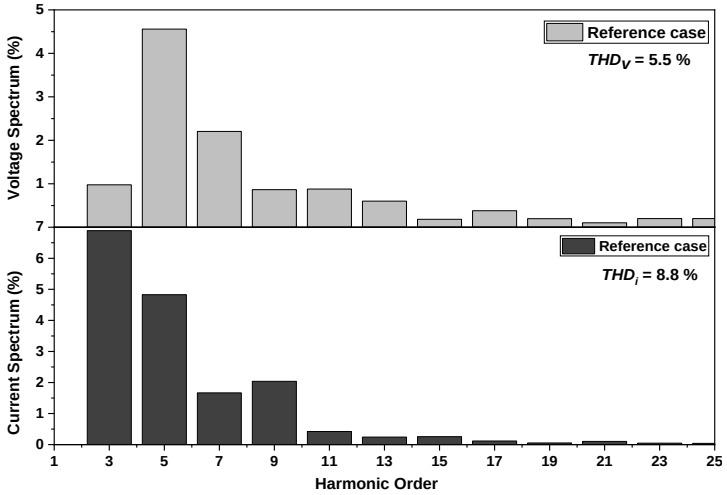

(b)

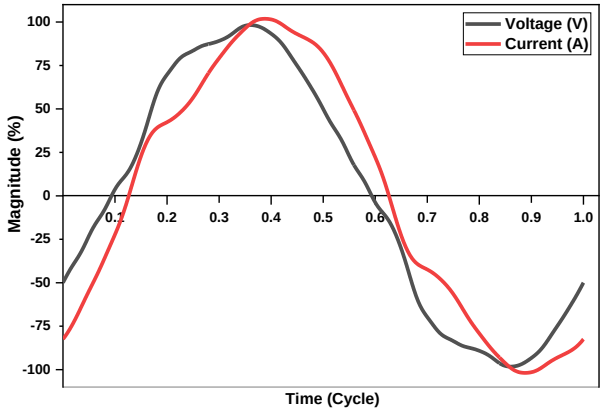

(c)

Figure 5.4 (a) Per unit (p.u.) voltage profile of the system (b) voltage and current spectrum with respect to harmonic orders at PCC (c) voltage and current waveforms at PCC.

Table 5.4 Total active (kW), reactive (kVar) and complex power loss (kVA) for the reference case in percentage (% age) of the total load of the network (%).

Type	Power Loss
Active (kW)	3.13
Reactive (kVar)	5.8
Complex (kVA)	6.6

5.3.2 33% PV Penetration (Case 1)

In this case, it is considered that 33% of the nodes are installed with rooftop solar PV, shown in Appendix D3. The per unit (p.u.) voltage at each bus for the four scenarios of case 1 shows that for scenario 1 and 3 (PV panels with overall high generations i.e., 3.3 kW_P and 3.1 kW_P during summers and winters, respectively), fewer buses are critically loaded (15 buses i.e., 832-848 and 858-890) as compared to the reference case (18 buses). However, for scenarios 2 and 4 (due to an overall low generation of 0.6 kW_p both during summers and winters), the voltage profiles of the buses remain fairly similar to case 0. Additionally, the harmonic spectrums of voltage and current at PCC for scenarios 1-4 shows that the total harmonic distortion (THD_v and THD_i) levels at PCC gets raised due to the insertion of harmonics at the output of PV inverters. The highest amount of current distortion (THD_i = 9.3%) is noted in scenario 1 with high generation during the summer season, illustrating that the current distortion increases with the power production at the output of the PV inverter.

5.3.3 50% PV penetration (Case 2)

The single line diagram (SLD*)* for case 2 is shown in Figure 5.5. It shows that 50% of the buses are connected with three-phase solar PV systems. 4kWp rooftop PV systems are installed at alternate buses along with the presence of three single-phase non-linear household connections at each node. The per unit (p.u.) voltage profile of the distribution network for case 2 during four scenarios is shown in Figure 5.6. It shows that for scenario 1 (PV panels with overall high generations of 3.3 kW_P at 50% buses), only four buses i.e., 838, 844, 846 and 848 are critically loaded. Similarly, for scenario 3 (50% buses installed with generations of 3.1 kW_P), only five buses

remain critically loaded i.e., 838, 844, 846, 848 and 862. Nevertheless, for scenarios 2 and 4, fourteen buses are critically loaded while others remain marginally loaded. It can be explained due to low DG at 50% of the buses (0.6 kW_P), resulting in more buses with critical loading.

Additionally, the voltage and current waveforms for each scenario of case 2 is shown in Figure 5.7. It shows that the highest distortion in the current and voltage waveforms is observed during scenario 1 and scenario 3. Further, the harmonic spectrums at PCC for scenarios 1-4 are shown in Figure 5.8 (a-b). Figure 5.8 (a) shows that during summers with the maximum generation, the highest levels of current distortion (10.2%) at PCC are observed due to higher harmonic currents from the PV inverter. The maximum amount of voltage distortion (5.2%) is seen in scenario 3 with high generation (3.1 kW_p) during the winter season, as shown in Figure 5.8 (b). It can be observed that during scenario 1, the voltage profile of the network gets better since only 4 out of 34 buses are under critical loading conditions along with the total harmonic distortion (THD_i and THD_v) values under acceptable limits according to IEEE-standards. Hence, this type of setting with solar PV generation installed at every other bus can be the optimal choice for rooftop grid-connected photovoltaic systems.

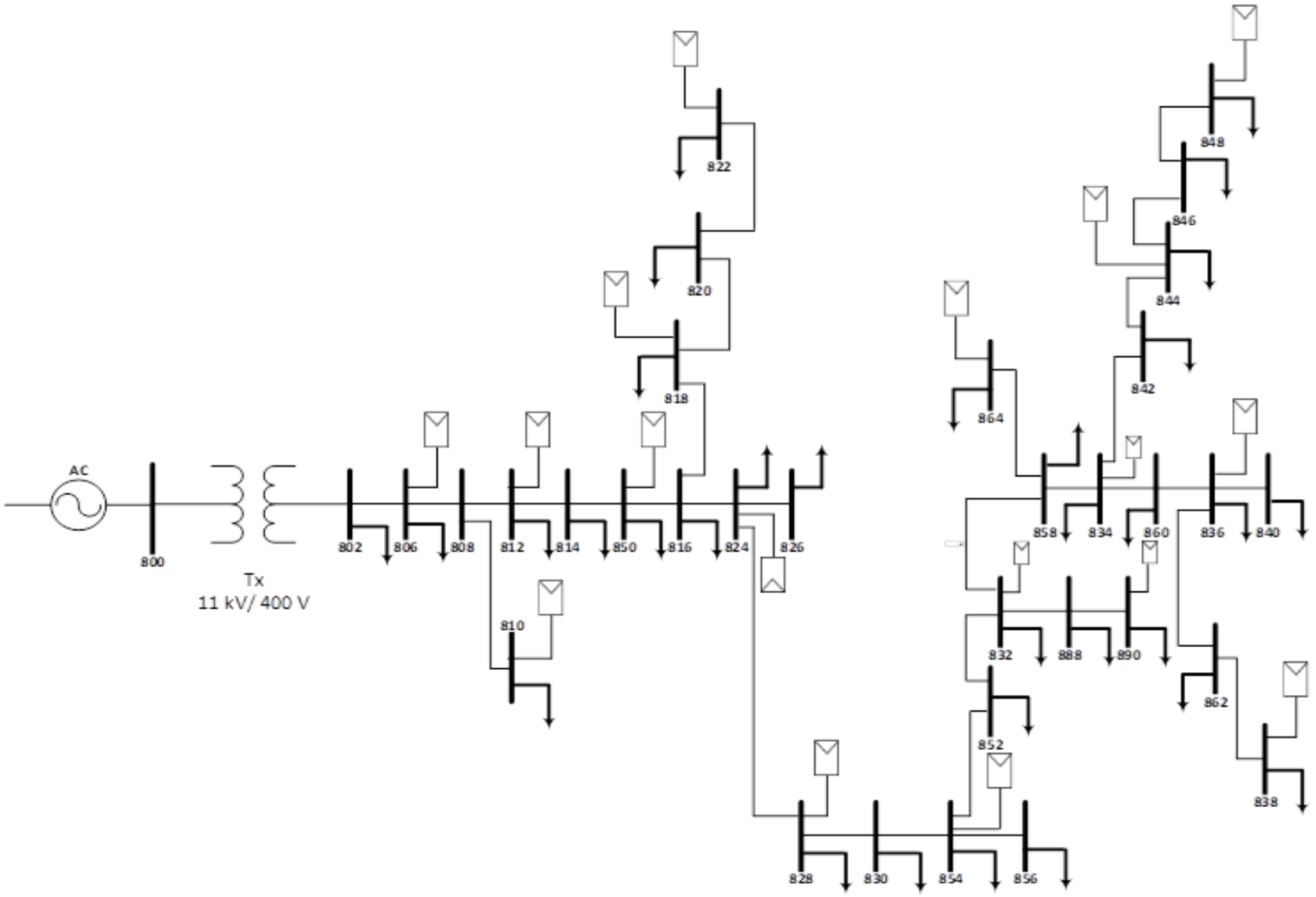

Figure 5.5 Single Line Diagram (SLD) of modified IEEE-34 bus distribution network with 50 % PV penetration.

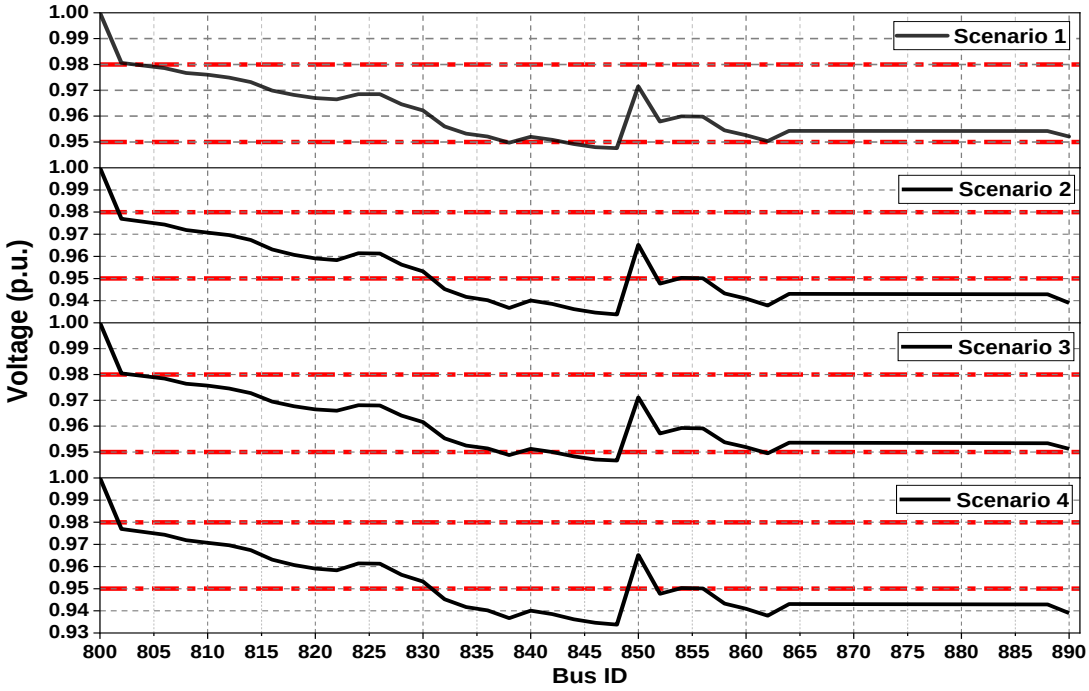

Figure 5.6 Per unit (p.u.) voltage profile of the system for scenario 1-4, respectively of case 2 (50% PV penetration).

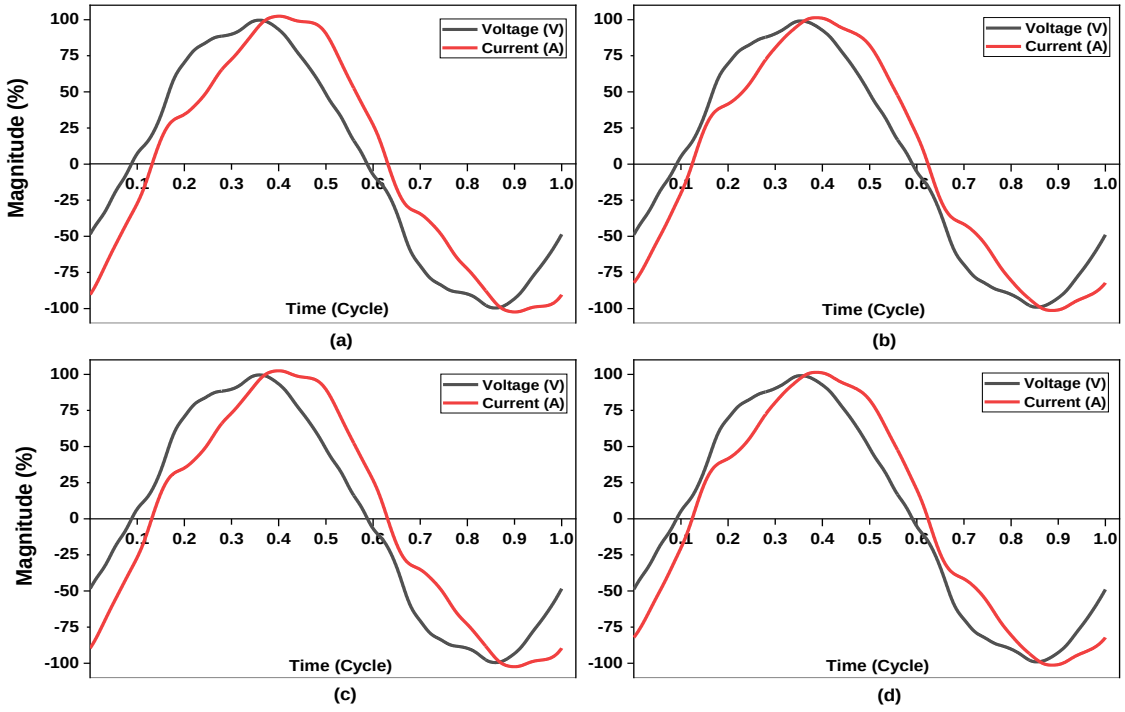

Figure 5.7 Voltage and current waveforms at PCC for a complete cycle for scenario 1-4, respectively of case 2 (50% PV penetration).

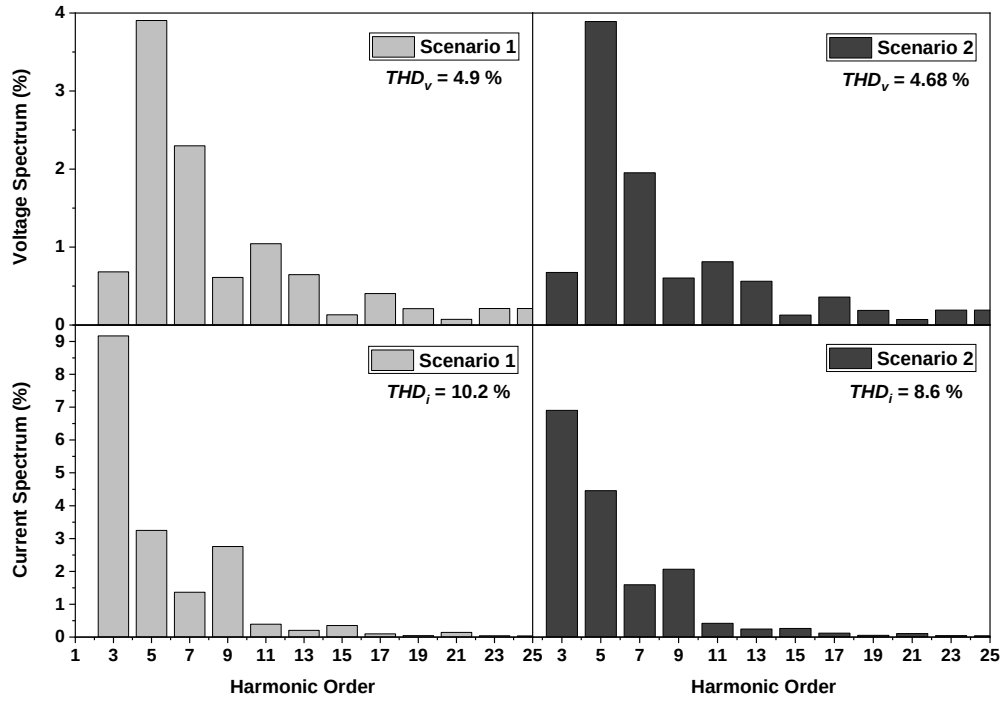

(a)

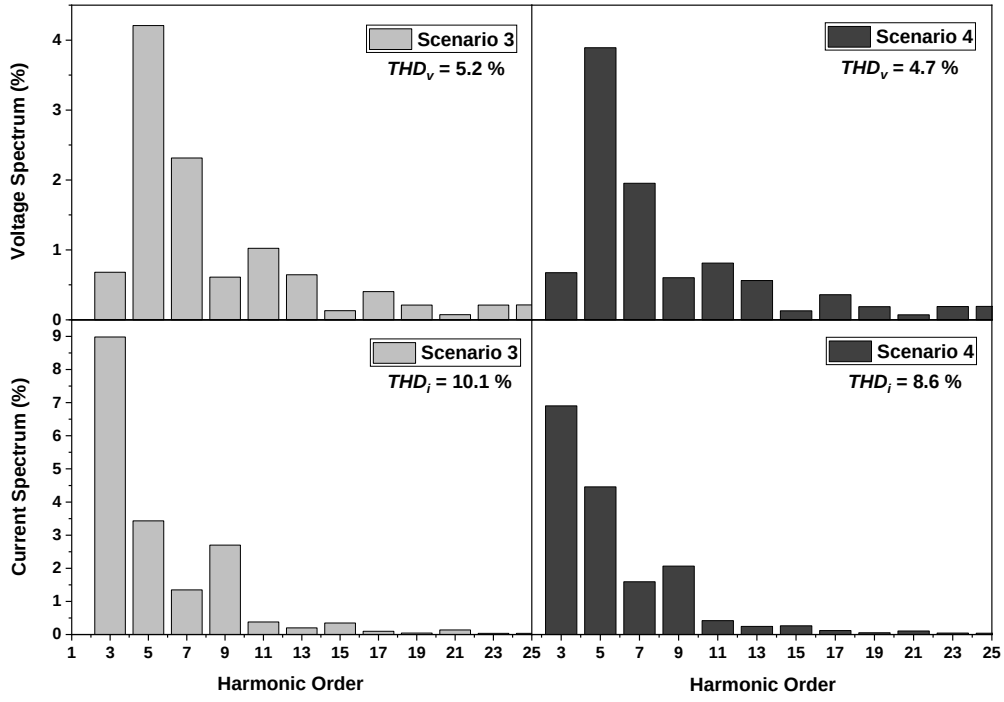

(b)

Figure 5.8 Voltage and current harmonic spectrum along with THDv and THDi at PCC for case 2 in the distribution network in (a) scenario 1-2 and (b) scenario 3-4.

5.3.4 100% PV Penetration (Case 3)

Lastly, it is considered that all buses have the deployment of 4 kW_p solar PV system (case 3). The SLD for case 3 shown in Appendix D3 indicates that each node has a solar PV system plus three single-phase residential connections. Henceforth, each node has a distributed generation of 4 kW_p and a cumulative load of 6 kW with non-linear characteristics. The voltage profile of the system for case 3 shows that for scenarios 1 and 3, none of the buses are critically loaded. Also, few buses adjacent to the distribution transformer i.e., 802-810 do not operate as marginally or critically loaded, rather the p.u. voltages are close to unity. However, during the low generation period for scenario 2 and 4, around half of the buses (far end buses) operate in the critically loaded condition (p.u. voltage less than 0.95. Also, the highest amount of distortions in the current and voltage waveforms are seen in scenario 1 and scenario 2, respectively. Furthermore, the harmonic spectrums at PCC for scenarios 1-4 shows that the highest levels of total harmonic distortion in voltage and current waveform, THD_v and THD_i, at PCC are observed as 14.5% and 4.3%, respectively. This level of THD_i is significantly greater than the IEEE-limits i.e., 8% at PCC; therefore, this case cannot be considered as an optimum choice in terms of grid-connected rooftop solar PV installations.

5.3.5 Detailed Power Loss Analysis

The summary of active, reactive, and apparent power losses for all cases and scenarios is discussed in Table 5.5. It shows that the maximum and minimum amount of percentage power losses with reference to total load at the LV network are obtained for case 1 and case 3, respectively. Intermediate levels of power losses are observed during case 2 with 50% PV penetration levels for all scenarios. Added to the reflections, the highest amount of percentage power losses is noted during scenarios 2 and 4 when generation levels are low. Hence, it is suggested that the losses in the LV network can be minimized through the high penetration levels of distributed generation (DG) with high generation levels. However, the harmonic pollution levels at PCC also get raised with incoming solar PV inverters' saturation.

Table 5.5 Summary of total active (kW), reactive (kVar) and apparent power loss (kVA) in percentage (% age) of total load of the network.

Type of Power Loss	**Reference Case (Case 0)**	**Case 1**				**Case 2**				**Case 3**			
		S1	S2	S3	S4	S1	S2	S3	S4	S1	S2	S3	S4
Active	3.13	2.2	3.1	2.3	3.3	1.9	3.3	2.0	3.3	0.9	3.3	1.0	3.3
Reactive	5.8	4.2	5.9	4.3	4.6	2.6	4.6	2.8	4.6	1.3	4.6	1.4	4.6
Apparent	6.6	4.8	6.7	4.9	5.7	3.3	5.7	3.4	5.7	1.6	5.7	1.7	5.7

Chapter 6

Conclusions and Perspectives

This thesis makes a contribution to modern power system operations by proposing a comprehensive and profitable power sharing mechanism between the inter-connected buildings. The main findings and future research directions are summarized in this chapter.

6.1 Overview of Contributions

This thesis first addressed the installation of optimum rooftop solar PV technology for buildings under low irradiance and partial shading conditions. Starting with **[Paper A/Chapter 2]**, the low irradiance loss for CdTe thin film panels (TFP) is explicitly quantified in this thesis and then compared with crystalline silicon (c-Si) PV panels. Detailed analysis of results based on sparse data at 1-hr interval shows that c-Si panel produces annually on average of 1.05% lower yield compared to CdTe panels for four consecutive years i.e., 2011-2014 available from NREL. Additionally, measured insolation values for 8 days, combined for winter and summer, shows 1.09 % higher energy yield for CdTe based PV systems compared to c-Si due to their higher bandgap and better spectral response at lower irradiances. Overall, it is suggested that TF solar PV modules perform better under low irradiance conditions and are very suitable for regions with larger irradiance variations. To further facilitate the selection of accurate solar PV technology for large-scale rooftop deployments, in **[Paper B/Chapter 2]**, a fair comparison is made between the TF and c-Si solar PV modules under partial shade. It is concluded that the performance of TF panels is better under partial shading conditions as compared to c-Si panels. Higher hotspots are formed in c-Si solar panels, which are confirmed by the thermographic analysis under realistic operating conditions. Furthermore, the power output during shading for a typical system is higher for the TF panel in comparison to the c-Si panels due to the internal structure, where cells are monolithically integrated and have long rectangular structure. This inherent orientation and

superior junction properties in TF modules lead to the high potential tolerance levels during the events of extreme shading scenarios, which has been revealed in this paper. Therefore, lower hot spot damages are practically observed in TF PV modules, as validated through the thermal images.

We further presented a comprehensive architecture for the profit maximization of inter-connected buildings, with one of the buildings installed with rooftop solar PV and storage. In **[Paper C/Chapter 3]**, we established a new framework to maximize profits linked with the installation of rooftop solar photovoltaics coupled with energy storage system at commercial/industrial/educational buildings. Based on the diversified load nature of secondary building(s), minimum contracted load can be bilaterally decided between the primary and secondary buildings. The proposed model is universal and applicable to agreed contracts and condition(s). The utility of the model is demonstrated via application to three participating buildings along with the actual time-of-use pricing. Profits of the primary and secondary buildings are assessed based on varying contracted rates and minimum agreement loads. It is concluded that nature of bilateral contracts, time-of-use utility tariffs, diverse nature of load profile, amount of minimum contracted load and contract rates between primary and secondary buildings are the key parameters that affect the overall profits of each building. For the scenarios discussed in **[Paper C/Chapter 3]**, the profits of primary building (B_1 with rooftop solar PV and storage) varied from 10-43% depending upon the minimum contracted load and tariffs. Secondary buildings without solar or storage (B_2 and B_3) can also make significant cost saving in terms of reduced electricity payments to the utility. The overall saving secured varied from 6-16% and 3-12% for B_2 and B_3, respectively in the current framework of minimum contracted load and prices. The addition of lithium-ion storage raised the profits of primary building around 25% for each scenario in comparison to solar PV only case. The presented framework targeted a more integrated approach to utilize solar and storage through bilateral contracts and net-metering for multiple agents/building resulting in improved economics for involved parties in comparison to business as usual i.e., grid only option. It is suggested that the developed framework enables and promotes inter-connected buildings to invest in rooftop solar in a more lucrative manner,

especially in the countries with vast solar resource and diminishing feed-in-tariffs or net-metering benefits.

To facilitate the integration of electric vehicles (EVs) in smart building, we developed a framework in **[Paper D/Chapter 4]**. It allowed the EV integration at a lucrative rate (1.25x of grid TOU price) and allows daily earnings of around 50 % for the primary building (B_1) and up to 14 % for secondary buildings (B_2 and B_3), respectively. The profits of B_1 increased by further 30 % after the inclusion of storage (Li-ion battery banks) due to its optimum power scheduling during peak hours. The proposed business architecture can be applied to *N* buildings with any single building owning the solar photovoltaic-battery system and charging infrastructure for EVs (primary), having bilateral contracts with remaining of *N-1* buildings (secondary).

Towards the introduction of vehicle-to-everything (V2X) concept in smart building, in **[Paper E/Chapter 4]**, we proposed a new framework for maximizing financial gains associated with the deployment of rooftop solar photovoltaics combined with energy storage systems and charging stations (a fleet of EVs) in smart building. It is suggested that model is generic and is pertinent to suitable pricing and load contracts. The model's effectiveness is illustrated by its deployment to three buildings and a fleet of fifteen electric vehicles in conjunction with the actual time-of-use pricing. It is concluded that the design of bilateral contracts, time-of-use tariffs, the varied nature of load profiles, the volume of minimum negotiated load, contract prices between primary and secondary buildings and charging and purchasing rates for the electric vehicles are the main criteria that influence the profits and savings of each building and fleet of electric vehicles. The dependency of EVs on the grid gets significantly reduced due to optimized charging through solar or storage. Further, it is determined that the profits of primary buildings (with rooftop solar PV, storage and charging infrastructure) range from 2 – 62% based on the minimum agreement load, contract tariffs and selling and purchasing tariff for the electric vehicle. The electricity cost savings of secondary buildings (without solar, storage and charging station) ranged from 8 – 20% and 2 – 15% for B_2 and B_3, respectively. The financial gains of the fleet of EVs varied from 35 – 66% based on the charging and selling tariff structure and availability of local resources (solar and storage) for charging of the electric vehicles. The profits of B_1 (primary building), B_2(secondary building), B_3 (secondary building) and EVs increased around 54%, 4%, 6% and 20%, respectively,

with the addition of storage besides the availability of solar PV and charging station. It is suggested that, the proposed paradigm aims for a more unified methodology to using solar and storage through bilateral contracts for multiple buildings and optimized charging and discharging of electric vehicles in the charging station.

Concerning the power quality issues attributed to the installation of rooftop solar PV panels, **[Paper F/Chapter 5]** identified the optimized arrangement of grid-connected solar PV panels. We characterized the potential harmonic impacts of grid-connected rooftop solar PV in the presence of diverse non-linear load profiles of residential devices for a weak grid. The performance of the low voltage (LV) network is benchmarked based on the penetration levels of solar PV, varying from low (0%) to high (100%) with the different seasonal generations along with the real load data. The total harmonic distortion in current and voltage waveforms (THD_v and THD_i) at the point of common coupling (PCC) is compared to IEEE-2014 standards and observed as overall harmonic index pollution. We modelled an off-the shelf inverter typically used in the rooftop solar PV installations. It is concluded that case 2 serves as the optimum case with the installation of solar PV panels at alternate buses (50% PV penetration) of the distribution system. The highest THD_i and THD_v with values 10.2% and 5.2% respectively, are reasonably comparable to the IEEE-benchmarks (8% both for THD_v and THD_i). Additionally, the system's voltage profile gets improved with significantly reduced losses of 1.9%, 2.6% and 3.3% for active, reactive, and apparent power, respectively compared to the base case. It is suggested that the integration of rooftop solar PV panels at alternated nodes of the modified IEEE-34 bus system improves both the voltage profile and minimize the power losses along with the compliance of *THD* limits as per IEEE-standards.

6.2 Future Research

The major findings of this thesis stimulate several future research directions concerning a paradigm shift towards a techno-economic model with bilateral contracts in smart building(s).

Towards the identification of optimum solar PV technology under low irradiance, the uncertainty in the measured irradiance values is not assessed. It is generally linked with the measurement

accuracy and it can be considered while evaluating the energy yield of crystalline silicon and thin film PV panels under low irradiance.

The profits maximization of multiple buildings in bilateral contracts is studied without explicitly accounting for the uncertainties and variabilities in the inputs of the model. The impact of uncertainties in load demand forecast, solar variation and utility pricing can be evaluated further for online solutions. A stochastic model dealing with the uncertainties in the inputs of the model will serve as a more generic model with regards to the its implementation in the real-world. The cost of battery degradation has not been incorporated in the proposed model; however, it can be considered for accurate evaluation of the profit margins. Further, a hardware-in-loop (HIL) setup can be considered for the experimental validation of the results as a future research thread. Also, a more comprehensive and precise models can be used to find the arrival times and initial state-of-power of the fleet of electric vehicles. This drives the research on the development of a stochastic model which caters for uncertainties in the inputs of the model.

On terms of maximizing the efficiency of grid-connected rooftop solar PV systems in low-voltage networks, a potential area of research is to perform the simulations for a complete day with a granularity of 1-hr. The model should incorporate the solar variations throughout the day, resultantly producing different amount of total harmonic distortions in voltage and current at point of common coupling for the whole course of day. Further, the presented framework can be applied to multiple feeders in the low voltage network as future investigations. The load dynamics depending upon the feeder's nature may affect the overall harmonic pollution inserted into the distribution network.

Lastly, towards the implementation of local electricity markets and competitive trading bilateral contract market (CTBCM) model in Pakistan, the existing legal and regulatory architecture needs to be adjusted accordingly. In this regard, some of the issues that need to be investigated further includes, i) a comprehensive government level policy for the establishment of a wholesale electricity market and the beginning of commercial operations, ii) the market rules, which regulate the market operator's functions and represent the different sorts of participants and service providers, iii) the commercial code and iv) grid code.

Appendix A1

The measured values of irradiance for four winter and summer days are shown in Figs. A1(i) and A1(ii), respectively.

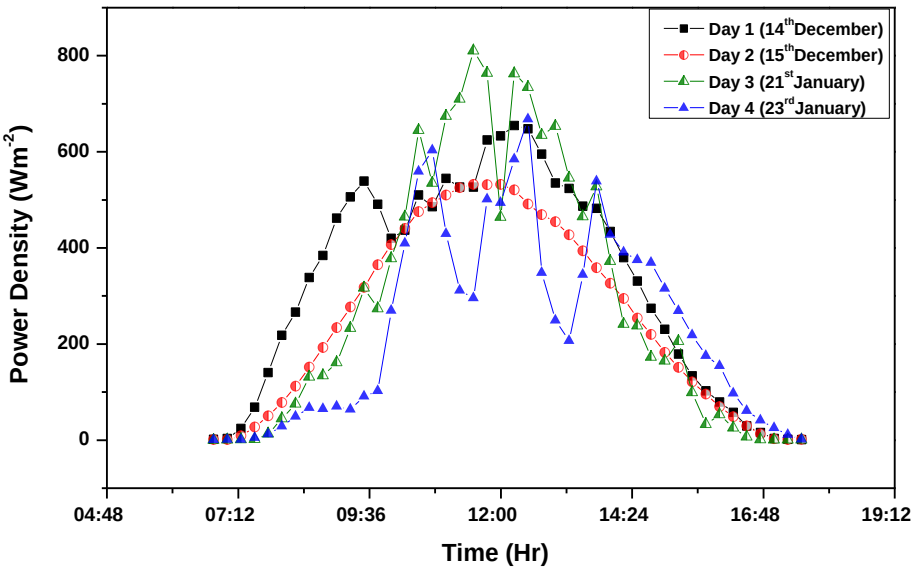

Figure A1(i) Measured irradiance values for 4 winter days.

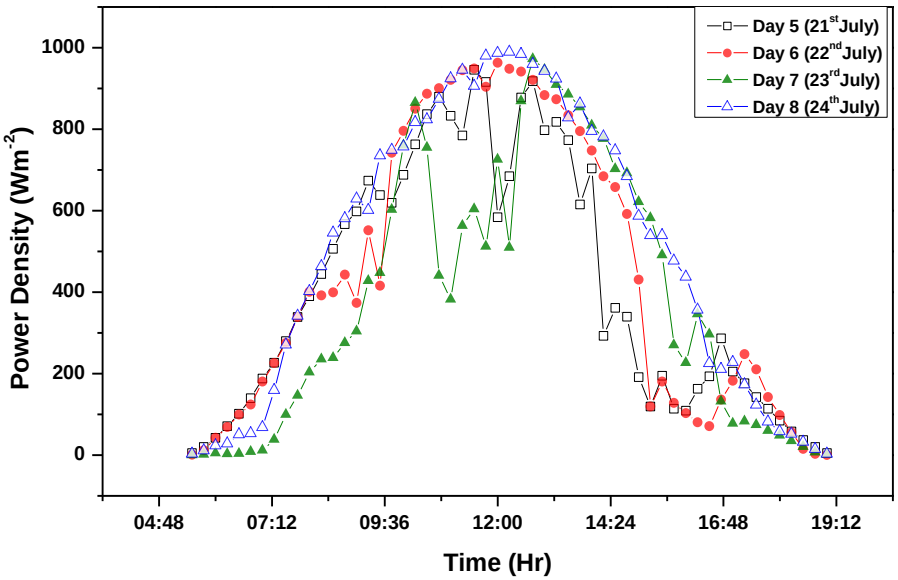

Figure A1(ii) Measured irradiance values for 4 summer days.

Appendix A2

The ideal energy yield and actual energy yields of Si and CdTe for four years are given in Table A2(i).

Table A2(i) Ideal energy available under STC and annual percentage difference between the two energy productions for c-Si and CdTe under low irradiance for all years (2011-2014).

Year	E_{STC}, Ideal Energy Available (kWhr/kW) for Whole Year	E_L(Si), Energy Yield of Si (kWhr/kW) for Whole Year	E_L(CdTe), Energy Yield of CdTe (kWhr/kW) for Whole Year	Annual Energy difference of c-Si compared to Ideal ($\Delta E/E_{STC}$ (%))	Annual Energy difference of CdTe compared to Ideal ($\Delta E/E_{STC}$ (%))
2011	1782.7	1736.3	1754.9	2.60	1.56
2012	1827.1	1781.2	1799.6	2.51	1.51
2013	1784.7	1738.6	1757.0	2.58	1.55
2014	1797.2	1751.2	1769.6	2.55	1.54
Total	7191.7	7007.3	7081.1	2.56(Avg.)	1.54(Avg.)

The additional energy yield from CdTe for four years under low irradiance is given in Table A2(ii).

Table A2(ii) Additional production output of CdTe for all years (2011-2014) under low irradiance.

Year	Energy Yield of Si ($kWhr/kW_{pk}$) for Whole Year	Energy Yield of CdTe ($kWhr/kW_{pk}$) for Whole Year	Additional Production Output of CdTe (%)
2011	1736.3	1754.9	1.07
2012	1781.2	1799.6	1.03
2013	1738.6	1757.0	1.05
2014	1751.2	1769.6	1.05
Total	7007.3	7081.1	1.05(Average)

Appendix B1

Hourly actual load demands of building 1 (primary) and buildings 2 and 3 (secondary) are shown in Figs. B1(i), B1(ii), and B1(iii), respectively.

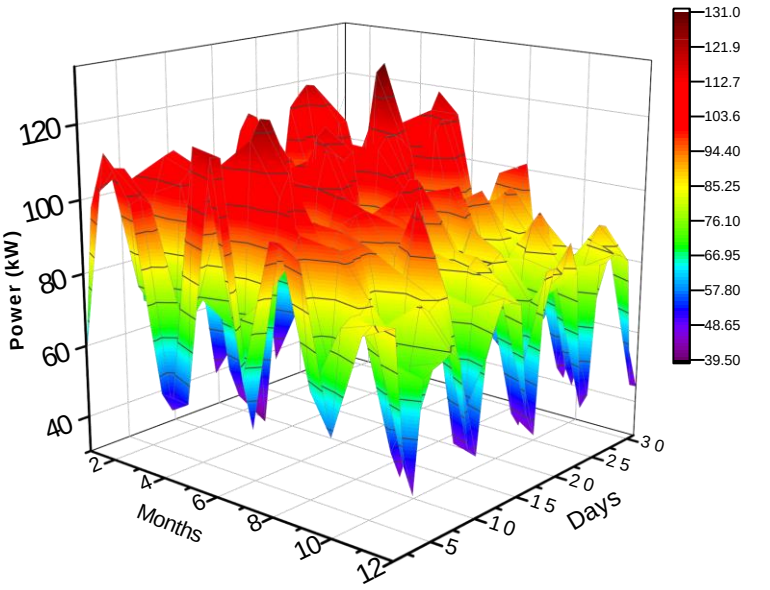

Figure B1(i) Annual real-time hourly load demand (kW) for building 1.

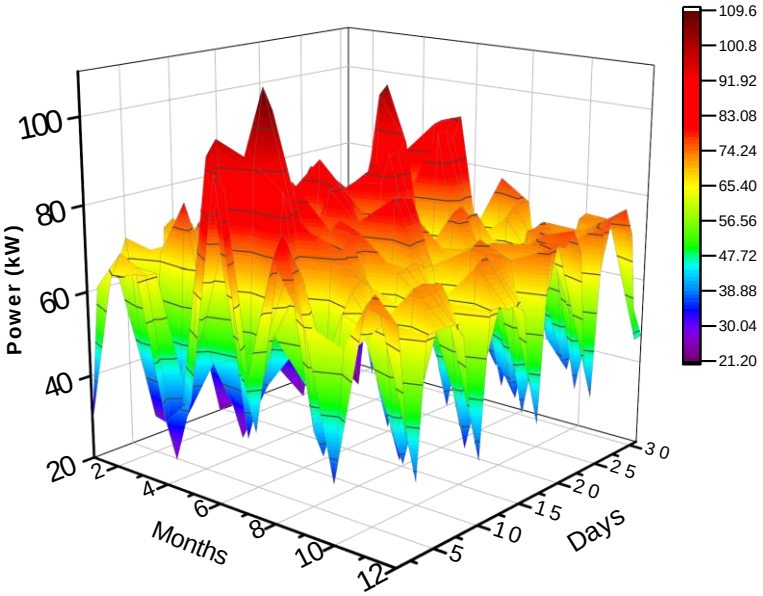

Figure B1(ii) Annual real-time hourly load demand (kW) for building 2.

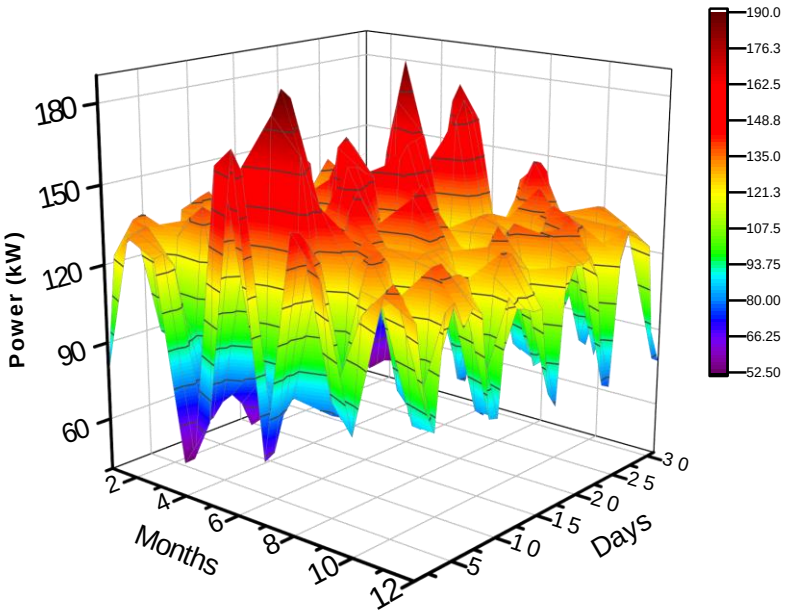

Figure B1(iii) Annual real-time hourly load demand (kW) for building 3.

Appendix B2

The annual payments and revenues (NZ$) for each sub-case are listed in the respective tables (B4(i)-B4(iii) for each building (primary and secondary).

Table B4(i) Annual financial analysis of Building 1 (B_1).

Type of Annual Payments/ Revenue	**Reference Case**		**Case 1**		**Case 2**	
Payments to the utility by B_1 for electricity units procured (C_{B_1}) (NZ$)	$C_{B_1}^0$	a. 48,710 b. 48,710 c. 48,710	$C_{B_1}^1$	a. 43,729 b. 52,044 c. 54,520	$C_{B_1}^2$	a. 19,308 b. 37,060 c. 44,841
Remarks	The payments to the grid are highest in case 1 since B_1 has to buy additional units from the grid to meet the contracted load demand of B_2 and B_3.					
Revenue of B_1 from power exports to the grid (N_G) (NZ$)	N_G^0	a. 0 b. 0 c. 0	N_G^1	a. 70 b. 70 c. 70	N_G^2	a. 277 b. 277 c. 277
Remarks	As in reference case there is no local generation or storage, there are no earnings from exports to the grid. Earnings as a result of exports to the grid are also given for case 1 and case 2.					

Revenue of B_1 from power exports to Building 2 (D_{B_2}) (NZ$)	$D^0_{B_2}$	a. 0 b. 0 c. 0	$D^1_{B_2}$	a. 3,479 b. 8,963 c. 3,325	$D^2_{B_2}$	a. 4,736 b. 16,763 c. 3,603
Remarks	In reference case there is no contract of B_2 with B_1, hence revenue is zero. For the other two cases the amounts vary based on contract prices as described earlier.					
Revenue of B_1 from power exports to Building 3 (D_{B_3}) (NZ$)	$D^0_{B_3}$	a. 0 b. 0 c. 0	$D^1_{B_3}$	a. 7,257 b. 6,762 c. 13,885	$D^2_{B_3}$	a. 9,335 b. 7,957 c. 25,775
Remarks	Again, the revenue is zero in reference case due to no contract of B_3 with B_1. However, the revenue from selling to B_3 is higher in case 2 compared to case 1 due to storage availability in case 2. In addition, for 2(c), highest revenue is attained due to higher contract prices.					
Net revenue of B_1 (NP_{B_1}) (NZ$)	$NP^0_{B_1}$	a. 0 b. 0 c. 0	$NP^1_{B_1}$	a. 11,539 b. 13,945 c. 15,413	$NP^2_{B_1}$	a. 31,508 b. 35,853 c. 38,314
Remarks	The profit earned by B_1 is highest in case 2(c), owing to more usage of battery during peak hours.					

Table B4(ii) Annual financial analysis of Building 2 (B_2).

Type of Annual Payments/ Revenue	**Reference Case**		**Case 1**		**Case 2**	
Payments by B_2 to the utility for electricity units procured (C_{B_2}) (NZ$)	$C^0_{B_2}$	a. 35,479 b. 35,479 c. 35,479	$C^1_{B_2}$	a. 29,680 b. 20,541 c. 29,938	$C^2_{B_2}$	a. 27,586 b. 7,541 c. 29,473
Remarks	The payments to the utility are least in case 2, since the units bought from the grid are minimum.					
Payments to B_1 by B_2 for electricity units purchased from B_1 (D_{B_2}) (NZ$)	$D^0_{B_2}$	a. 0 b. 0 c. 0	$D^1_{B_2}$	a. 3,479 b. 11,951 c. 3,325	$D^2_{B_2}$	a. 4,735 b. 22,351 c. 3,603
Remarks	B_2 earnings are highest in case 2 due to maximum import of units from B_1.					
Net revenue earned by B_2 (NP_{B_2}) (NZ$)	$NP^0_{B_2}$	a. 0 b. 0 c. 0	$NP^1_{B_2}$	a. 2,319 b. 2,987 c. 2,217	$NP^2_{B_2}$	a. 3,157 b. 5,587 c. 2,402
Remarks	The highest profit is earned by B_2 in case 2(b) regardless of the higher contracted rates with B_1.					

Table B4(iii) Annual financial analysis of Building 3 (B_3).

Type of Annual Payments/ Revenue	**Reference Case**		**Case 1**		**Case 2**	
Payments to the utility by B_3 for electricity units procured (C_{B_3}) (NZ$)	$C^0_{B_3}$	a. 69,434 b. 69,434 c. 69,434	$C^1_{B_3}$	a. 57,339 b. 58,164 c. 46,292	$C^2_{B_3}$	a. 53,874 b. 56,172 c. 26,475

Remarks	The annual cost of purchasing electricity units from the grid is minimum in case 2(c) attributed to higher number of units purchased by B_3 from B_1.					
Payments to B_1 for electricity units purchased from B_1 (D_{B_3}) (NZ$)	$D_{B_3}^0$	a. 0 b. 0 c. 0	$D_{B_2}^1$	a. 7,257 b. 6,762 c. 18,514	$D_{B_2}^2$	a. 9,335 b. 7,957 c. 34,367
Remarks	B_3 procures maximum number of units in case 2(c) from B_1 installed with solar PV and storage system					
Net revenue earned by B_3 (NP_{B_3}) (NZ$)	$NP_{B_3}^0$	a. 0 b. 0 c. 0	$NP_{B_3}^1$	a. 4,838 b. 4,508 c. 4,628	$NP_{B_3}^2$	a. 6,224 b. 5,305 c. 8,592
Remarks	B_3 earns highest profit in case 2(c) owing to maximum number of units purchased from B_1 at reduced rates as compared to TOU tariff.					

Appendix B3

The net present value (NPV) is given as:

$$NPV = \sum_{n=1}^{N} \frac{C_n}{(1+r)^n} - Initial\ Investment$$

where, C_n = cash flow at year n, r = discount rate, n = time period and initial investment is the total price of the system.

Appendix B4

The percentage annual savings earned by B_1, B_2 and B_3 after the application of profit model are given as follows:

$$Annual\ Savings\ (\%)\ for\ B_1 = \frac{P_{B_1}^0 - (P_{B_1}^0 - NP_{B_1})}{P_{B_1}^0} * 100$$

$$Annual\ Savings\ (\%)\ for\ B_2 = \frac{P_{B_2}^0 - (P_{B_2}^0 - NP_{B_2})}{P_{B_2}^0} * 100$$

$$Annual\ Savings\ (\%)\ for\ B_3 = \frac{P_{B_3}^0 - (P_{B_3}^0 - NP_{B_3})}{P_{B_3}^0} * 100$$

Appendix C1

The terms in (4.1) are defined as follows:

$$N_G = \sum_{t=1}^{24} (P_{RE2G}(t) * R_{sell}(t) + P_{ESS2G}(t)/\eta_{disch} * R_{sell}(t)) * \Delta t$$

$$D_{B_2} = \sum_{t=1}^{24} (P_{RE2B_2}(t) * R_{cont_2}(t) + P_{ESS2B_2}(t)/\eta_{disch} * R_{cont_2}(t)) * \Delta t$$

$$D_{B_3} = \sum_{t=1}^{24} (P_{RE2B_3}(t) * R_{cont_3}(t) + P_{ESS2B_3}(t)/\eta_{disch} * R_{cont_3}(t)) * \Delta t$$

$$D_{EV_n} = \sum_{n=1}^{30} \sum_{t=1}^{24} \Big(\big(P_{ESS2EV_n}(t) * \eta_{char} * R_{EV}(t) + P_{RE2EV_n}(t) * \eta_{char} * R_{EV}(t) + P_{G2EV_n}(t) * \eta_{char} * R_{EV}(t) \big) \Big) * \Delta t$$

$$S_{B_1} = \sum_{t=1}^{24} P_{RE2B_1}(t) * \Big(R_{pur}(t) - R_{sell}(t) \Big) + P_{ESS2B_1}(t)/\eta_{disch} * \Big(R_{pur}(t) - R_{sell}(t) \Big) * \Delta t$$

$$C_{B_1} = \sum_{t=1}^{24} \Big(P_{G2B_1}(t) * R_{pur}(t) \Big) * \Delta t$$

$$P_{EV} = \sum_{n=1}^{30} \sum_{t=1}^{24} \Big(P_{G2EV_n}(t) * \Big(R_{pur}(t) \Big) \Big) * \Delta t$$

$$E_{B_1} = \sum_{t=1}^{24} \Big(P_{G2ESS}(t) * \eta_{char} * R_{pur}(t) \Big) * \Delta t$$

$$P_{B_2} = \sum_{t=1}^{24} \left(P_{G2B_2}(t) * \left(R_{pur}(t) - R_{cont_2}(t) \right) \right) * \Delta t$$

$$P_{B_3} = \sum_{t=1}^{24} \left(P_{G2B_3}(t) * \left(R_{pur}(t) - R_{cont_3}(t) \right) \right) * \Delta t$$

Appendix C2

The additional terms in (4.17) are defined as follows:

$$C_{EV_{B_1}} = \sum_{n=1}^{15} \sum_{t=1}^{24} \left(P_{EV_n 2B_1}(t) * R_{EV_{pur}}(t) \right) * \Delta t$$

$$C_{EV_{ESS}} = \sum_{n=1}^{15} \sum_{t=1}^{24} \left(P_{EV_n 2ESS}(t) * R_{EV_{pur}}(t) \right) * \Delta t$$

Appendix C3

The percentage savings received by B_1, B_2, B_3 and EVs through profit model are given as:

$$Daily\ Savings\ (\%)\ for\ B_1 = \frac{C^0_{B_1} - (C^0_{B_1} - NP_{B_1})}{C^0_{B_1}} * 100$$

$$Daily\ Savings\ (\%)\ for\ B_2 = \frac{C^0_{B_2} - (C^0_{B_2} - NP_{B_2})}{C^0_{B_2}} * 100$$

$$Daily\ Savings\ (\%)\ for\ B_3 = \frac{C^0_{B_3} - (C^0_{B_3} - NP_{B_3})}{C^0_{B_3}} * 100$$

$$Daily\ Savings\ (\%)\ for\ EVs = \frac{C^0_{EV} - (C^0_{EV} - NP_{EV})}{C^0_{EV}} * 100$$

Appendix D1

The power ratings, total harmonic distortions and power factors for household appliances connected to a typical LESCO feeder is given in Table D1.

Table D1 Power rating (W), THDi (%), and power factor of household appliances connected with the LESCO feeder.

Household Appliances	**Power Rating (Watt)**	***THD$_i$*** **(% age)**	**Power Factor (*PF*)**	**Fundamental Current, I_1 (A)(*RMS*)**
Laptop Charger	45	148.76	0.57	0.34
LED/LCD/TV	30	139.12	0.56	0.23
Mobile Charger	6	138.04	0.48	0.054
CFL	24	100.96	0.67	0.15
Microwave Owen	1000	19.48	0.97	4.46
Refrigerator	150	17.1	0.53	1.22
Washing Machine	500	11.63	0.99	2.18
Fan	100	6.14	0.87	0.49
Water Dispenser	500	2.24	0.99	2.18
Electric Kettle	1000	1.89	0.97	4.46
Electric Heater	1000	1.87	0.99	4.37
Air conditioner	1300	50	0.95	5.92

Appendix D2

Modelling of modified IEEE 34-bus system and non-linear loads in ETAP is shown in Figures D4(i) and D4(ii), respectively.

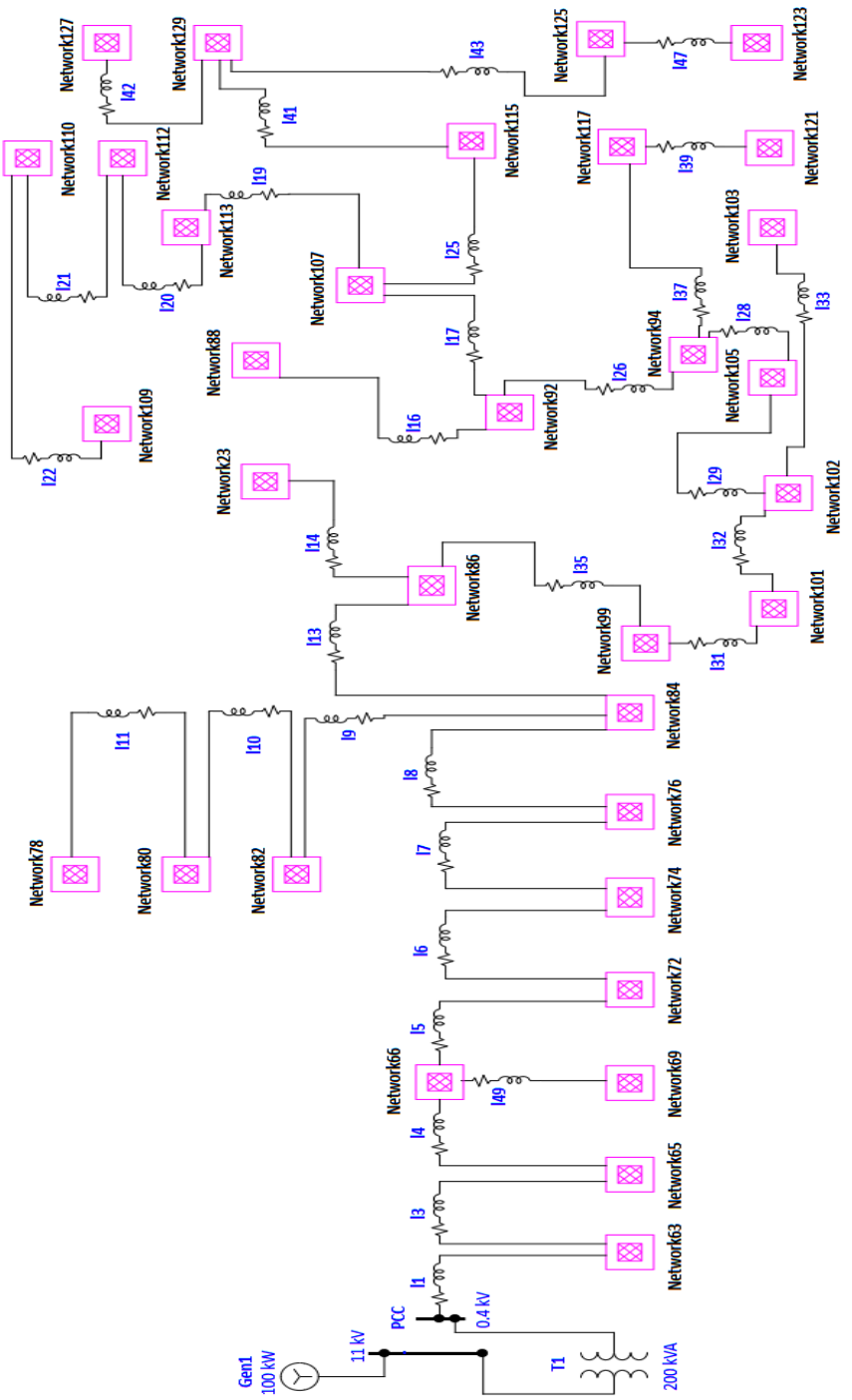

Figure D2(i). Modeling of modified IEEE-34 bus distribution network in ETAP 20.0.0 with 34 sub-networks (buses).

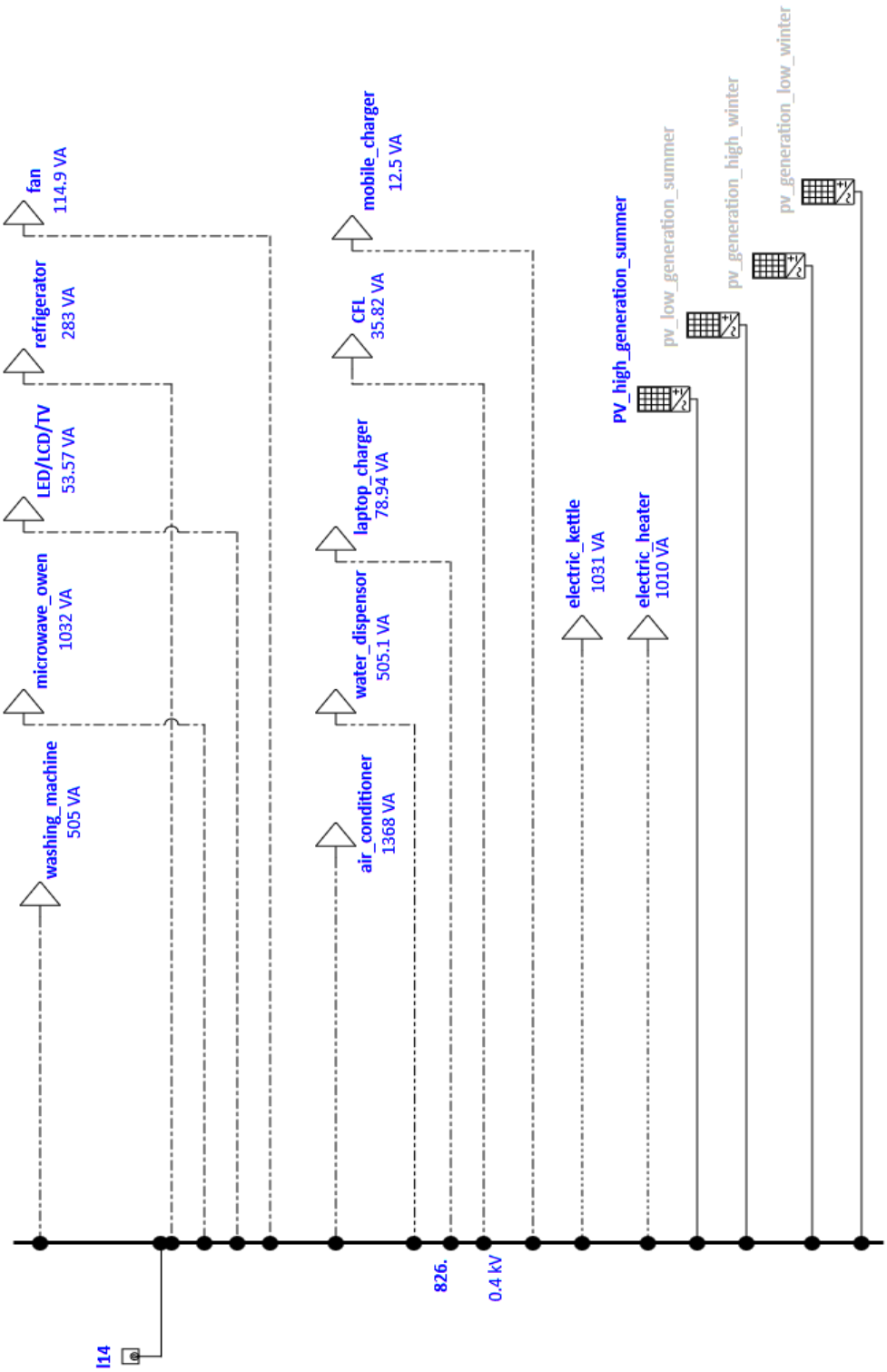

Figure D2(ii). Details of each sub-network in ETAP with three single-phase connections (non-linear loads) along with the integration of PV panels.

Appendix D3

Single Line Diagrams of the modified IEEE-34 bus system with 33% and 50% solar PV penetration are shown in Figures D3(i) and D3(ii), respectively.

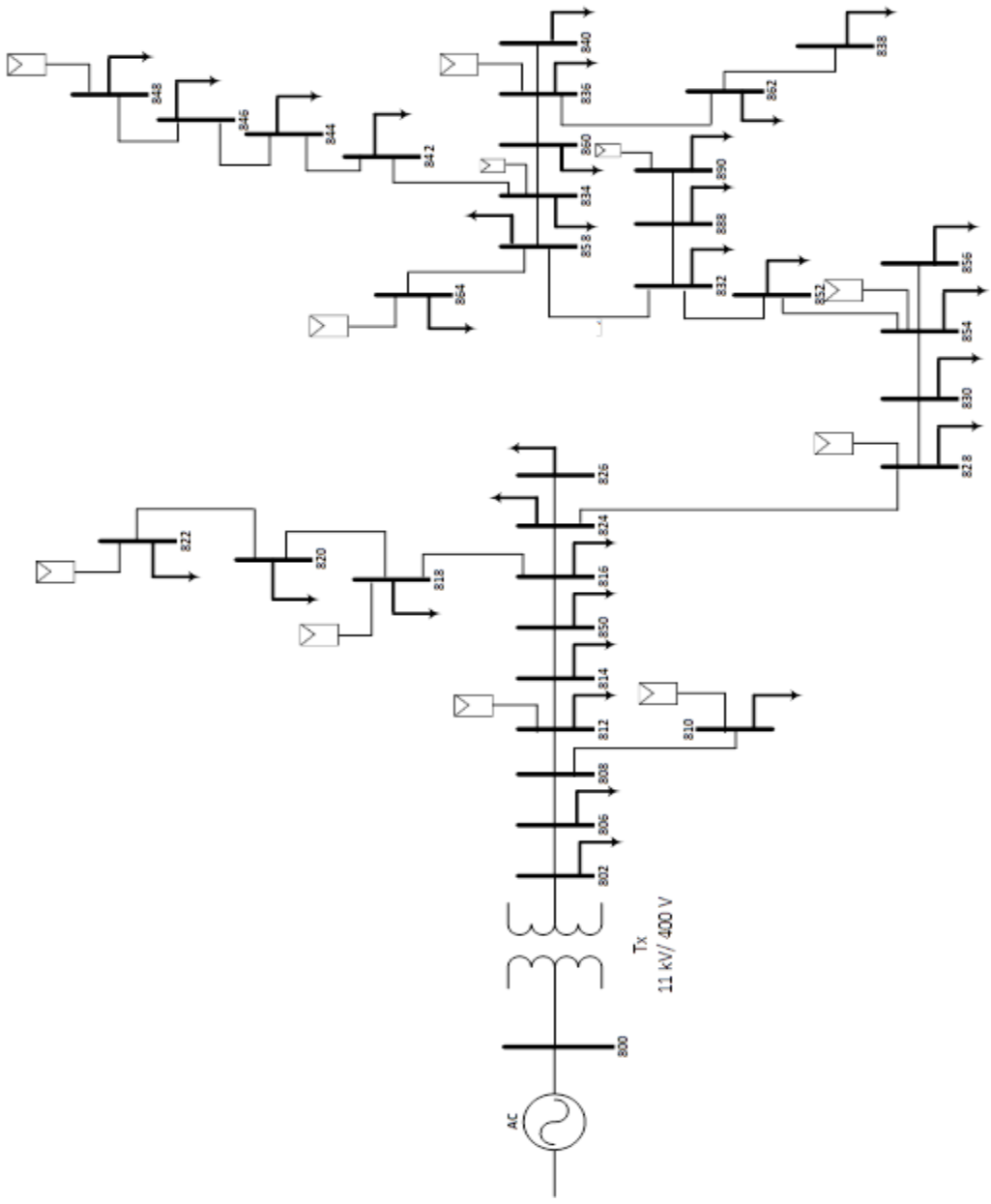

Figure D3(i). Single Line Diagram (SLD) of modified IEEE-34 bus distribution network with 33 % PV penetration.

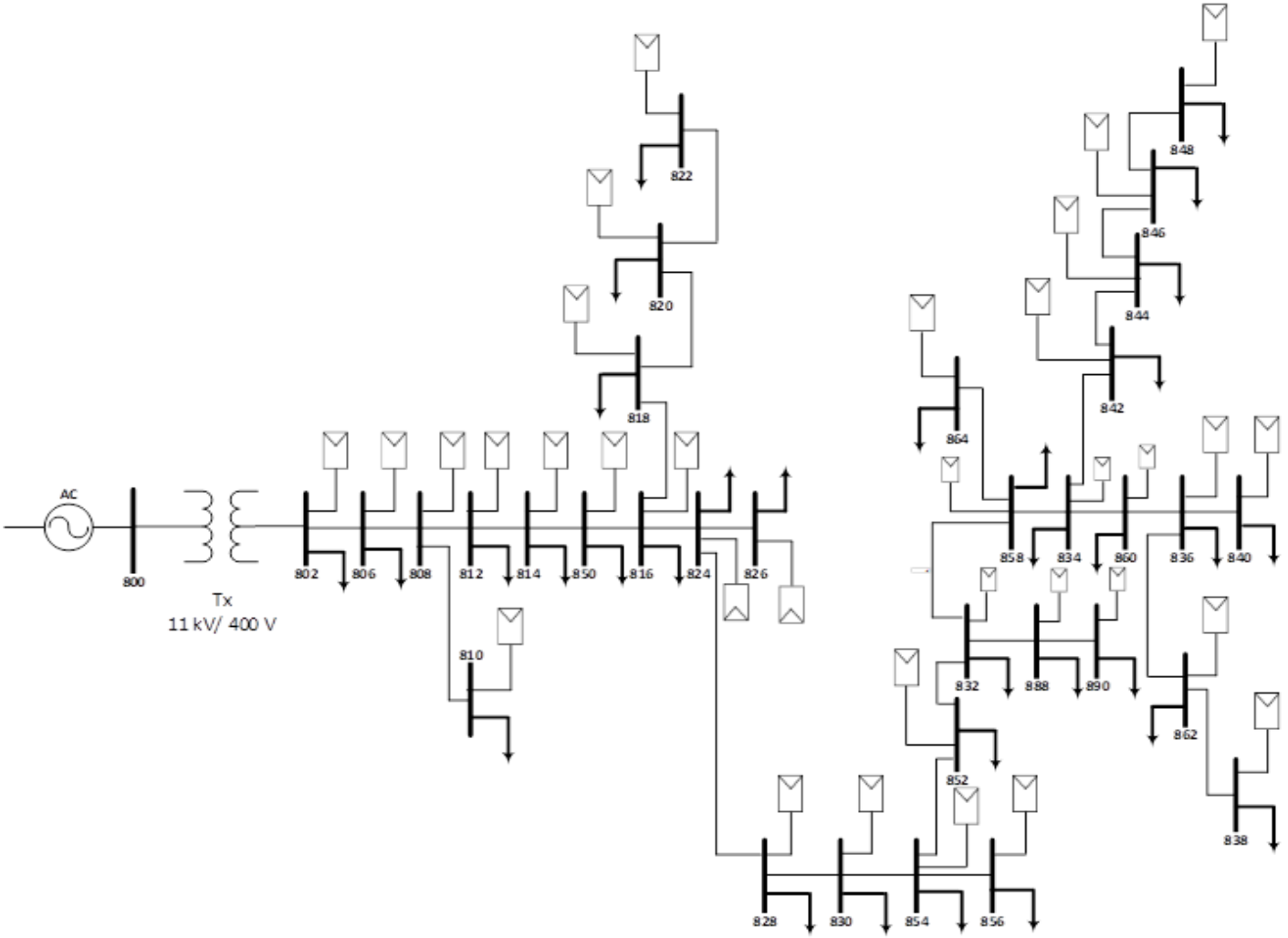

Figure D3(ii). Single Line Diagram (SLD) of modified IEEE-34 bus distribution network with 100 % PV penetration.

Bibliography

[1] Ministry of Finance (Government of Pakistan). [Online]. Available: http://www.finance.gov.pk/rebuttals_details1.html

[2] F. Abid Lateef Lodhi, "Future of Competitive Electricity Market in Pakistan."

[3] A. Malik, "In power projects: History, Policy and Politics."

[4] S. Malik, M. Qasim, and H. Saeed, "Green finance in Pakistan: Barriers and solutions," ADBI Working Paper2018.

[5] National Electric Power Regulatory Authority (NEPRA), "Annual Report," 2021.

[6] Central Power Purchasing Agency (CPPA), "Annual Report " 2020.

[7] R. Faia, F. Lezama, and J. M. Corchado, "Local electricity markets—practical implementations," in *Local Electricity Markets*, ed: Elsevier, 2021, pp. 127-140.

[8] A. Lüth, J. M. Zepter, P. C. del Granado, and R. Egging, "Local electricity market designs for peer-to-peer trading: The role of battery flexibility," *Applied energy,* vol. 229, pp. 1233-1243, 2018.

[9] M. F. Dynge, P. C. del Granado, N. Hashemipour, and M. Korpås, "Impact of local electricity markets and peer-to-peer trading on low-voltage grid operations," *Applied Energy,* vol. 301, p. 117404, 2021.

[10] S. Bjarghov, M. Löschenbrand, A. I. Saif, R. A. Pedrero, C. Pfeiffer, S. K. Khadem*, et al.*, "Developments and challenges in local electricity markets: A comprehensive review," *IEEE Access,* vol. 9, pp. 58910-58943, 2021.

[11] A. Cabrera-Tobar, E. Bullich-Massagué, M. Aragüés-Peñalba, and O. Gomis-Bellmunt, "Topologies for large scale photovoltaic power plants," *Renewable and Sustainable Energy Reviews,* vol. 59, pp. 309-319, 2016.

[12] A. Ferreira, S. S. Kunh, K. C. Fagnani, T. A. De Souza, C. Tonezer, G. R. Dos Santos*, et al.*, "Economic overview of the use and production of photovoltaic solar energy in brazil," *Renewable and Sustainable Energy Reviews,* vol. 81, pp. 181-191, 2018.

[13] V. Tyagi, N. A. Rahim, N. Rahim, A. Jeyraj, and L. Selvaraj, "Progress in solar PV technology: Research and achievement," *Renewable and sustainable energy reviews,* vol. 20, pp. 443-461, 2013.

[14] M. Bazilian, I. Onyeji, M. Liebreich, I. MacGill, J. Chase, J. Shah, *et al.*, "Re-considering the economics of photovoltaic power," *Renewable Energy,* vol. 53, pp. 329-338, 2013.

[15] M. A. Green, "Commercial progress and challenges for photovoltaics," *Nature Energy,* vol. 1, p. 15015, 2016.

[16] C. Lupangu and R. Bansal, "A review of technical issues on the development of solar photovoltaic systems," *Renewable and Sustainable Energy Reviews,* vol. 73, pp. 950-965, 2017.

[17] D. S. Albin, J. N. Johnson, Y. Zhao, and B. A. Korevaar, "Varying cadmium telluride growth temperature during deposition to increase solar cell reliability," ed: Google Patents, 2016.

[18] G. Data, "Thin Film Photovoltaics Market, 2017-2030," LONDON, Report 4335273, June 2017.

[19] K. Burrows and V. Fthenakis, "Glass needs for a growing photovoltaics industry," *Solar Energy Materials and Solar Cells,* vol. 132, pp. 455-459, 2015.

[20] J. Khan and M. H. Arsalan, "Solar power technologies for sustainable electricity generation–A review," *Renewable and Sustainable Energy Reviews,* vol. 55, pp. 414-425, 2016.

[21] M. Vellini, M. Gambini, and V. Prattella, "Environmental impacts of PV technology throughout the life cycle: Importance of the end-of-life management for Si-panels and CdTe-panels," *Energy,* vol. 138, pp. 1099-1111, 2017.

[22] J. A. Ruiz-Arias, E. F. Fernández, Á. Linares-Rodríguez, and F. Almonacid, "Analysis of the spatiotemporal characteristics of high concentrator photovoltaics energy yield and performance ratio," *IEEE Journal of Photovoltaics,* vol. 7, pp. 359-366, 2017.

[23] A. M. Khalid, I. Mitra, W. Warmuth, and V. Schacht, "Performance ratio–Crucial parameter for grid connected PV plants," *Renewable and Sustainable Energy Reviews,* vol. 65, pp. 1139-1158, 2016.

[24] A. E. Ghitas, "Studying the effect of spectral variations intensity of the incident solar radiation on the Si solar cells performance," *NRIAG Journal of Astronomy and Geophysics,* vol. 1, pp. 165-171, 2012.

[25] J. Bai, Y. Cao, Y. Hao, Z. Zhang, S. Liu, and F. Cao, "Characteristic output of PV systems under partial shading or mismatch conditions," *Solar Energy,* vol. 112, pp. 41-54, 2015.

[26] D. La Manna, V. L. Vigni, E. R. Sanseverino, V. Di Dio, and P. Romano, "Reconfigurable electrical interconnection strategies for photovoltaic arrays: A review," *Renewable and Sustainable Energy Reviews,* vol. 33, pp. 412-426, 2014.

[27] J. Peng, L. Lu, and H. Yang, "Review on life cycle assessment of energy payback and greenhouse gas emission of solar photovoltaic systems," *Renewable and Sustainable Energy Reviews,* vol. 19, pp. 255-274, 2013.

[28] P. Sivakumar and M. Arutchelvi, "Maximum power extractions in a single stage PV sourced grid connected inverter during low irradiations and nonlinear loads," *Renewable Energy,* vol. 107, pp. 262-270, 2017/07/01/ 2017.

[29] N. v. Reich, W. Van Sark, E. Alsema, R. Lof, R. Schropp, W. Sinke*, et al.*, "Crystalline silicon cell performance at low light intensities," *Solar Energy Materials and Solar Cells,* vol. 93, pp. 1471-1481, 2009.

[30] F. Bizzarri, M. Bongiorno, A. Brambilla, G. Gruosso, and G. S. Gajani, "Model of photovoltaic power plants for performance analysis and production forecast," *IEEE transactions on sustainable energy,* vol. 4, pp. 278-285, 2013.

[31] S. Pervaiz and H. A. Khan, "Low irradiance loss quantification in c-Si panels for photovoltaic systems," *Journal of Renewable and Sustainable Energy,* vol. 7, p. 013129, 2015.

[32] A. Thomson, M. Ernst, I. Haedrich, and J. Qian, "Impact of PV module configuration on energy yield under realistic conditions," *Optical and Quantum Electronics,* vol. 49, p. 82, 2017.

[33] M. Schweiger, W. Herrmann, A. Gerber, and U. Rau, "Understanding the energy yield of photovoltaic modules in different climates by linear performance loss analysis of the module performance ratio," *IET Renewable Power Generation,* vol. 11, pp. 558-565, 2017.

[34] T. Ozden, B. G. Akinoglu, and R. Turan, "Long term outdoor performances of three different on-grid PV arrays in central Anatolia – An extended analysis," *Renewable Energy,* vol. 101, pp. 182-195, 2017/02/01/ 2017.

[35] T. Huld, R. Gottschalg, H. G. Beyer, and M. Topič, "Mapping the performance of PV modules, effects of module type and data averaging," *Solar Energy,* vol. 84, pp. 324-338, 2010.

[36] C. Cañete, J. Carretero, and M. Sidrach-de-Cardona, "Energy performance of different photovoltaic module technologies under outdoor conditions," *Energy,* vol. 65, pp. 295-302, 2014/02/01/ 2014.

[37] H. Liu, A. M. Nobre, D. Yang, J. Y. Ye, F. R. Martins, R. Rüther*, et al.*, "The impact of haze on performance ratio and short-circuit current of pv systems in Singapore," *IEEE Journal of Photovoltaics,* vol. 4, pp. 1585-1592, 2014.

[38] A. M. Nobre, S. Karthik, H. Liu, D. Yang, F. R. Martins, E. B. Pereira*, et al.*, "On the impact of haze on the yield of photovoltaic systems in Singapore," *Renewable Energy,* vol. 89, pp. 389-400, 2016/04/01/ 2016.

[39] H. A. AlBusairi and H. J. Möller, "Performance evaluation of CdTe PV modules under natural outdoor conditions in Kuwait," in *25th European Solar Energy Conference and Exhibition/5th World Conference on Photovoltaic Energy Conversion, Valencia, Spain, September*, 2010, pp. 6-10.

[40] C. Candelise, J. F. Speirs, and R. J. Gross, "Materials availability for thin film (TF) PV technologies development: A real concern?," *Renewable and Sustainable Energy Reviews,* vol. 15, pp. 4972-4981, 2011.

[41] N. R. E. Laboratory. Solar Resource Data [Online]. Available: pvwatts.nrel.gov

[42] M. K. Juhl, M. D. Abbott, and T. Trupke, "Relative external quantum efficiency of crystalline silicon wafers from photoluminescence," *IEEE Journal of Photovoltaics,* vol. 7, pp. 1074-1080, 2017.

[43] S. Hosseini, S. Taheri, M. Farzaneh, H. Taheri, and M. Narimani, "Determination of Photovoltaic Characteristics in Real Field Conditions," *IEEE Journal of Photovoltaics,* vol. 8, pp. 572-580, 2018.

[44] M. Padilla, B. Michl, B. Thaidigsmann, W. Warta, and M. Schubert, "Short-circuit current density mapping for solar cells," *Solar Energy Materials and Solar Cells,* vol. 120, pp. 282-288, 2014.

[45] P. Singh and N. M. Ravindra, "Temperature dependence of solar cell performance—an analysis," *Solar Energy Materials and Solar Cells,* vol. 101, pp. 36-45, 2012.

[46] A. S. Rana and H. A. Khan, "String level optimization on grid-tied solar PV systems for minimizing soft shading power loss," 2016.

[47] T. D. Lee and A. U. Ebong, "A review of thin film solar cell technologies and challenges," *Renewable and Sustainable Energy Reviews,* vol. 70, pp. 1286-1297, 2017.

[48] C. S. Solanki, *Solar photovoltaics: fundamentals, technologies and applications*: PHI Learning Pvt. Ltd., 2015.

[49] A. Polman, M. Knight, E. C. Garnett, B. Ehrler, and W. C. Sinke, "Photovoltaic materials: Present efficiencies and future challenges," *Science,* vol. 352, p. aad4424, 2016.

[50] D. Mello, R. Ricciari, A. Battaglia, M. Foti, and C. Gerardi, "Case study of failure analysis in thin film silicon solar cell," *Microelectronics Reliability,* vol. 55, pp. 1800-1803, 2015.

[51] A. Pandey, V. Tyagi, A. Jeyraj, L. Selvaraj, N. Rahim, and S. Tyagi, "Recent advances in solar photovoltaic systems for emerging trends and advanced applications," *Renewable and Sustainable Energy Reviews,* vol. 53, pp. 859-884, 2016.

[52] J. Solórzano and M. Egido, "Hot-spot mitigation in PV arrays with distributed MPPT (DMPPT)," *Solar Energy,* vol. 101, pp. 131-137, 2014.

[53] K. A. Kim, G.-S. Seo, B.-H. Cho, and P. T. Krein, "Photovoltaic hot-spot detection for solar panel substrings using AC parameter characterization," *IEEE Transactions on Power Electronics,* vol. 31, pp. 1121-1130, 2016.

[54] N. Kaushika and A. K. Rai, "An investigation of mismatch losses in solar photovoltaic cell networks," *Energy,* vol. 32, pp. 755-759, 2007.

[55] S. Dongaonkar and M. A. Alam, "Geometrical design of thin film photovoltaic modules for improved shade tolerance and performance," *Progress in Photovoltaics: Research and Applications,* vol. 23, pp. 170-181, 2015.

[56] S. Daliento, F. Di Napoli, P. Guerriero, and V. d'Alessandro, "A modified bypass circuit for improved hot spot reliability of solar panels subject to partial shading," *Solar Energy,* vol. 134, pp. 211-218, 2016.

[57] P. Manganiello, M. Balato, and M. Vitelli, "A survey on mismatching and aging of PV modules: The closed loop," *IEEE Transactions on Industrial Electronics,* vol. 62, pp. 7276-7286, 2015.

[58] D. C. Jordan, T. J. Silverman, B. Sekulic, and S. R. Kurtz, "PV degradation curves: non-linearities and failure modes," *Progress in Photovoltaics: Research and Applications,* vol. 25, pp. 583-591, 2017.

[59] M. Q. Duong, G. N. Sava, G. Ionescu, H. Necula, S. Leva, and M. Mussetta, "Optimal bypass diode configuration for PV arrays under shading influence," in *Environment and Electrical Engineering and 2017 IEEE Industrial and Commercial Power Systems Europe (EEEIC/I&CPS Europe), 2017 IEEE International Conference on*, 2017, pp. 1-5.

[60] C. Tzikas, G. Gómez, M. van den Donker, K. Bakker, A. H. Smets, and W. Folkerts, "Do thin film PV modules offer an advantage under partial shading conditions?," *Presented at: EUPVSEC,* vol. 25, p. 29, 2017.

[61] S. Dongaonkar, C. Deline, and M. A. Alam, "Performance and reliability implications of two-dimensional shading in monolithic thin-film photovoltaic modules," *IEEE Journal of Photovoltaics,* vol. 3, pp. 1367-1375, 2013.

[62] K. Seshan and D. Schepis, *Handbook of thin film deposition*: William Andrew, 2018.

[63] X. Sun, J. Raguse, R. Garris, C. Deline, T. Silverman, and M. A. Alam, "A physics-based compact model for CIGS and CdTe solar cells: from voltage-dependent carrier collection to light-enhanced reverse breakdown," in *Photovoltaic Specialist Conference (PVSC), 2015 IEEE 42nd*, 2015, pp. 1-6.

[64] A. S. Rana, M. Nasir, and H. A. Khan, "String level optimisation on grid-tied solar PV systems to reduce partial shading loss," *IET Renewable Power Generation,* vol. 12, pp. 143 – 148, 2018.

[65] S. WrÜth. "Módulo solar GeneCIS 51,3W|WRG1005" [Online]. Available: https://abonahora.files.wordpress.com/2012/04/wrg1005_es.pdf

[66] K. A. Kim and P. T. Krein, "Hot spotting and second breakdown effects on reverse IV characteristics for mono-crystalline Si photovoltaics," in *Energy Conversion Congress and Exposition (ECCE), 2013 IEEE*, 2013, pp. 1007-1014.

[67] R. Moretón, E. Lorenzo, and L. Narvarte, "Experimental observations on hot-spots and derived acceptance/rejection criteria," *Solar energy,* vol. 118, pp. 28-40, 2015.

[68] S. Armstrong and W. Hurley, "A new methodology to optimise solar energy extraction under cloudy conditions," *Renewable Energy,* vol. 35, pp. 780-787, 2010.

[69] "BYD240P6-30 Polycrystalline Silicon solar panel. 2011.," ed, 2011.

[70] K. Siraj and H. A. Khan, "DC distribution for residential power networks—A framework to analyze the impact of voltage levels on energy efficiency," *Energy Reports,* vol. 6, pp. 944-951, 2020.

[71] N. Martin and J. Rice, "Solar Feed-In Tariffs: Examining fair and reasonable retail rates using cost avoidance estimates," *Energy Policy,* vol. 112, pp. 19-28, 2018.

[72] J. Hirvonen, G. Kayo, S. Cao, A. Hasan, and K. Sirén, "Renewable energy production support schemes for residential-scale solar photovoltaic systems in Nordic conditions," *Energy Policy,* vol. 79, pp. 72-86, 2015.

[73] A. S. Rana, M. Nasir, and H. A. Khan, "String level optimisation on grid-tied solar PV systems to reduce partial shading loss," *IET Renewable Power Generation,* vol. 12, pp. 143-148, 2017.

[74] N. R. Darghouth, R. H. Wiser, G. Barbose, and A. D. Mills, "Net metering and market feedback loops: Exploring the impact of retail rate design on distributed PV deployment," *Applied Energy,* vol. 162, pp. 713-722, 2016.

[75] M. Nasir, H. A. Khan, I. Khan, N. A. Zaffar, A. Mehmood, T. Sauter*, et al.*, "Grid Load Reduction through Optimized PV Power Utilization in Intermittent Grids Using a Low-Cost Hardware Platform," *Energies,* vol. 12, p. 1764, 2019.

[76] M. T. Lawder, B. Suthar, P. W. Northrop, S. De, C. M. Hoff, O. Leitermann*, et al.*, "Battery energy storage system (BESS) and battery management system (BMS) for grid-scale applications," *Proceedings of the IEEE,* vol. 102, pp. 1014-1030, 2014.

[77] S. P. Ayeng'o, T. Schirmer, K.-P. Kairies, H. Axelsen, and D. U. Sauer, "Comparison of off-grid power supply systems using lead-acid and lithium-ion batteries," *Solar Energy,* vol. 162, pp. 140-152, 2018.

[78] H. A. Khan and S. Pervaiz, "Technological review on solar PV in Pakistan: Scope, practices and recommendations for optimized system design," *Renewable and Sustainable Energy Reviews,* vol. 23, pp. 147-154, 2013.

[79] N. Bashir, H. S. Sardar, M. Nasir, N. U. Hassan, and H. A. Khan, "Lifetime maximization of lead-acid batteries in small scale UPS and distributed generation systems," in *2017 IEEE Manchester PowerTech*, 2017, pp. 1-6.

[80] M. U. Tahir, T. Moaz, H. A. Khan, N. A. Zaffar, and I. Khan, "Accurate Modeling of Li-ion Cells Applied to LiFePO 4 and NMC Chemistries," in *2020 IEEE Texas Power and Energy Conference (TPEC)*, 2020, pp. 1-6.

[81] M. Y. Raza, M. Wasim, and M. S. Sarwar, "Development of Renewable Energy Technologies in rural areas of Pakistan," *Energy Sources, Part A: Recovery, Utilization, and Environmental Effects,* vol. 42, pp. 740-760, 2020.

[82] C. Curry, "Lithium-ion battery costs and market," *Bloomberg New Energy Finance,* vol. 5, 2017.

[83] B. Numbi and S. Malinga, "Optimal energy cost and economic analysis of a residential grid-interactive solar PV system-case of eThekwini municipality in South Africa," *Applied Energy,* vol. 186, pp. 28-45, 2017.

[84] E. O'Shaughnessy, D. Cutler, K. Ardani, and R. Margolis, "Solar plus: Optimization of distributed solar PV through battery storage and dispatchable load in residential buildings," *Applied Energy,* vol. 213, pp. 11-21, 2018.

[85] J. Jin, Y. Xu, Y. Khalid, and N. U. Hassan, "Optimal operation of energy storage with random renewable generation and AC/DC loads," *IEEE Transactions on Smart Grid,* vol. 9, pp. 2314-2326, 2018.

[86] B.-R. Ke, T.-T. Ku, Y.-L. Ke, C.-Y. Chuang, and H.-Z. Chen, "Sizing the battery energy storage system on a university campus with prediction of load and photovoltaic generation," *IEEE Transactions on Industry Applications,* vol. 52, pp. 1136-1147, 2016.

[87] E. L. Ratnam, S. R. Weller, and C. M. Kellett, "Scheduling residential battery storage with solar PV: Assessing the benefits of net metering," *Applied Energy,* vol. 155, pp. 881-891, 2015.

[88] T. Anilkumar, S. P. Simon, and N. P. Padhy, "Residential electricity cost minimization model through open well-pico turbine pumped storage system," *Applied energy,* vol. 195, pp. 23-35, 2017.

[89] M. I. Azim, W. Tushar, and T. K. Saha, "Investigating the impact of P2P trading on power losses in grid-connected networks with prosumers," *Applied Energy,* vol. 263, p. 114687, 2020.

[90] J. Yuning, "LCA of Microgrid System: a Case Study at 'North-five Islands' of Changshan Archipelago, China," ed, 2019.

[91] C. S. Lai and M. D. McCulloch, "Levelized cost of electricity for solar photovoltaic and electrical energy storage," *Applied energy,* vol. 190, pp. 191-203, 2017.

[92] K. Branker, M. Pathak, and J. M. Pearce, "A review of solar photovoltaic levelized cost of electricity," *Renewable and sustainable energy reviews,* vol. 15, pp. 4470-4482, 2011.

[93] S. M. Ahsan and H. A. Khan, "Performance comparison of CdTe thin film modules with c-Si modules under low irradiance," *IET Renewable Power Generation,* 2019.

[94] NPV Calculator [Online]. Available: https://www.calculatestuff.com/financial/npv-calculator

[95] A. W. Thompson and Y. Perez, "Vehicle-to-Everything (V2X) energy services, value streams, and regulatory policy implications," *Energy Policy,* vol. 137, p. 111136, 2020.

[96] S. M. Ahsan, H. A. Khan, A. Hussain, S. Tariq, and N. A. Zaffar, "Harmonic Analysis of Grid-Connected Solar PV Systems with Nonlinear Household Loads in Low-Voltage Distribution Networks," *Sustainability,* vol. 13, p. 3709, 2021.

[97] S. M. Arif, T. T. Lie, B. C. Seet, S. M. Ahsan, and H. A. Khan, "Plug-In Electric Bus Depot Charging with PV and ESS and Their Impact on LV Feeder," *Energies,* vol. 13, p. 2139, 2020.

[98] T. Ma and O. A. Mohammed, "Optimal charging of plug-in electric vehicles for a car-park infrastructure," *IEEE Transactions on Industry Applications,* vol. 50, pp. 2323-2330, 2014.

[99] S. Wang, S. Bi, Y.-J. A. Zhang, and J. Huang, "Electrical vehicle charging station profit maximization: Admission, pricing, and online scheduling," *IEEE Transactions on Sustainable Energy,* vol. 9, pp. 1722-1731, 2018.

[100] M. Shafiullah, A. T. Al-Awami, and I. M. ElAmin, "Profit maximization planning of a Load Aggregator using Electric Vehicles through optimal scheduling of day ahead load," in *2015 18th International Conference on Intelligent System Application to Power Systems (ISAP)*, 2015, pp. 1-6.

[101] Z. Moghaddam, I. Ahmad, D. Habibi, and M. A. Masoum, "A coordinated dynamic pricing model for electric vehicle charging stations," *IEEE Transactions on Transportation Electrification,* vol. 5, pp. 226-238, 2019.

[102] A. Rabiee, A. Ghiasian, and M. A. Chermahini, "Long term profit maximization strategy for charging scheduling of electric vehicle charging station," *IET Generation, Transmission & Distribution,* vol. 12, pp. 4134-4141, 2018.

[103] S. Khemakhem, M. Rekik, and L. Krichen, "A collaborative energy management among plug-in electric vehicle, smart homes and neighbors' interaction for residential power load profile smoothing," *Journal of Building Engineering,* vol. 27, p. 100976, 2020.

[104] I. Gonçalves, Á. Gomes, and C. H. Antunes, "Optimizing the management of smart home energy resources under different power cost scenarios," *Applied Energy,* vol. 242, pp. 351-363, 2019.

[105] J. Chen, Y. Zhang, X. Li, B. Sun, Q. Liao, Y. Tao*, et al.*, "Strategic integration of vehicle-to-home system with home distributed photovoltaic power generation in Shanghai," *Applied Energy,* vol. 263, p. 114603, 2020.

[106] A. Ul-Haq, C. Cecati, and E. A. Al-Ammar, "Modeling of a photovoltaic-powered electric vehicle charging station with vehicle-to-grid implementation," *Energies,* vol. 10, p. 4, 2017.

[107] Q. Dai, J. Liu, and Q. Wei, "Optimal photovoltaic/battery energy storage/electric vehicle charging station design based on multi-agent particle swarm optimization algorithm," *Sustainability,* vol. 11, p. 1973, 2019.

[108] L. Luo, Z. Wu, W. Gu, H. Huang, S. Gao, and J. Han, "Coordinated allocation of distributed generation resources and electric vehicle charging stations in distribution systems with vehicle-to-grid interaction," *Energy,* vol. 192, p. 116631, 2020.

[109] L. Global, "GOGLA; ESMAP. Off-Grid Solar Market Trends Report 2020," 2020.

[110] D. Thomas, O. Deblecker, and C. S. Ioakimidis, "Optimal operation of an energy management system for a grid-connected smart building considering photovoltaics' uncertainty and stochastic electric vehicles' driving schedule," *Applied Energy,* vol. 210, pp. 1188-1206, 2018.

[111] S. Ayyadi and M. Maaroufi, "Optimal Framework to Maximize the Workplace Charging Station Owner Profit while Compensating Electric Vehicles Users," *Mathematical Problems in Engineering,* vol. 2020, 2020.

[112] S. M. Ahsan, H. A. Khan, N.-u. Hassan, S. M. Arif, and T.-T. Lie, "Optimized power dispatch for solar photovoltaic-storage system with multiple buildings in bilateral contracts," *Applied Energy,* vol. 273, p. 115253, 2020.

[113] M. Nicholas, "Estimating electric vehicle charging infrastructure costs across major US metropolitan areas," *URL: https://theicct. org/sites/default/files/publications/ICCT_EV_Charging_Cost_20190813. pdf,* 2019.

[114] T. A. Lehtola and A. Zahedi, "Electric vehicle battery cell cycle aging in vehicle to grid operations: A review," *IEEE Journal of Emerging and Selected Topics in Power Electronics,* vol. 9, pp. 423-437, 2019.

[115] G. Zhao and J. Baker, "Effects on environmental impacts of introducing electric vehicle batteries as storage-A case study of the United Kingdom," *Energy Strategy Reviews,* vol. 40, p. 100819, 2022.

[116] M. Petit, E. Prada, and V. Sauvant-Moynot, "Development of an empirical aging model for Li-ion batteries and application to assess the impact of Vehicle-to-Grid strategies on battery lifetime," *Applied energy,* vol. 172, pp. 398-407, 2016.

[117] S.-K. Kim, J.-H. Jeon, C.-H. Cho, E.-S. Kim, and J.-B. Ahn, "Modeling and simulation of a grid-connected PV generation system for electromagnetic transient analysis," *Solar Energy,* vol. 83, pp. 664-678, 2009.

[118] F. M. Camilo, V. F. Pires, R. Castro, and M. Almeida, "The impact of harmonics compensation ancillary services of photovoltaic microgeneration in low voltage distribution networks," *Sustainable cities and society,* vol. 39, pp. 449-458, 2018.

[119] A. Chidurala, T. K. Saha, N. Mithulananthan, and R. C. Bansal, "Harmonic emissions in grid connected PV systems: A case study on a large scale rooftop PV site," in *2014 IEEE PES General Meeting| Conference & Exposition*, 2014, pp. 1-5.

[120] A. Elkholy, "Harmonics assessment and mathematical modeling of power quality parameters for low voltage grid connected photovoltaic systems," *Solar Energy,* vol. 183, pp. 315-326, 2019.

[121] M. A. Eltawil and Z. Zhao, "Grid-connected photovoltaic power systems: Technical and potential problems—A review," *Renewable and sustainable energy reviews,* vol. 14, pp. 112-129, 2010.

[122] W. I. Gabr and W. A. Salem, "Impact of Grid Connected Photovoltaic System on Total Harmonics Distortion (THD) of Low Voltage Distribution Network: A Case Study," in *2018 Twentieth International Middle East Power Systems Conference (MEPCON)*, 2018, pp. 608-614.

[123] A. B. Nassif, H. Yazdanpanahi, and R. Torquato, "Harmonic Characterization of Modern Residential Distributed Energy Resources," in *2018 IEEE Canadian Conference on Electrical & Computer Engineering (CCECE)*, 2018, pp. 1-4.

[124] O. S. Nduka and B. C. Pal, "Harmonic domain modeling of PV system for the assessment of grid integration impact," *IEEE Transactions on Sustainable Energy,* vol. 8, pp. 1154-1165, 2017.

[125] M. Patsalides, A. Stavrou, V. Efthymiou, and G. E. Georghiou, "Towards the establishment of maximum PV generation limits due to power quality constraints," *International Journal of Electrical Power & Energy Systems,* vol. 42, pp. 285-298, 2012.

[126] H. A. Pereira, F. D. Freijedo, M. Silva, V. Mendes, and R. Teodorescu, "Harmonic current prediction by impedance modeling of grid-tied inverters: A 1.4 MW PV plant case study," *International Journal of Electrical Power & Energy Systems,* vol. 93, pp. 30-38, 2017.

[127] R. Pinto, S. Mariano, M. D. R. Calado, and J. F. De Souza, "Impact of rural grid-connected photovoltaic generation systems on power quality," *Energies,* vol. 9, p. 739, 2016.

[128] S. Sakar, M. E. Balci, S. H. A. Aleem, and A. F. Zobaa, "Integration of large-scale PV plants in non-sinusoidal environments: Considerations on hosting capacity and harmonic distortion limits," *Renewable and Sustainable Energy Reviews,* vol. 82, pp. 176-186, 2018.

[129] R. Torquato, F. C. Trindade, and W. Freitas, "Analysis of the harmonic distortion impact of photovoltaic generation in Brazilian residential networks," in *2014 16th International Conference on Harmonics and Quality of Power (ICHQP)*, 2014, pp. 239-243.

[130] K. Fekete, Z. Klaic, and L. Majdandzic, "Expansion of the residential photovoltaic systems and its harmonic impact on the distribution grid," *Renewable energy,* vol. 43, pp. 140-148, 2012.

[131] H. Dghim, A. El-Naggar, and I. Erlich, "Harmonic distortion in low voltage grid with grid-connected photovoltaic," in *2018 18th International Conference on Harmonics and Quality of Power (ICHQP)*, 2018, pp. 1-6.

[132] W. Miller, A. Liu, Z. Amin, and A. Wagner, "Power quality and rooftop-photovoltaic households: an examination of measured data at point of customer connection," *Sustainability,* vol. 10, p. 1224, 2018.

[133] M. Piccirilli, A. Reatti, F. Corti, M. K. Kazimierczuk, A. Ayachit, P. De La Pierre*, et al.*, "Distortion analysis and equivalent impedance estimation of a class-D full-wave rectifier," in *2017 IEEE International Conference on Environment and Electrical Engineering and 2017 IEEE Industrial and Commercial Power Systems Europe (EEEIC/I&CPS Europe)*, 2017, pp. 1-7.

[134] F. Corti, A. Laudani, G. M. Lozito, and A. Reatti, "Computationally Efficient Modeling of DC-DC Converters for PV Applications," *Energies,* vol. 13, p. 5100, 2020.

[135] A. Chidurala, T. K. Saha, and N. Mithulananthan, "Harmonic impact of high penetration photovoltaic system on unbalanced distribution networks–learning from an urban photovoltaic network," *IET Renewable Power Generation,* vol. 10, pp. 485-494, 2016.

[136] A. Kharrazi, V. Sreeram, and Y. Mishra, "Assessment techniques of the impact of grid-tied rooftop photovoltaic generation on the power quality of low voltage distribution network-A review," *Renewable and Sustainable Energy Reviews,* vol. 120, p. 109643, 2020.

[137] IEEE, "IEEE Recommended Practice and Requirements for Harmonic Control in Electric Power Systems," in *IEEE Standards Association*, ed: IEEE Power and Energy Society, 2014, p. 29.

[138] A. Ahmad, S. A. R. Kashif, M. A. Saqib, A. Ashraf, and U. T. Shami, "Tariff for reactive energy consumption in household appliances," *Energy,* vol. 186, p. 115818, 2019.